Italy,the Mediterranean, and Plate Tectonics

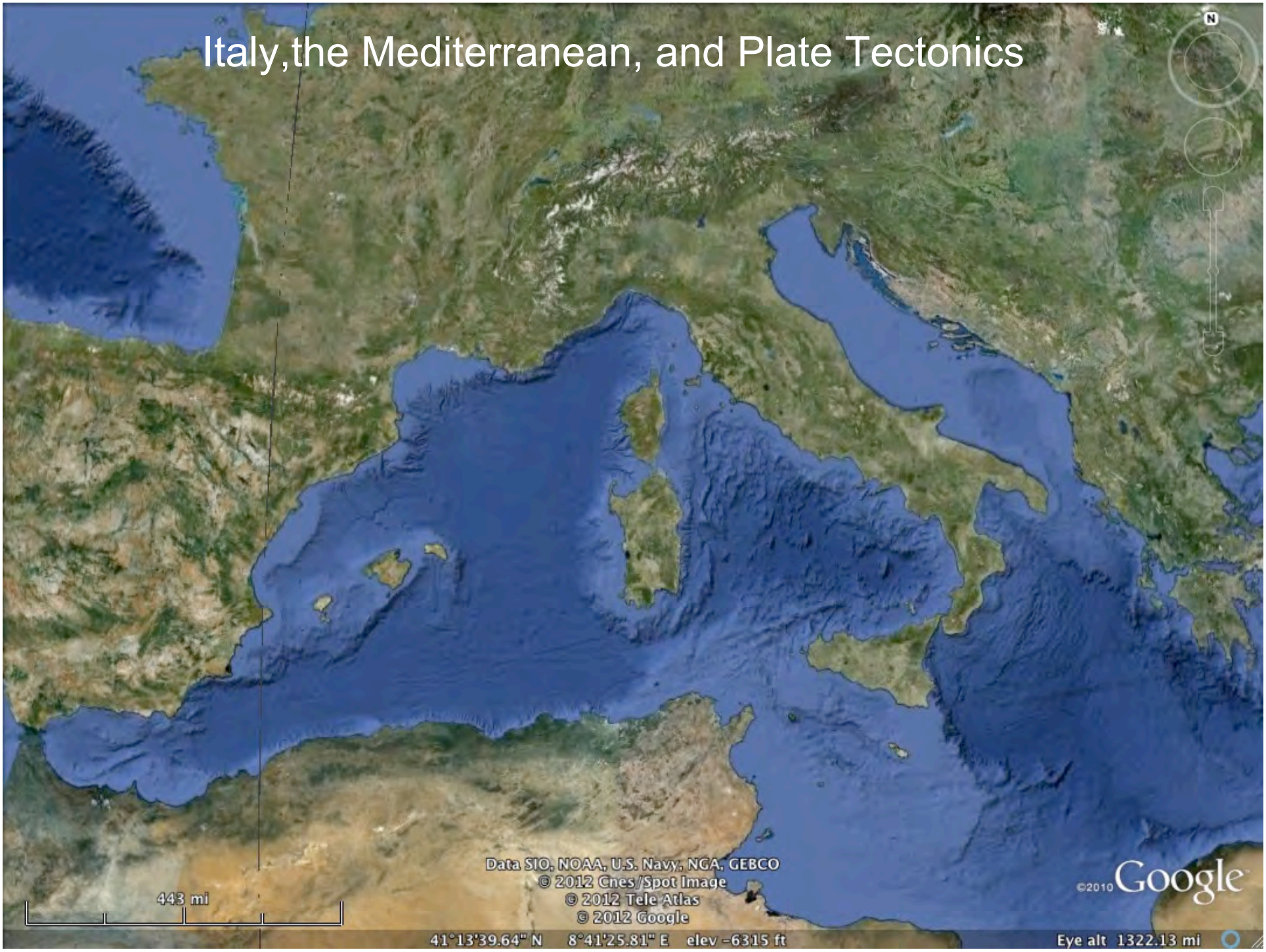

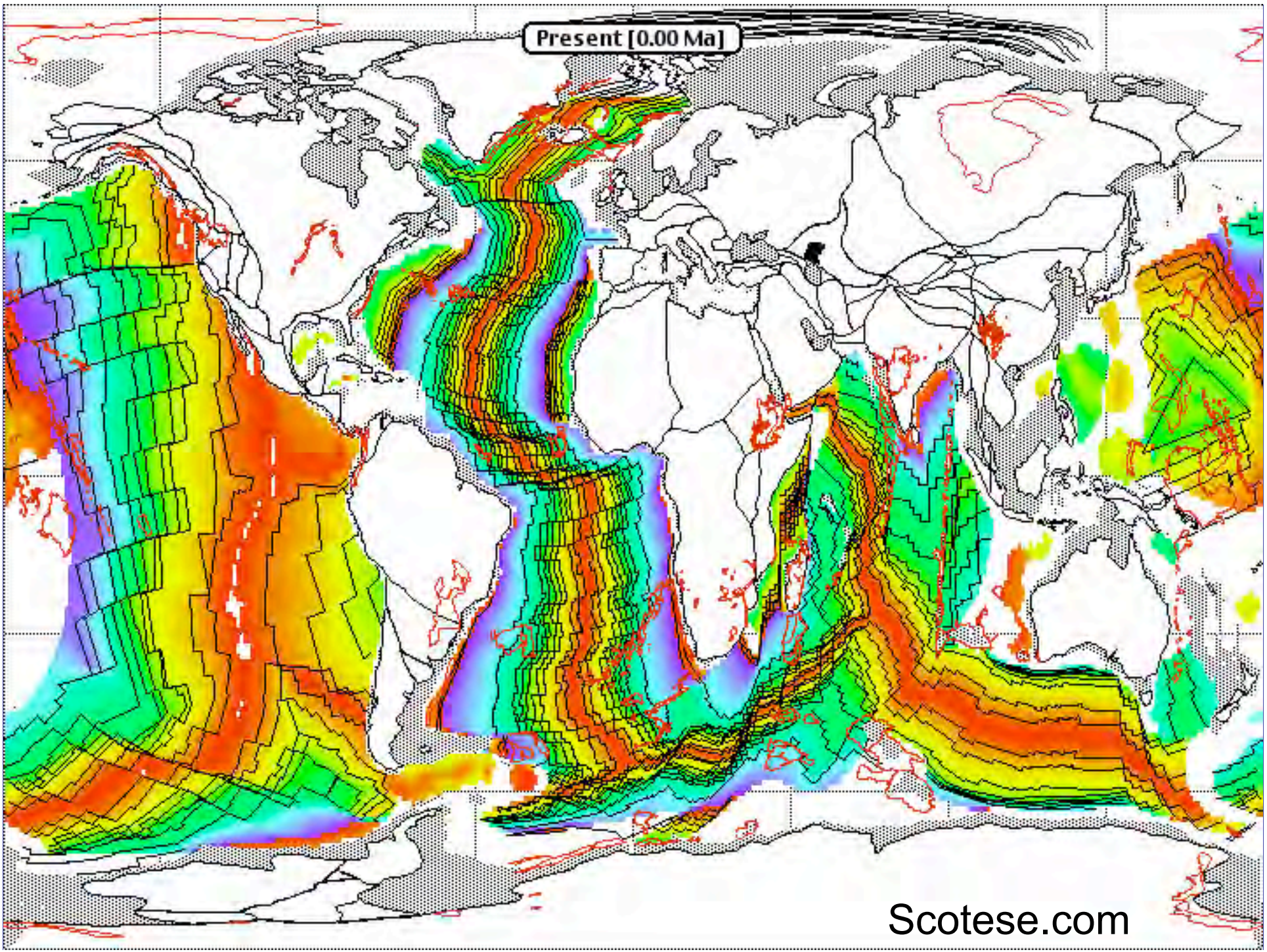
Present [0.00 Ma]
Scotese.com

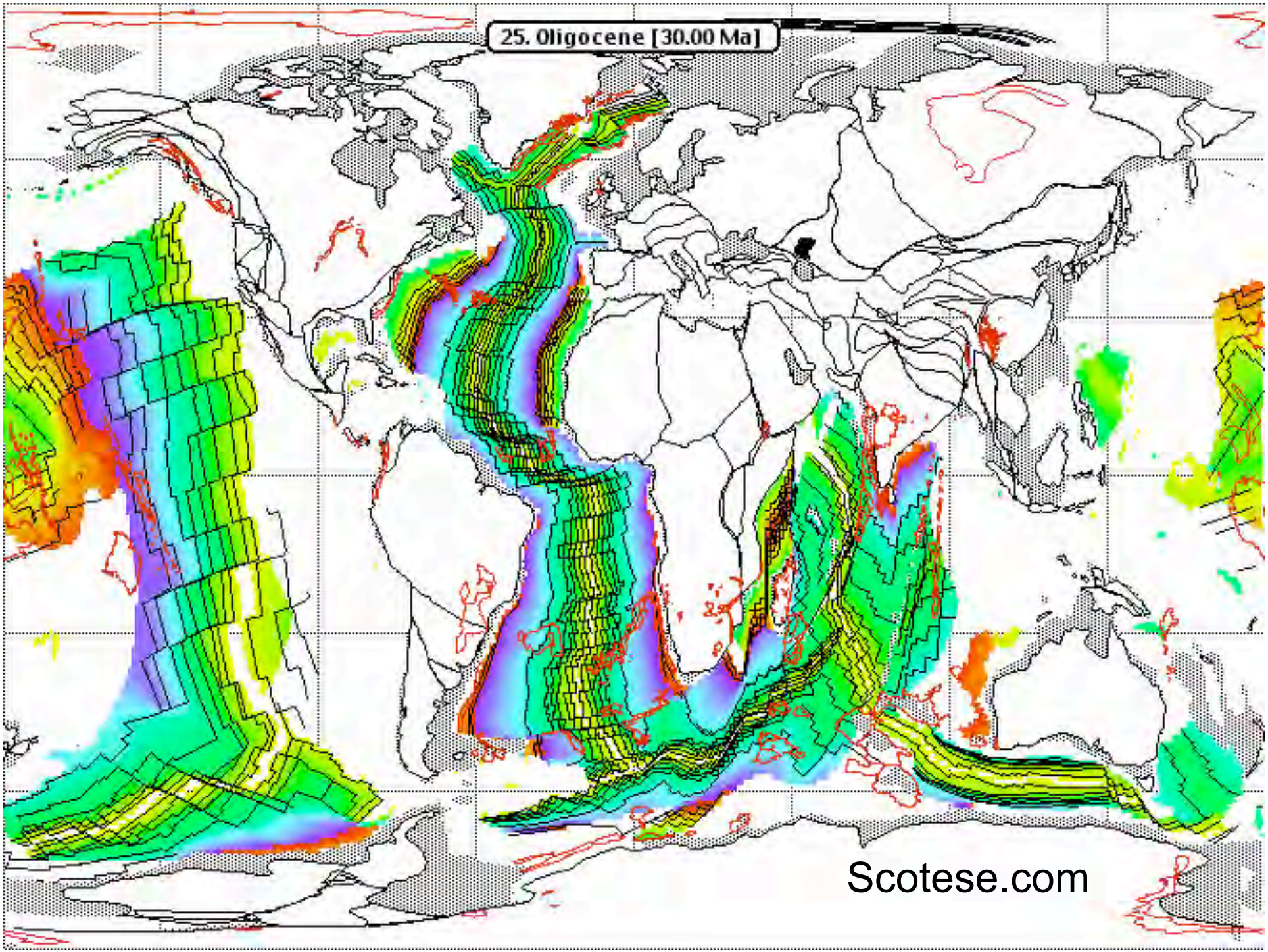
25. Oligocene [30.00 Ma]
Scotese.com

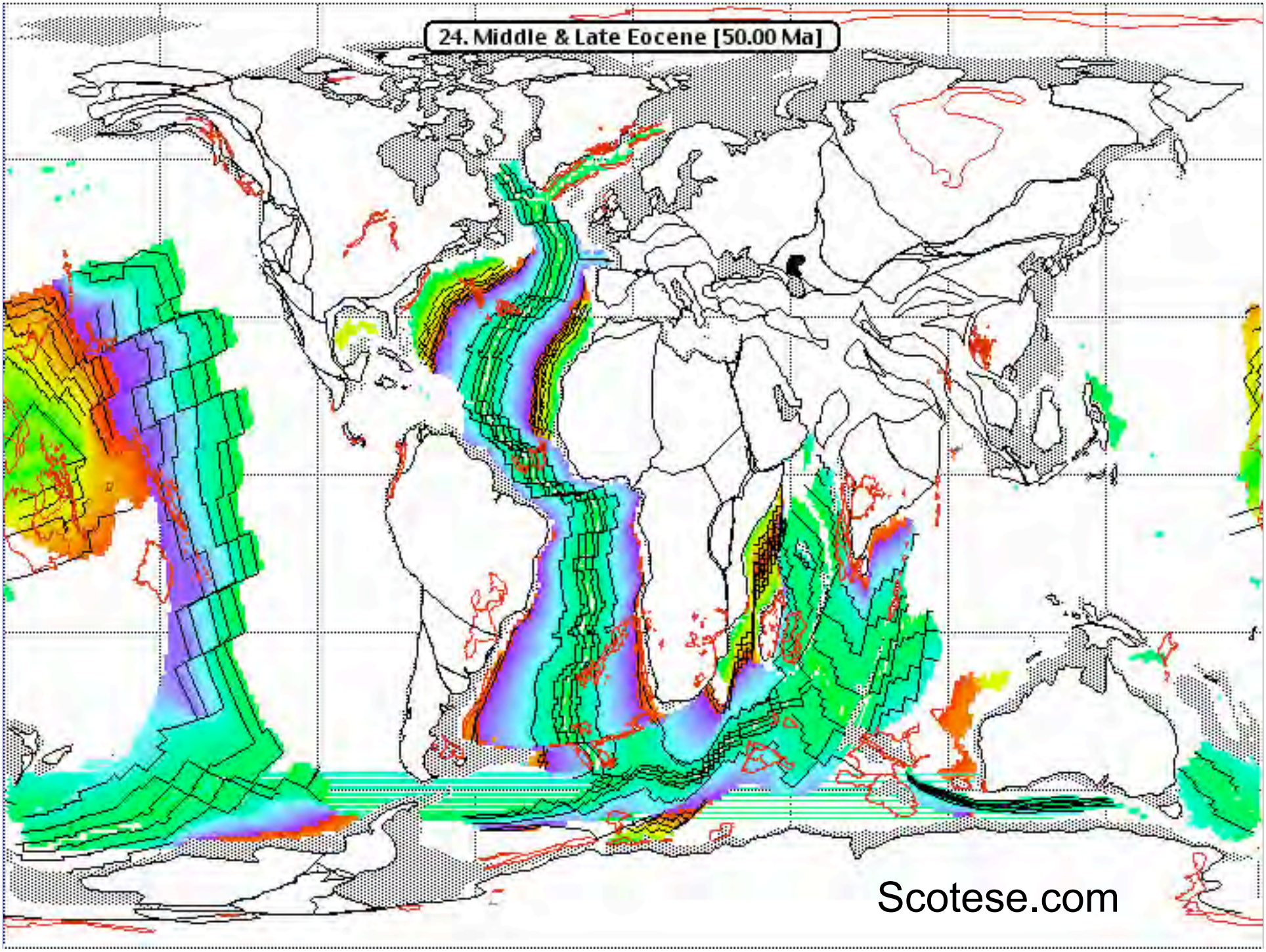
24. Middle & Late Eocene [50.00 Ma]
Scotese.com

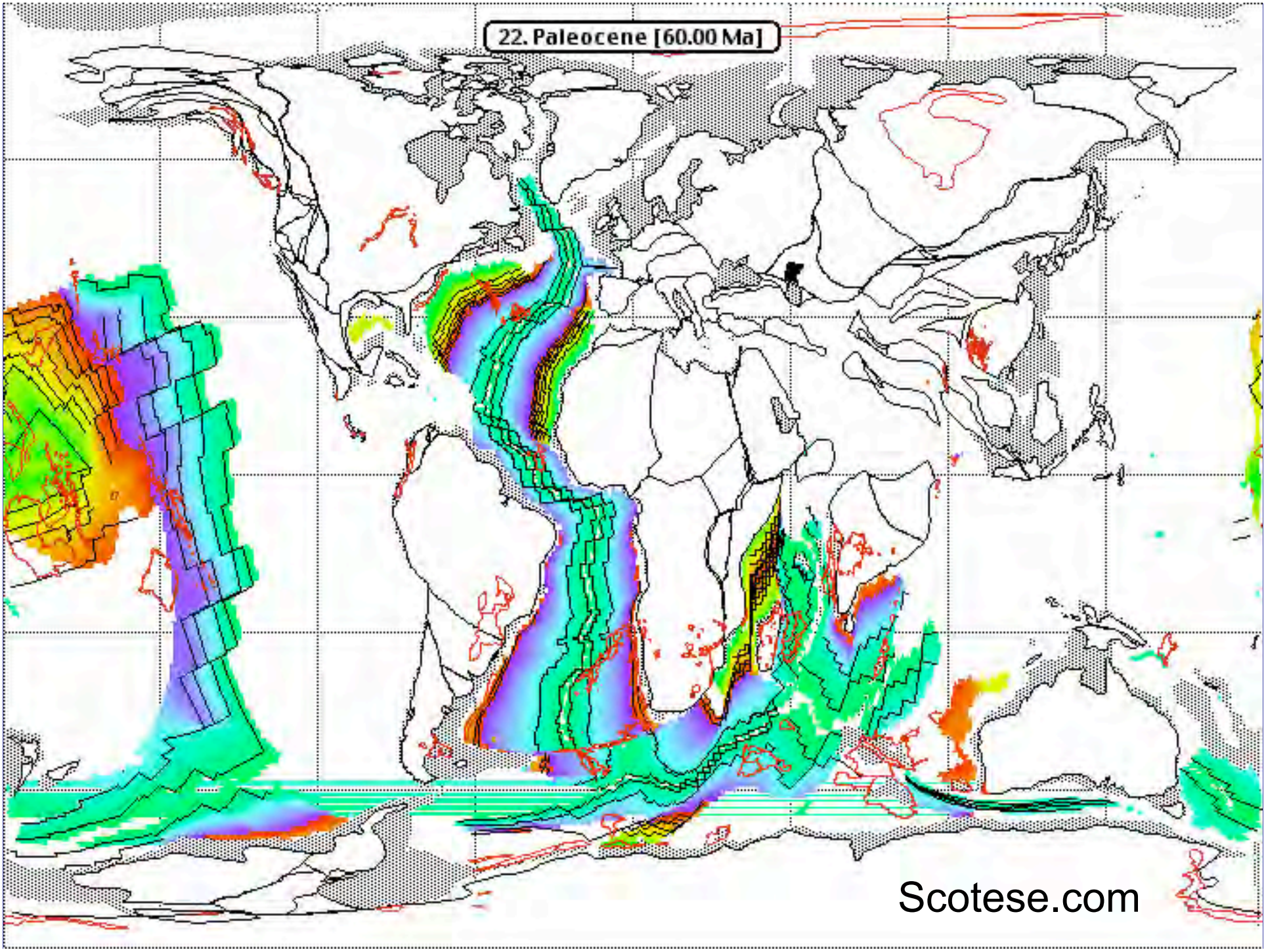
22. Paleocene [60.00 Ma]
Scotese.com

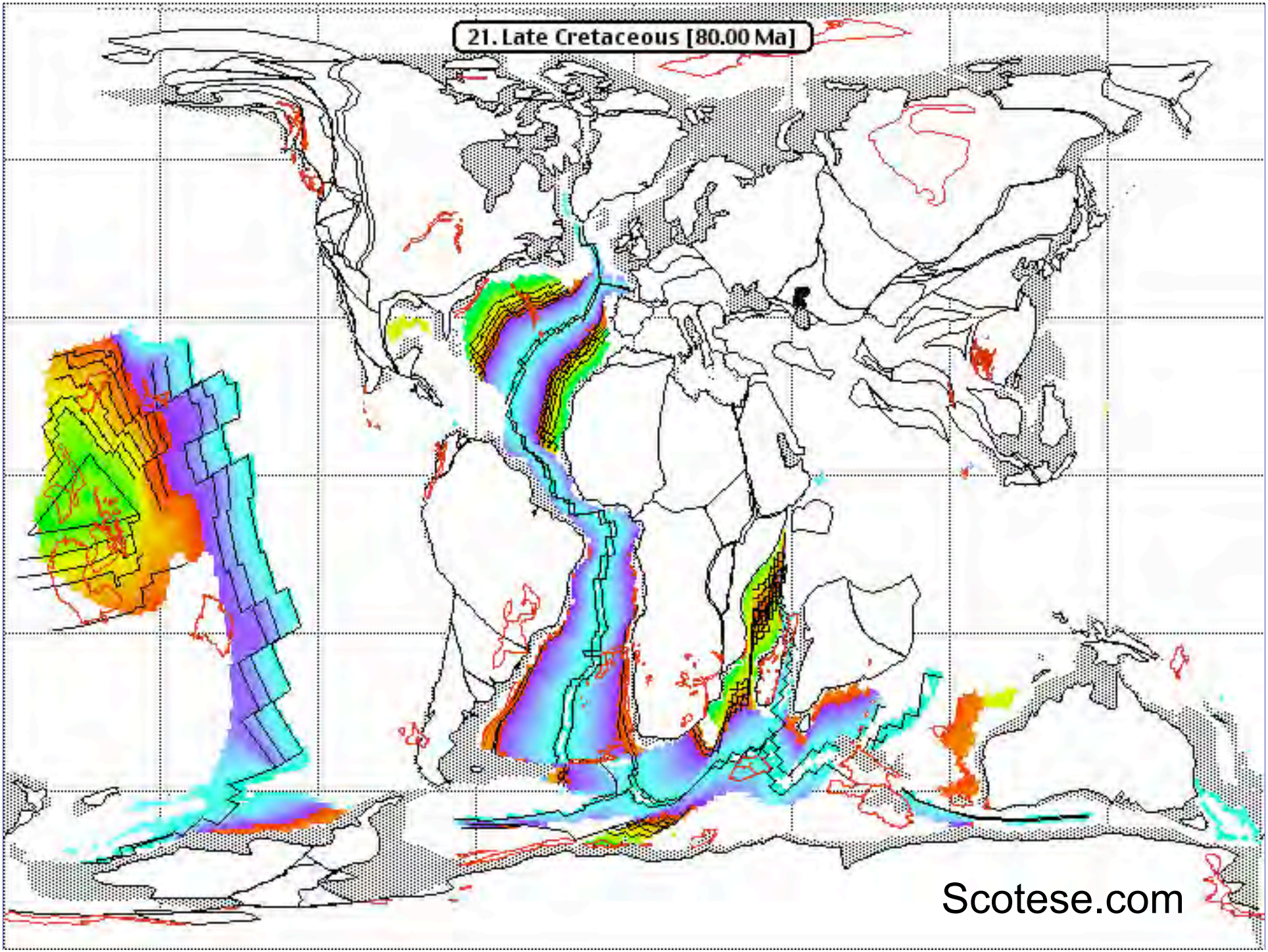
21. Late Cretaceous [80.00 Ma]
Scotese.com

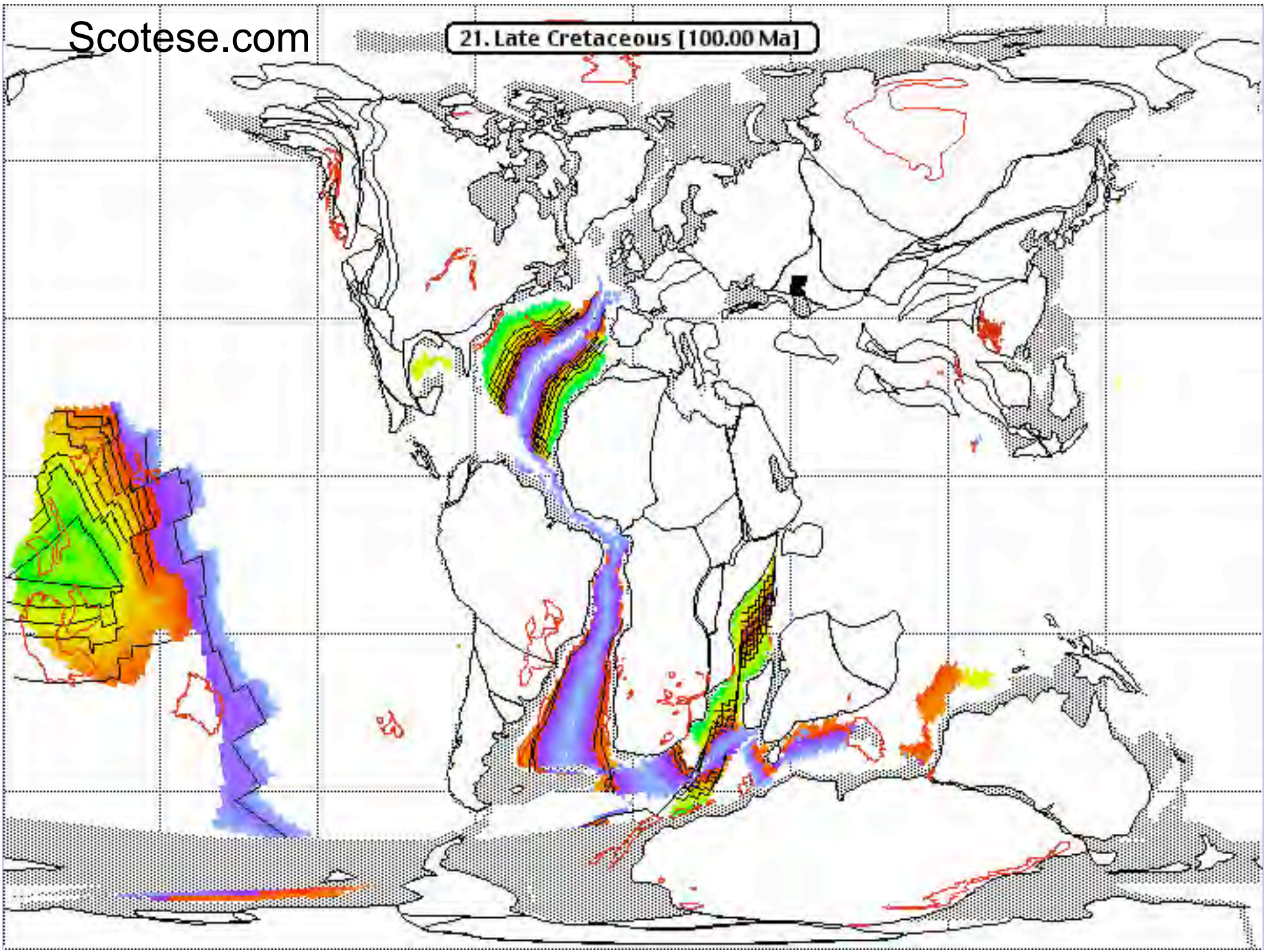
Scotese.com
21. Late Cretaceous [100.00 Ma]

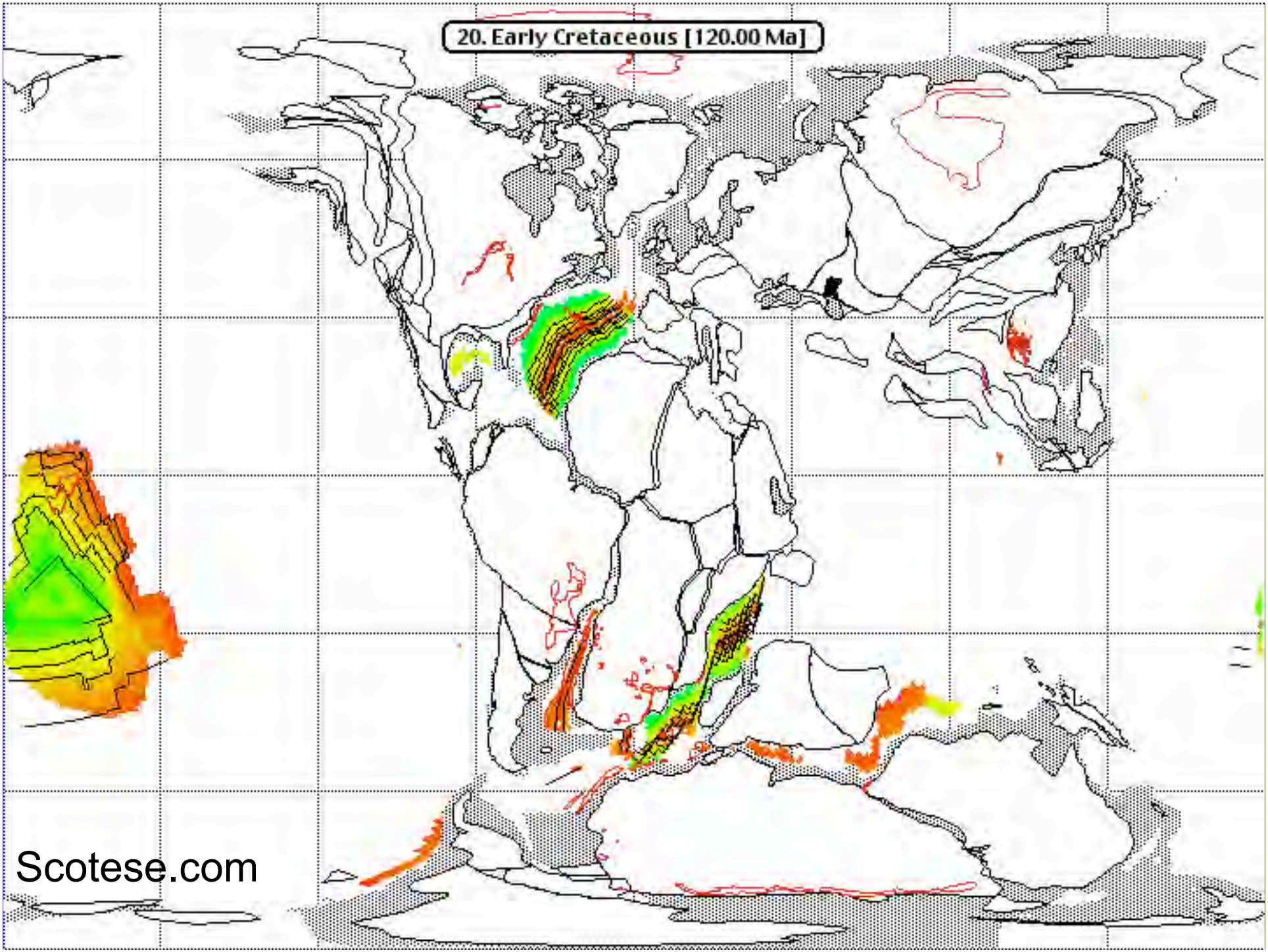
20. Early Cretaceous [120.00 Ma]
Scotese.com

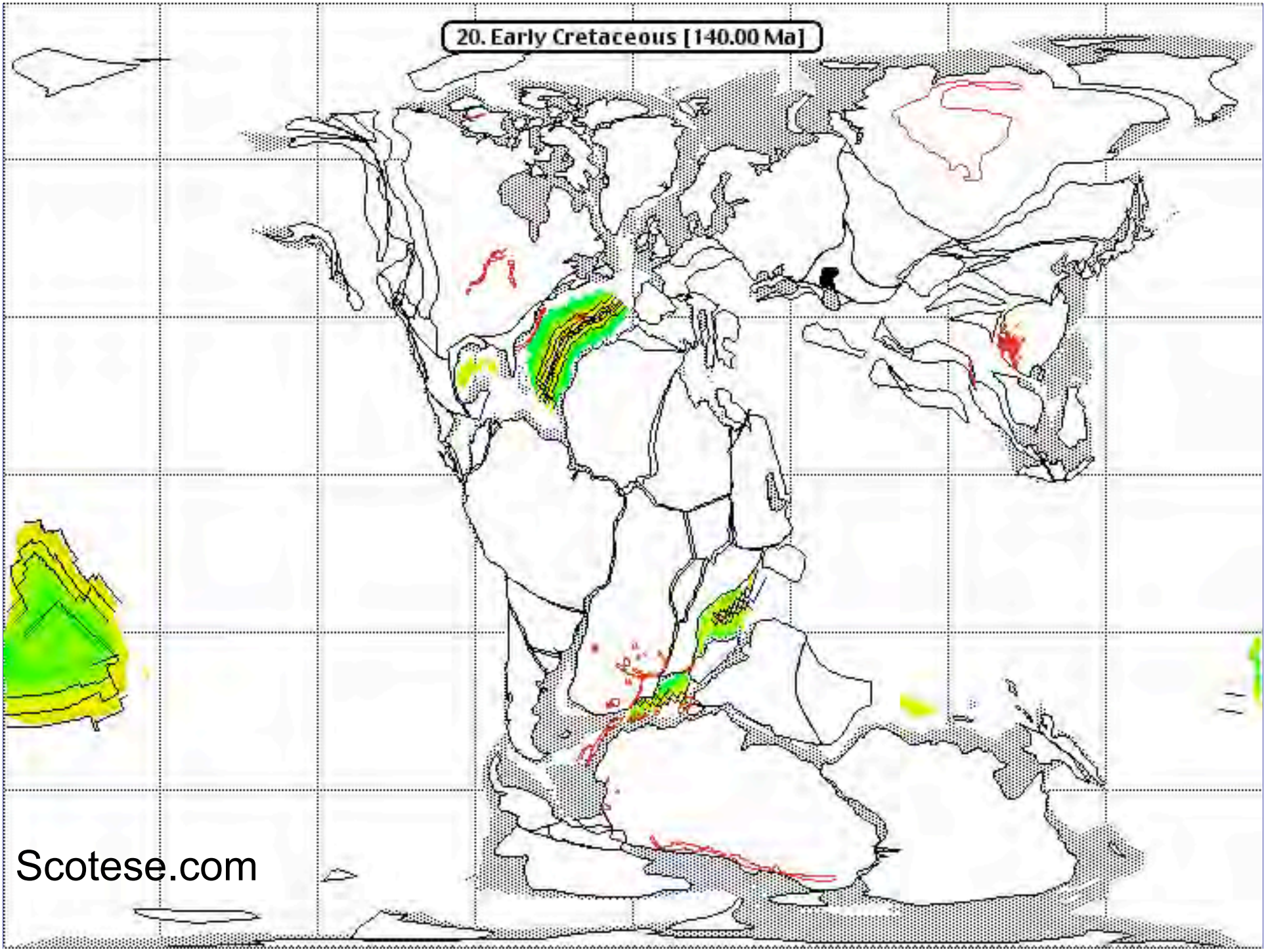
20. Early Cretaceous [140.00 Ma]
Scotese.com

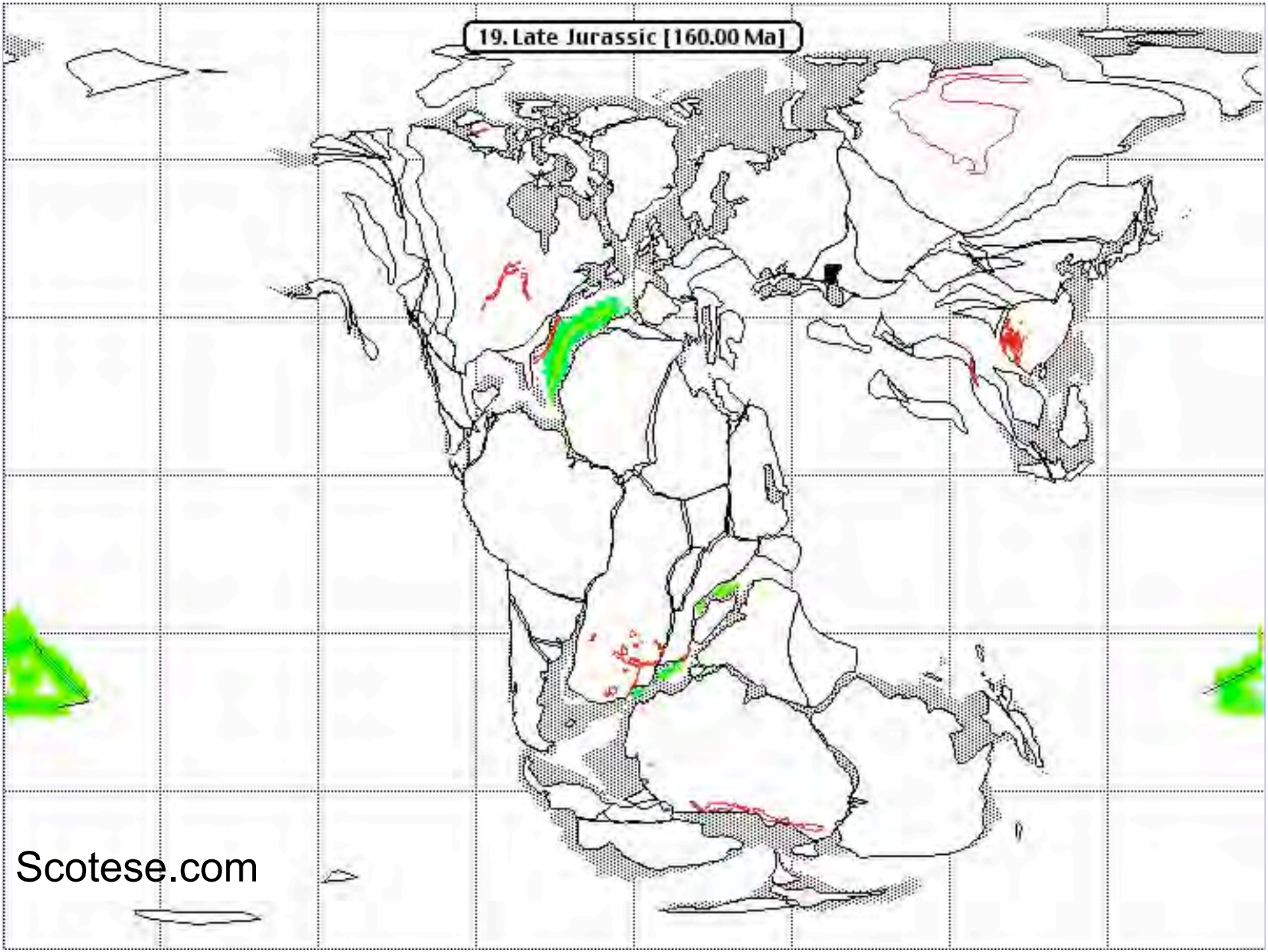
19. Late Jurassic [160.00 Ma]
Scotese.com

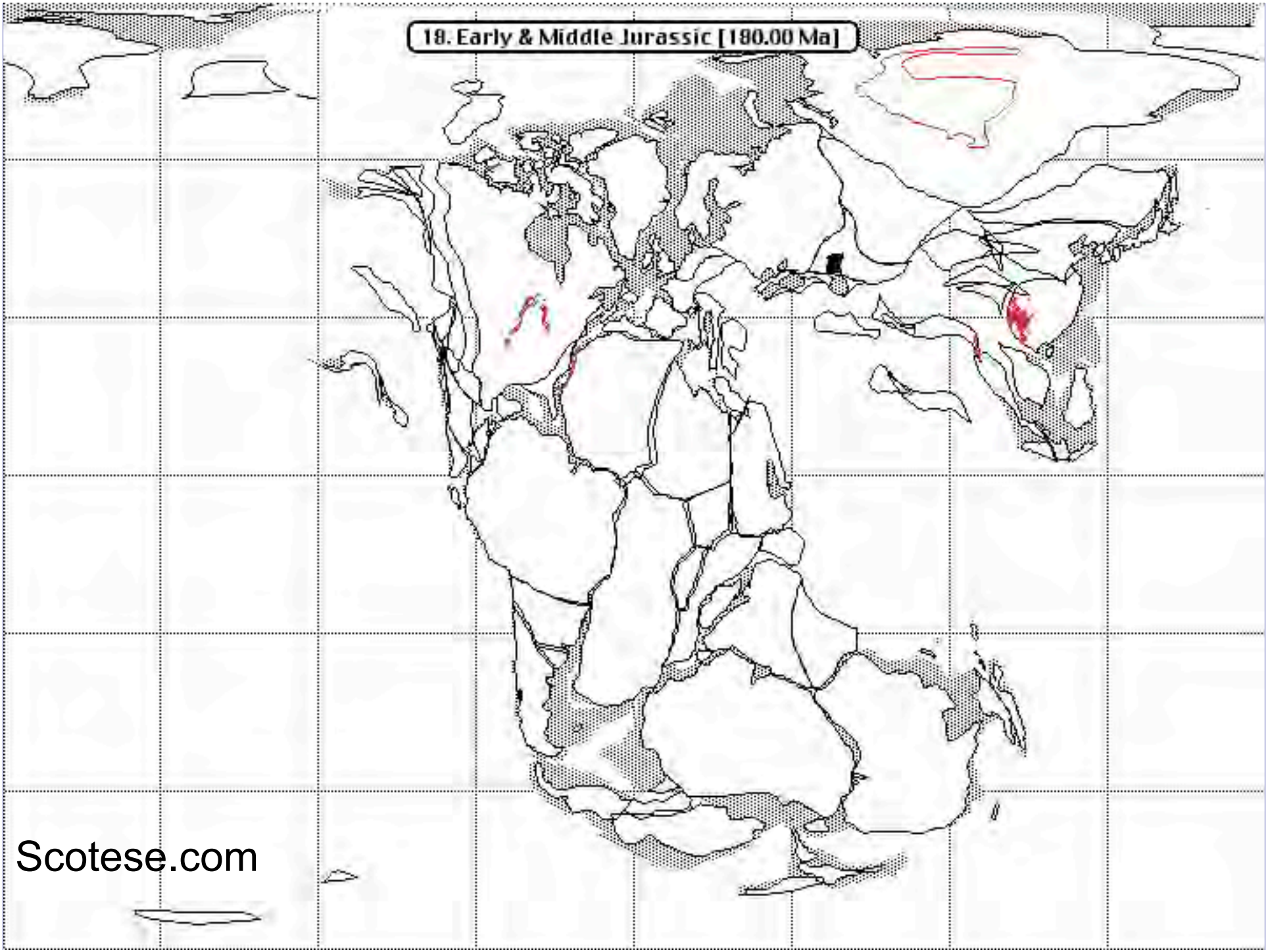
18. Early & Middle Jurassic [180.00 Ma]
Scotese.com

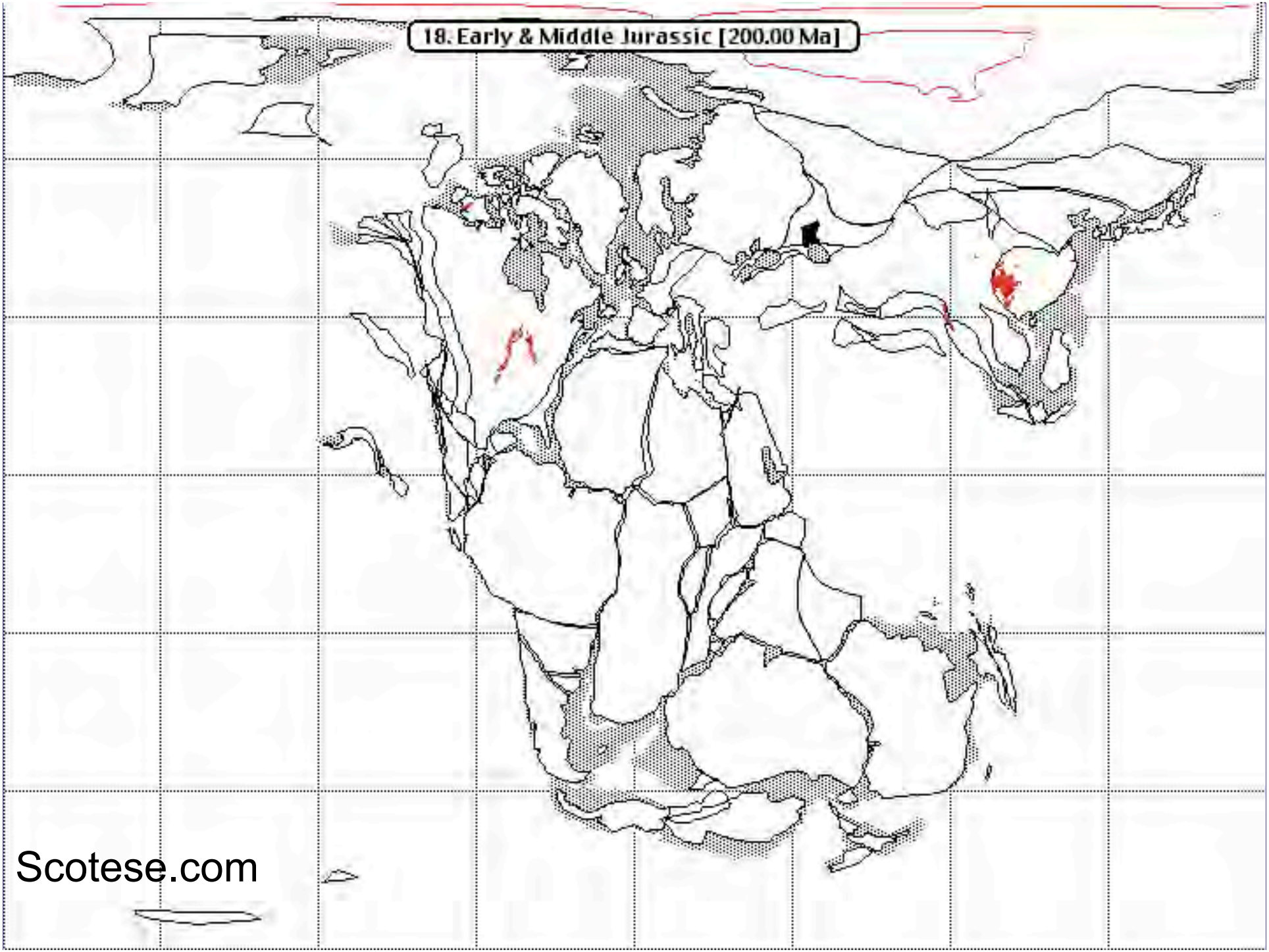
18. Early & Middle Jurassic [200.00 Ma]
Scotese.com

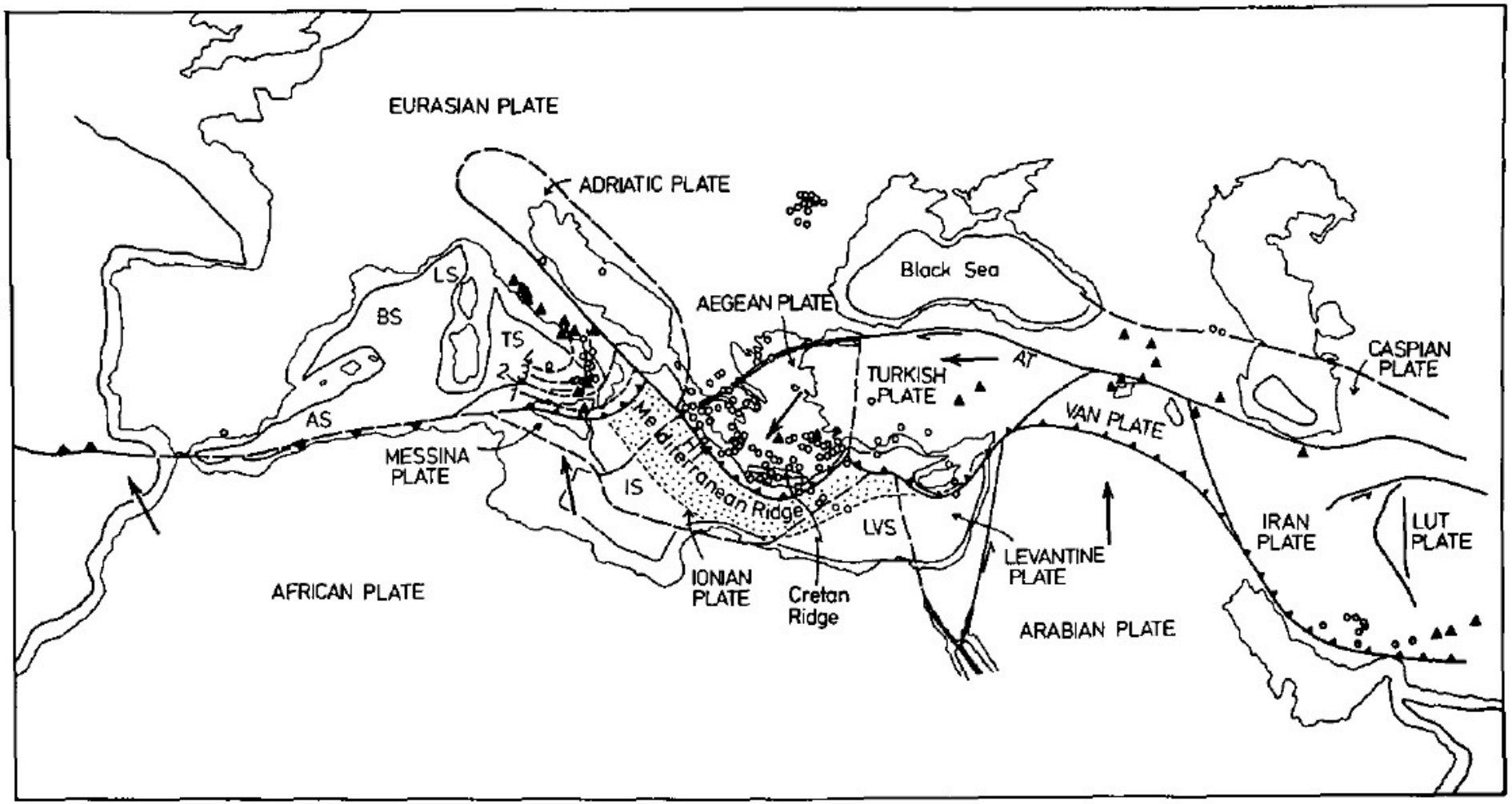

Figure 1. Neotectonics of the Alpine System. Plate boundary symbols as in Figure 9. Based mainly on Bogdanoff and others (1964), Choubert (1968), Stöcklin (1968), McKenzie (1970), and Ryan and others (1971). Key to symbols: triangles = Quaternary and Holocene volcanoes; circles = epicenters of earthquakes deeper than 100 km; arrows = slip directions of plates with respect to the Eurasian plate; dashed lines = contours on Benioff zone in hundreds of kilometers. Key to abbreviations: AS = Alboran Sea; AT = Anatolian Transform; BS = Balearic Sea; HT = Hellenic Trench; IS = Ionian Sea; LS = Ligurian Sea; LVS = Levantine Sea; TS = Tyrrhenian Sea.

Dewey et al 1973

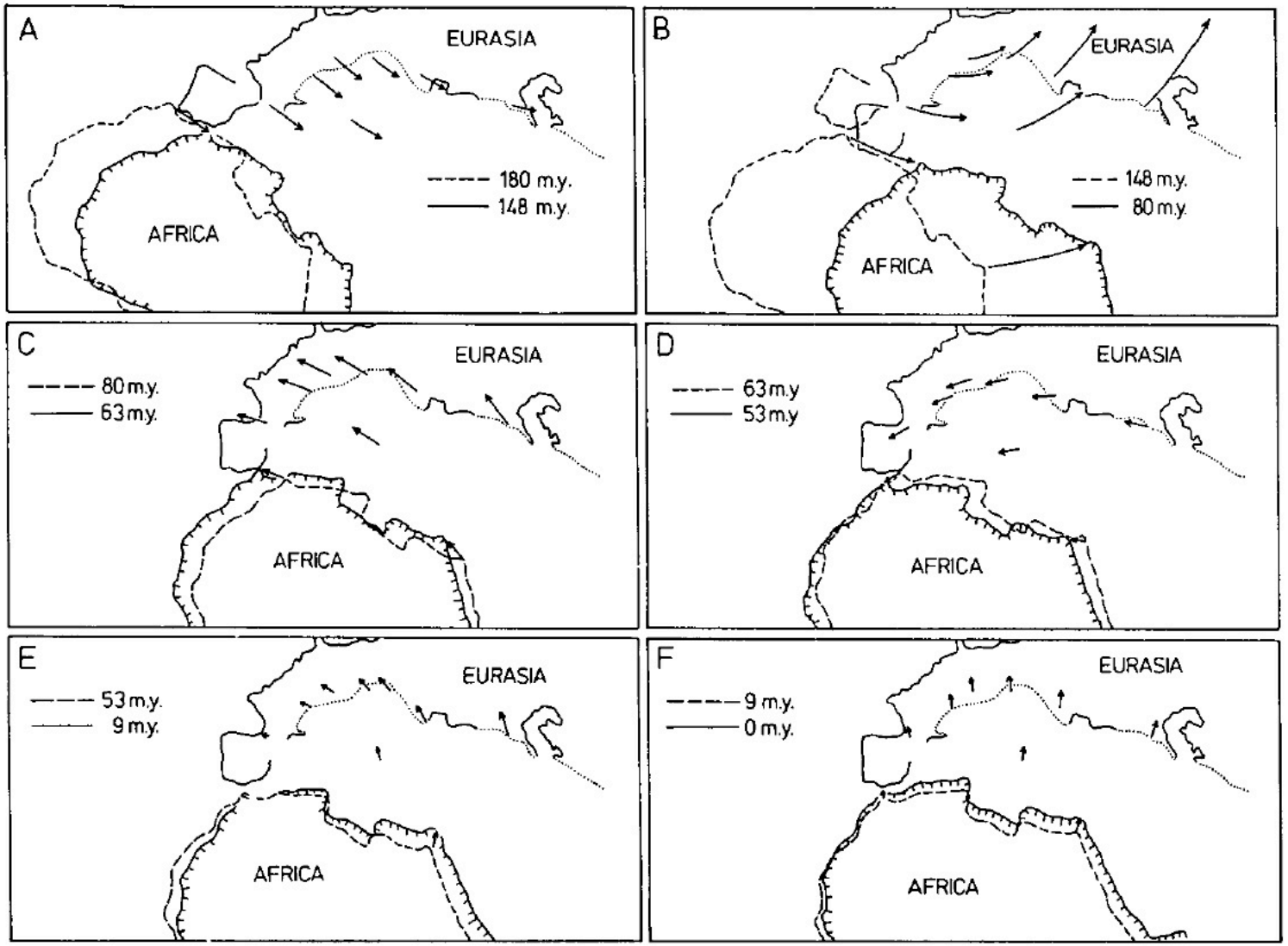

Figure 2. Successive positions of Africa relative to Europe at 180 m.y., 148 m.y., 80 m.y., 63 m.y., 53 m.y., 9 m.y., and present. In A through F, the dashed and hachured lines are the outline of Africa (taken as present-day shoreline) before and after, respectively, the six successive finite rotations θAE(180-148), θAE(148-80), and so on, given in Table 1. The arrows are finite slip vectors that represent the simplest path that Africa could have taken to move from its position, relative to Europe, at 180 m.y. to successive positions at 148 m.y., 80 m.y., and so on. In other words, the arrows show the simplest relative-motion paths for successive intervals and are segments of rotation circles around the successive θAE poles of Table 1.

Dewey et al 1973

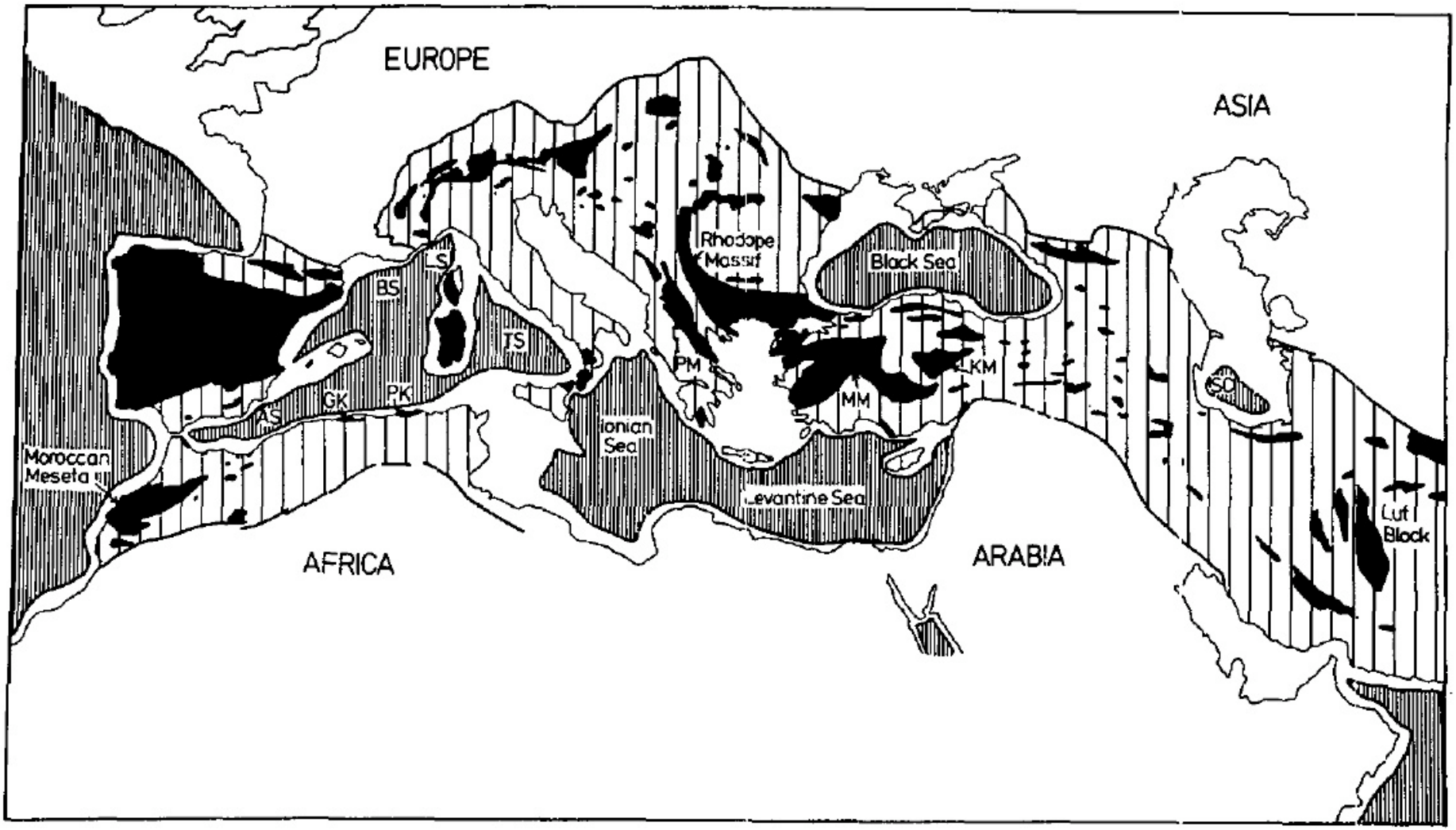

Figure 4. Distribution of pre-Alpine continental basement (black) and present oceans (narrowly spaced vertical lines) within the Alpine System (widely spaced vertical lines). Based mainly on Bogdanoff and others (1964), Choubert (1968), and Stöcklin (1968). Key to abbreviations: AS = Alboran Sea; BS = Balearic Sea; GK = Grand Kabylie; KM = Kirsehir Massif; LS = Ligurian Sea; MM = Menderes Massif; PK = Petit Kabylie; PM = Pelagonian Massif; SC = South Caspian Basin; TS = Tyrrhenian Sea.

Dewey et al 1973

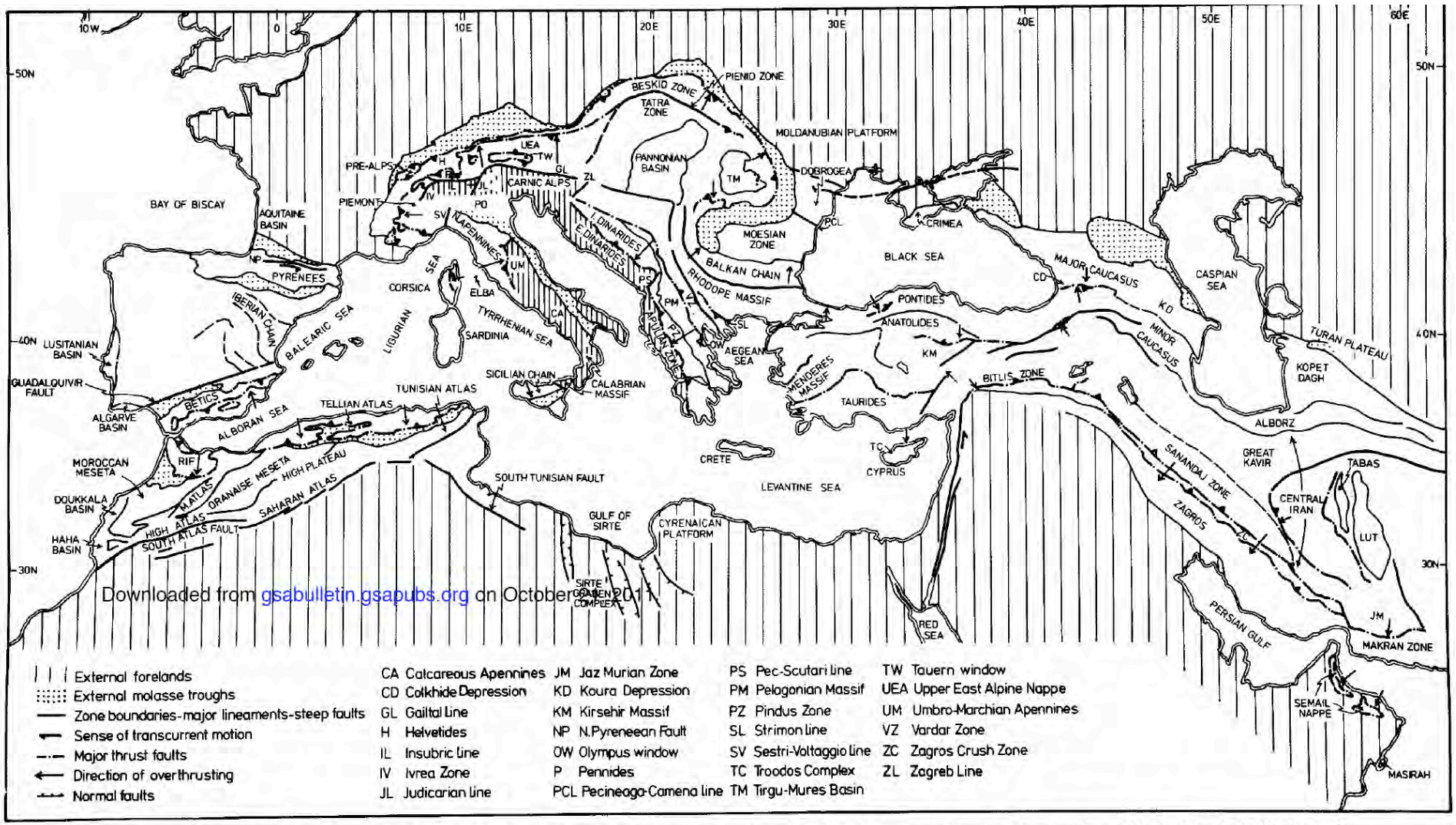

Figure 3. Schematic tectonic outline of the Alpine System of Europe, North Africa, and the Middle East in Transverse Mercator Projection, showing the zones and structures referred to in the text. Based mainly on Bogdanoff and others (1964), Choubert (1968), and Stöcklin (1968).

Dewey et al 1973

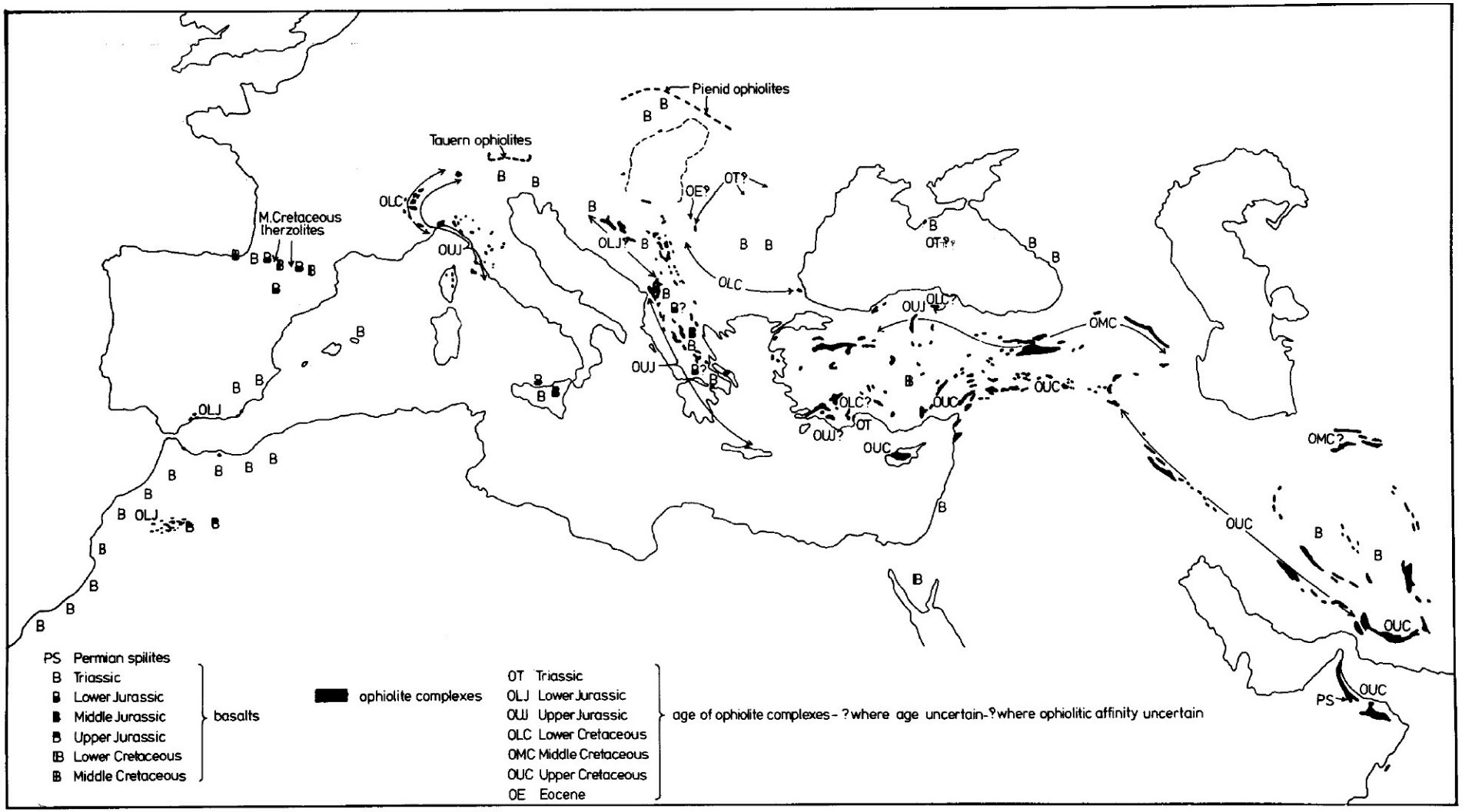

Figure 5. Distribution and age of origin of the ophiolite suite and basalts in the Alpine System. Based on Almela and Rios (1962), Andrusov (1963), Aubouin (1965), Aubouin and others (1963), Bailey and McCallien (1953), Belostotkiy and Kolbantsev (1969), Bezzi and Piccardo (1971), Blumenthal (1963), Bogdanoff and others (1964), Bousquet (1962), Brunn (1960, 1961), Brunn and others (1971), Choubert (1968), Choubert and Faure-Muret (1962), Ciocardelli and Socolescu (1969), Ciric (1963), Debelmas and Lemoine (1964, 1970), Dercourt (1970), Dubar (1962), Dubertret (1953), Gansser (1959), Gass (1968), Görler and Reutter (1963), Grunau (1965), Jenkyns (1970d), Ketin (1964), Khain and Milanovskii (1963), Ksiazkiewicz (1963), Milanovskii and Khain (1964a, 1964b), Moores (1969), Moores and Vine (1971), Moseley (1969), Mouratov (1964), Reinhardt (1969), Rigo de Righi and Cortesina (1964), Sander (1970), Steinmann (1926), Stöcklin (1968), Trümpy (1958), van der Kaaden (1963), and Wilson (1969).

Dewey et al 1973

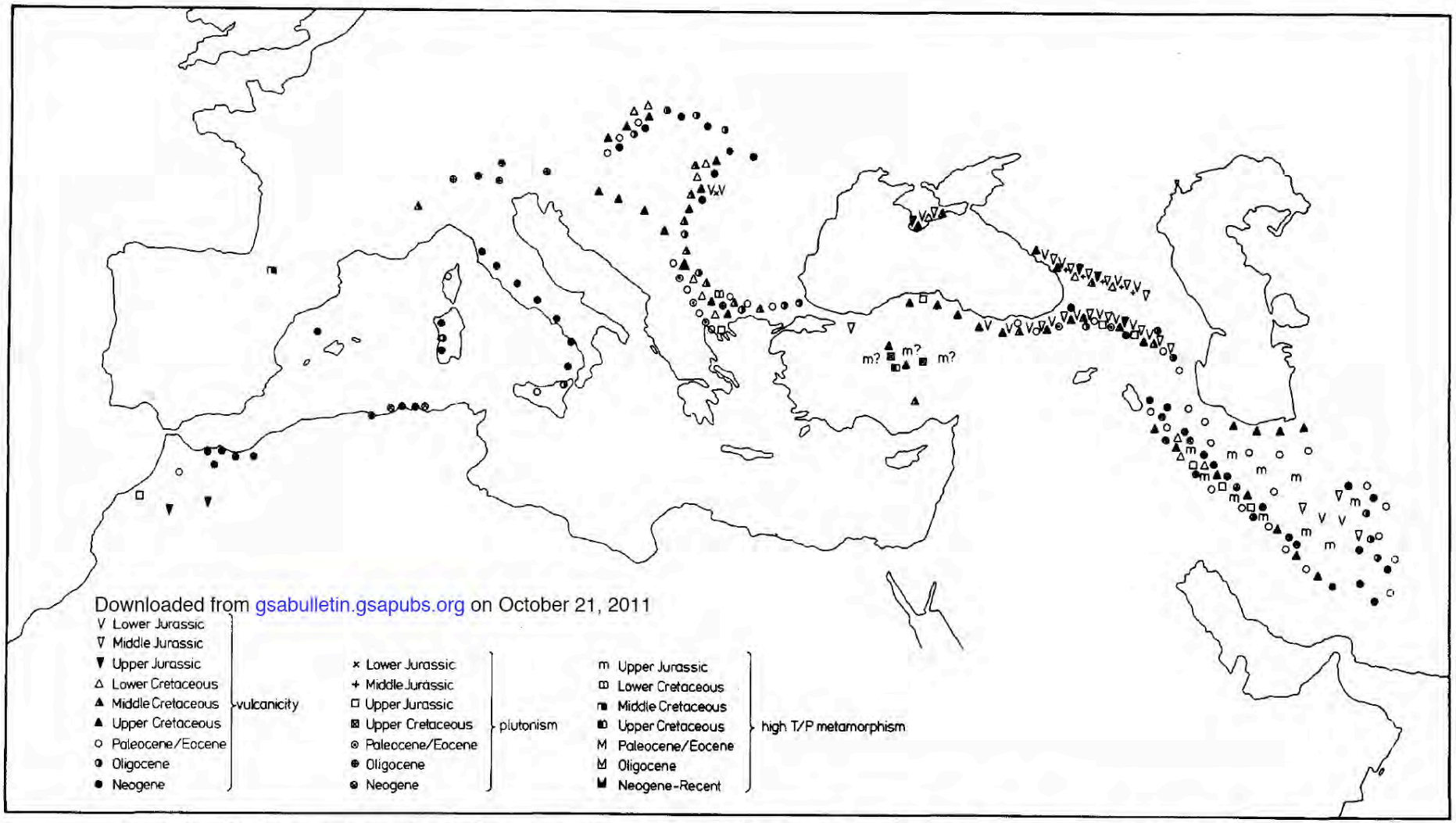

Figure 6. Distribution and age of volcanism, plutonism, and metamorphism believed to be related to past subduction in the Alpine System. Based on Andrusov (1963), Arkell (1956), Aubouin and others (1963), Bleahu and others (1967), Boccaletti and Guazzone (1971), Borsi and others (1966), Ciocardelli and Socolescu (1969), Ciric (1963), Debelmas and Lemoine (1964, 1970), de Sitter (1965), Dzotsenidze (1968), Faure-Muret (1964), Forgac and others (1968), Glangeaud (1956), Ivanov (1968), Khain (1964a, 1964b), Kieken (1962), Klemme (1958), Mercier (1966), Milanovskii and Khain (1964a, 1964b), Mouratov (1964), Sander (1970), Stöcklin (1968), Trümpy (1960), and Zwart (1967).

Dewey et al 1973

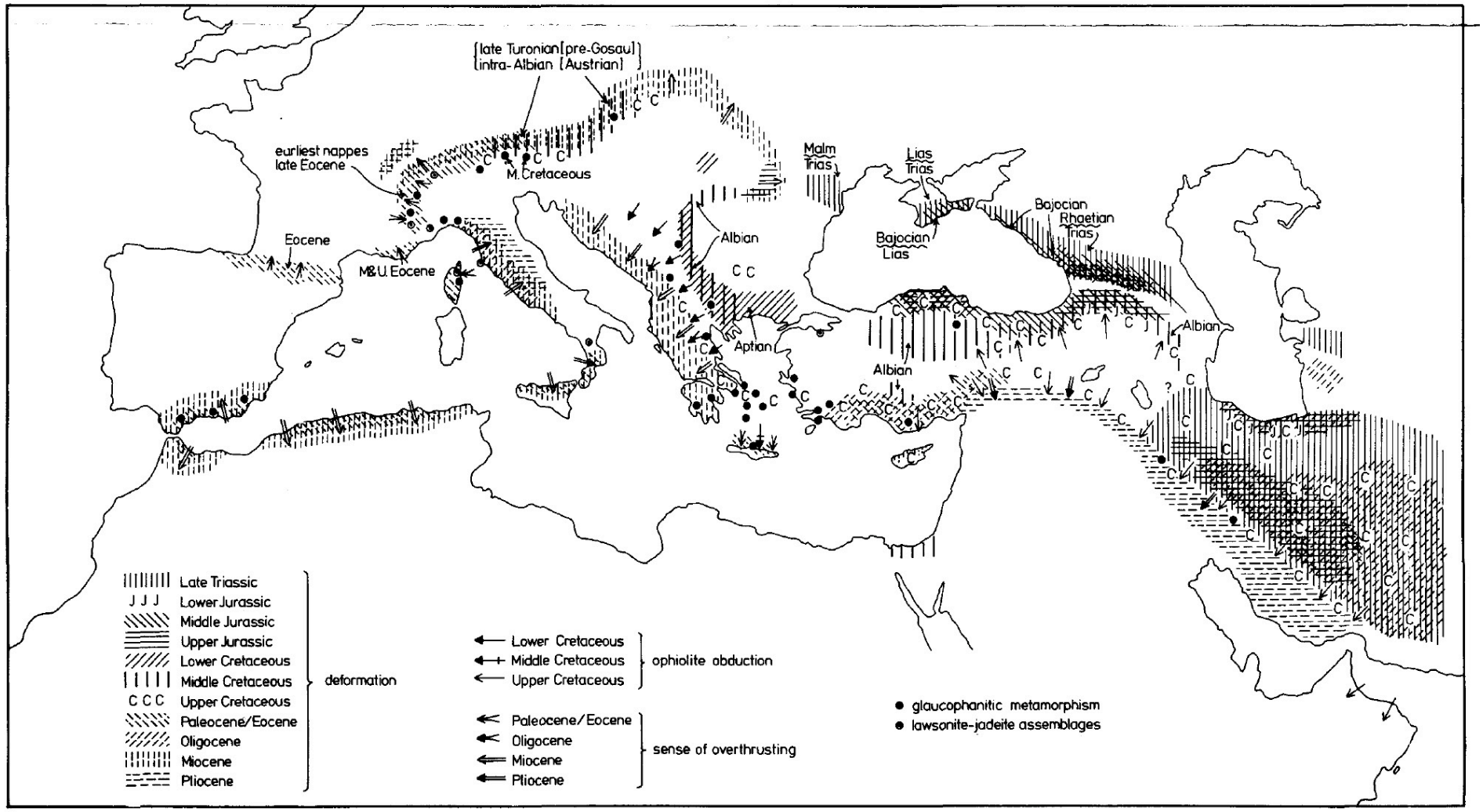

Figure 7. Distribution and age of deformation, ophiolite obduction, and high-pressure metamorphism in the Alpine System. Based upon Almela and Rios (1962), Andrieux and others (1971), Andrusov (1963), Arkell (1956), Aubouin (1965), Aubouin and others (1963), Aubouin and Mennesier (1963), Bancila (1968), Beloussov and Sorski (1962), Blanchet (1969), Blumenthal (1963), Bodechtel (1964), Brouwer (1963), Brunn (1960), Brunn and others (1971), Burollet (1967), Choubert and Faure-Muret (1962), Ciocardelli and Socolescu (1969), Ciric (1963), Debelmas and Lemoine (1964, 1970), de Sitter (1965). Faure-Muret (1964), Freund (1965), Godfriaux (1964), Hsü and Schlanger (1971), Ianchin (1964), Ketin (1964), Khain (1964a, 1964b), Khain and Milanovskii (1963, 1968), Kieken (1962), Ksiazkiewicz (1963), Lanteaume and others (1963), Mercier (1966) Migliorini (1948) Milanovskii and Khain (1964a, 1964b), Mouratov (1964), Oxburgh (1968), Paquet (1968), Ramsay (1963), Reinhardt (1969), Rigo de Righi and Cortesina (1964), Sander (1970), Scholle (1970), Stöcklin (1968), Tollman (1963), Trümpy (1960), Wezel (1970a), Wilson (1969), Youssef (1968), and Zwart (1967).

Dewey et al 1973

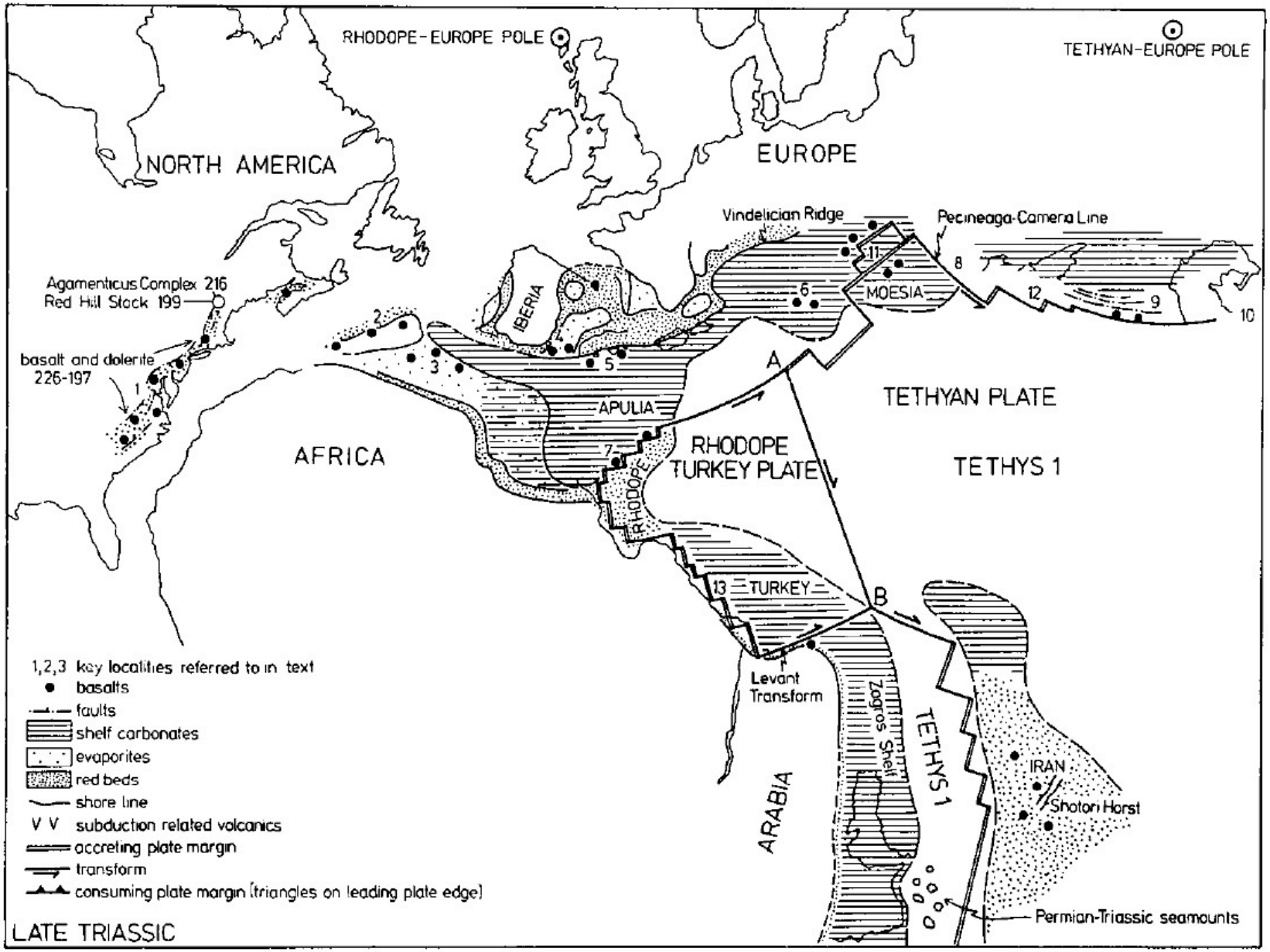

Figure 9. Proposed Late Triassic paleographic reconstruction and plate margins. Numbers indicate key position of data referred to in the text. Includes data from Armstrong and Besancon (1970), Armstrong and Stump (1971), Aubouin (1965), Burollet (1967), Choubert and Faure-Muret (1962), Khain and Milanovskii (1963), Sander (1970), Stöcklin (1968), Warrington (1970), and Wills (1970).

Dewey et al 1973

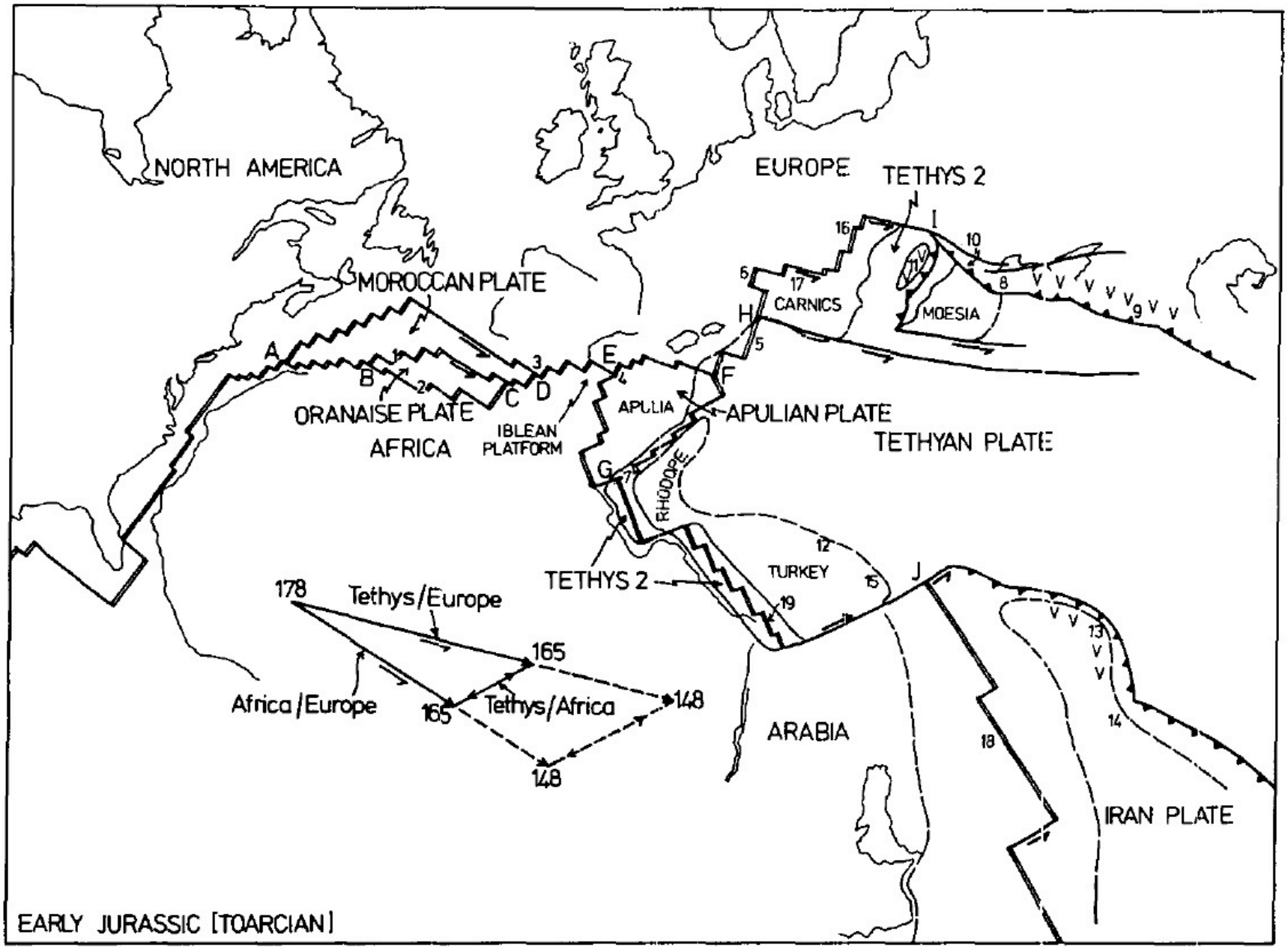

Figure 10. Proposed Toarcian plate-boundary scheme. Numbers indicate key data referred to in the text. Key to symbols in Figure 9.

Dewey et al 1973

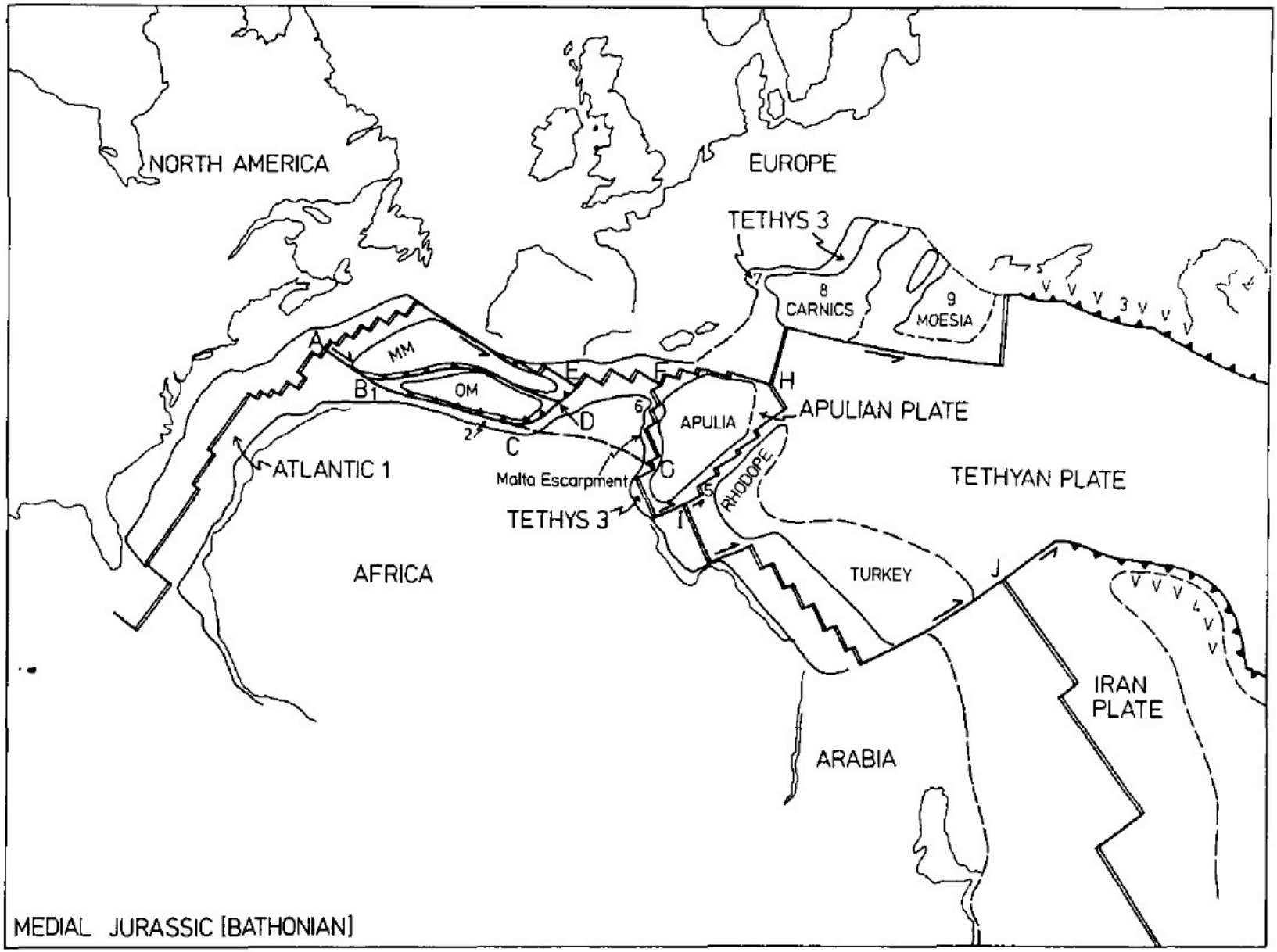

Figure 11. Proposed Bathonian plate-boundary scheme. Numbers indicate key data referred to in the text. Key to symbols in Figure 9. Abbreviations: MM = Moroccan Meseta, OM = Oran Meseta.

Dewey et al 1973

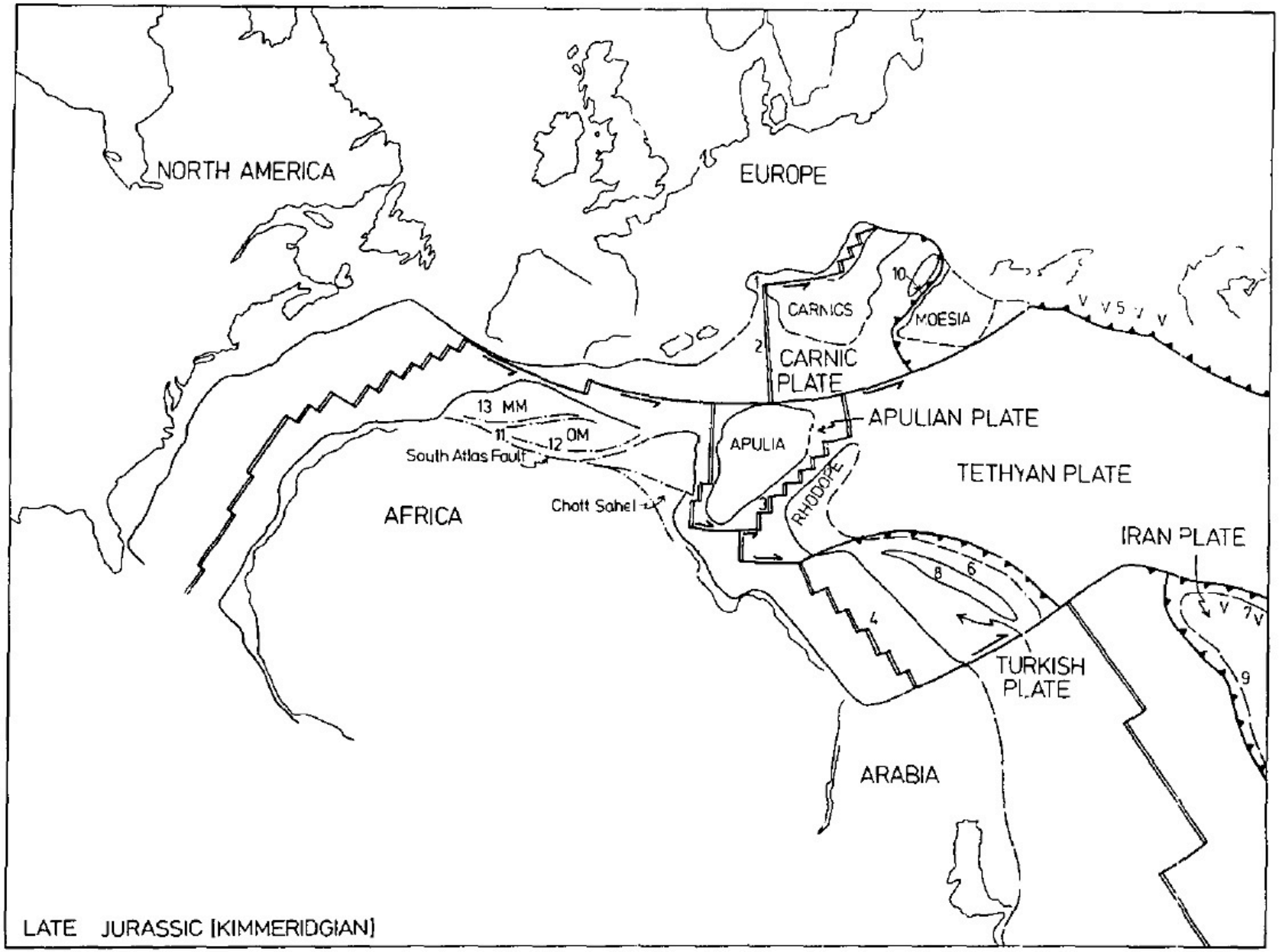

Figure 12. Proposed Kimmeridgian plate-boundary scheme. Numbers indicate key data referred to in the text. Key to symbols in Figure 9. Abbreviations: MM = Moroccan Meseta, OM = Oran Meseta.

Dewey et al 1973

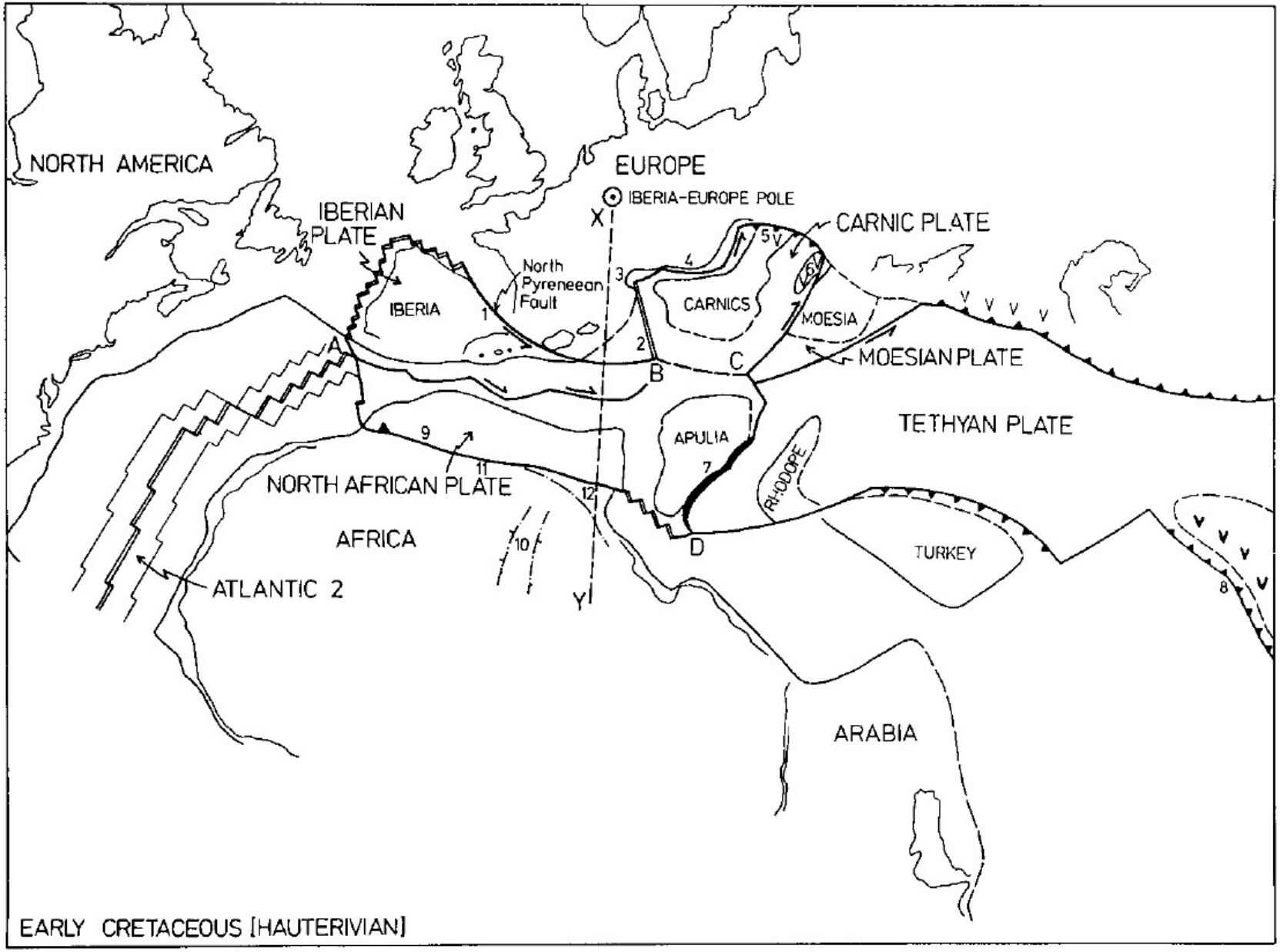

Figure 13. Proposed Hauterivian plate-boundary scheme. Numbers indicate key data referred to in the text. Key to symbols in Figure 9.

Dewey et al 1973

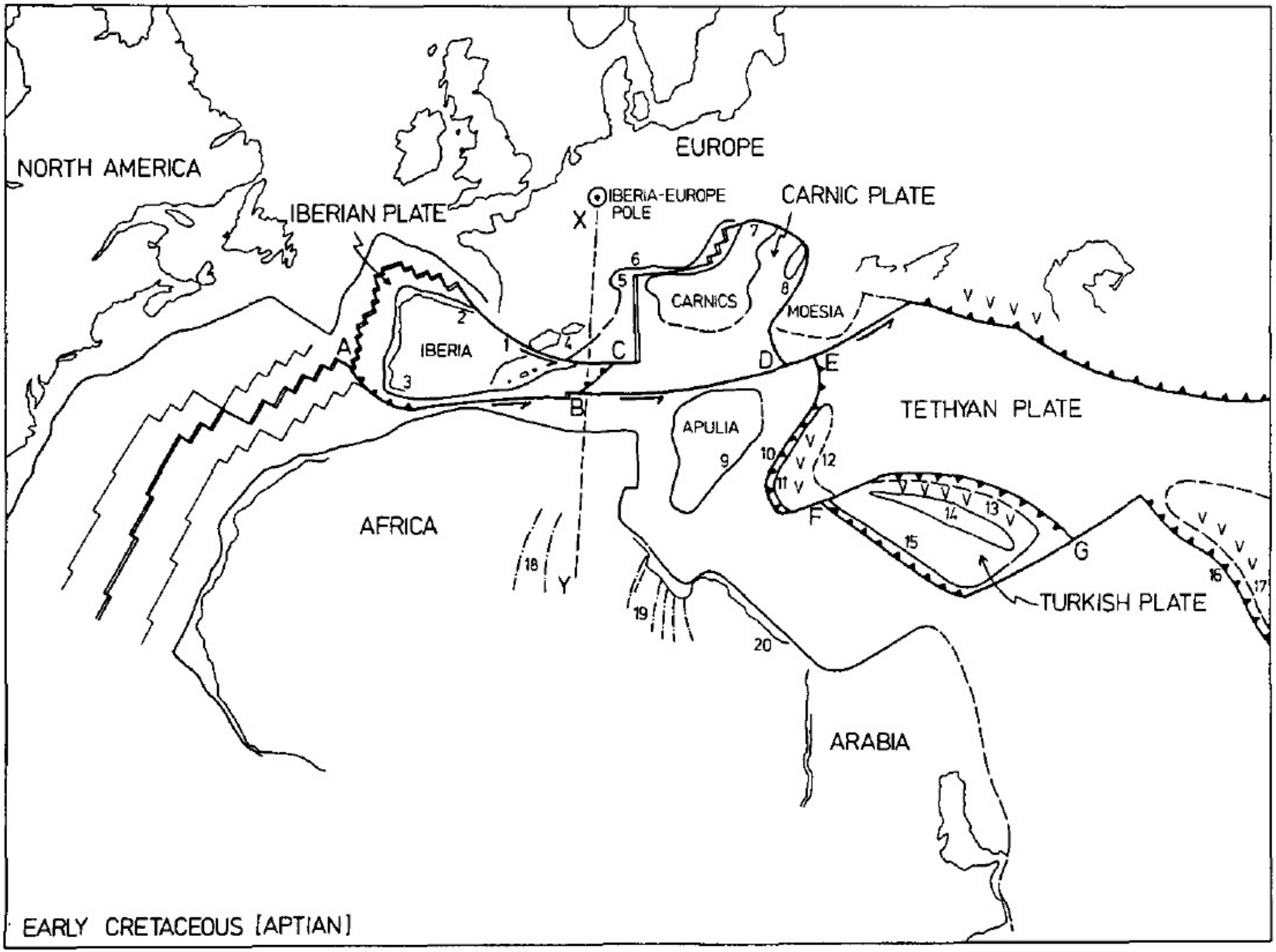

Figure 14. Proposed Aptian plate-boundary scheme. Numbers indicate key data referred to in the text. Key to symbols in Figure 9.

Dewey
et al 1973

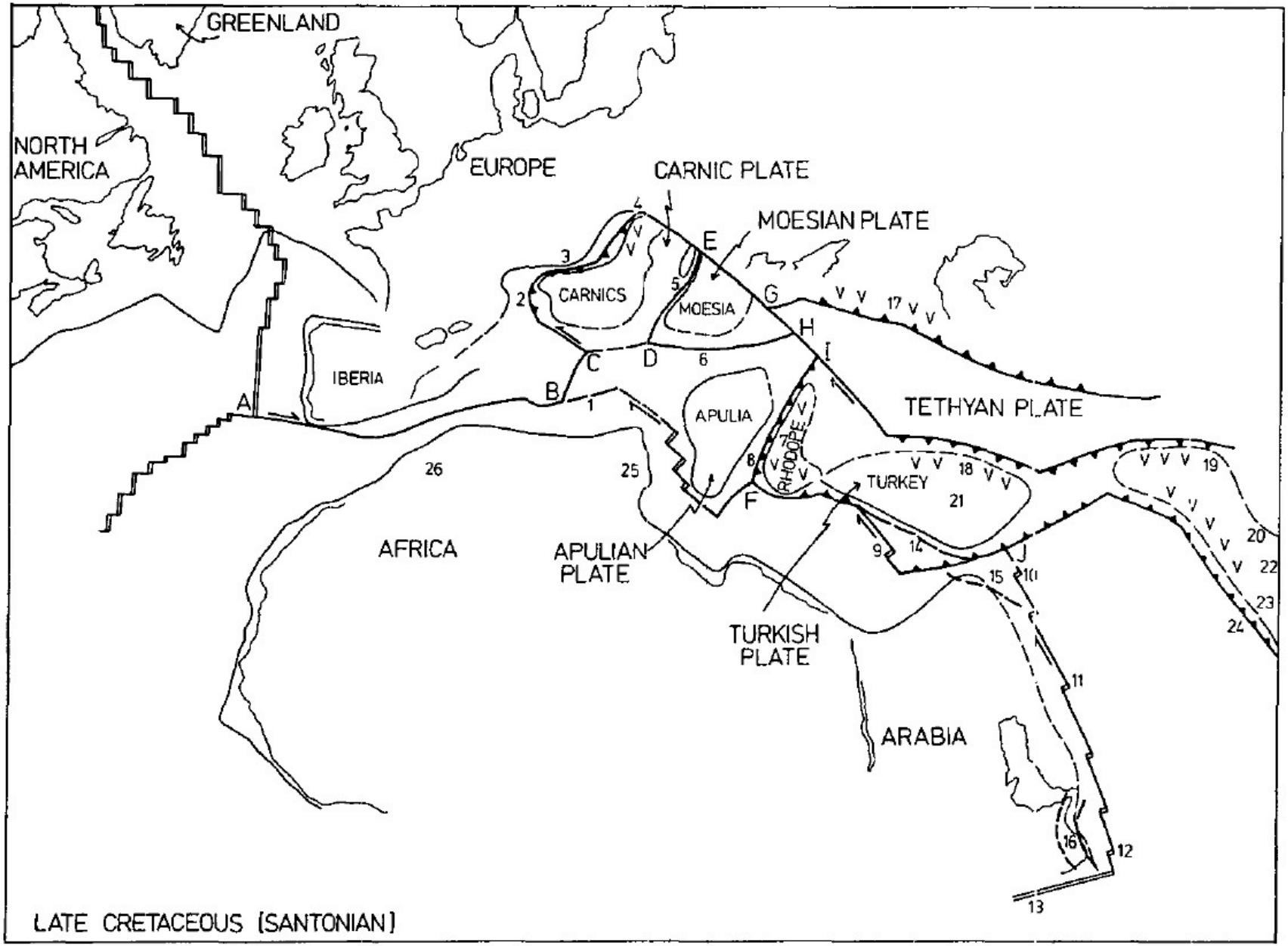

Figure 15. Proposed Santonian plate boundary. Numbers indicate key data referred to in the text. Key to symbols in Figure 9.

Dewey et al 1973

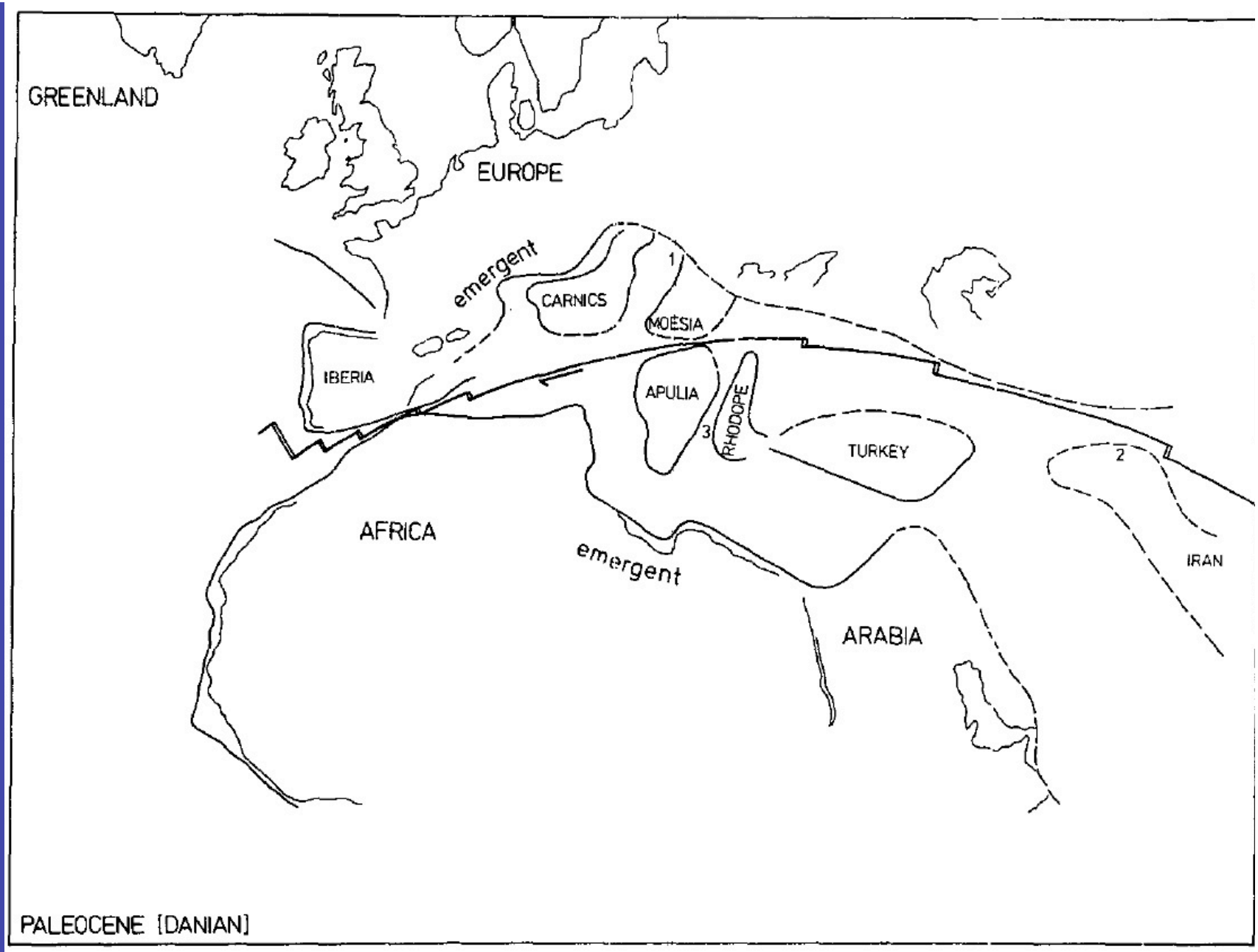

Figure 16. Proposed Danian plate boundary. Numbers indicate data referred to in the text. Key to symbol in Figure 9.

Dewey et al 1973

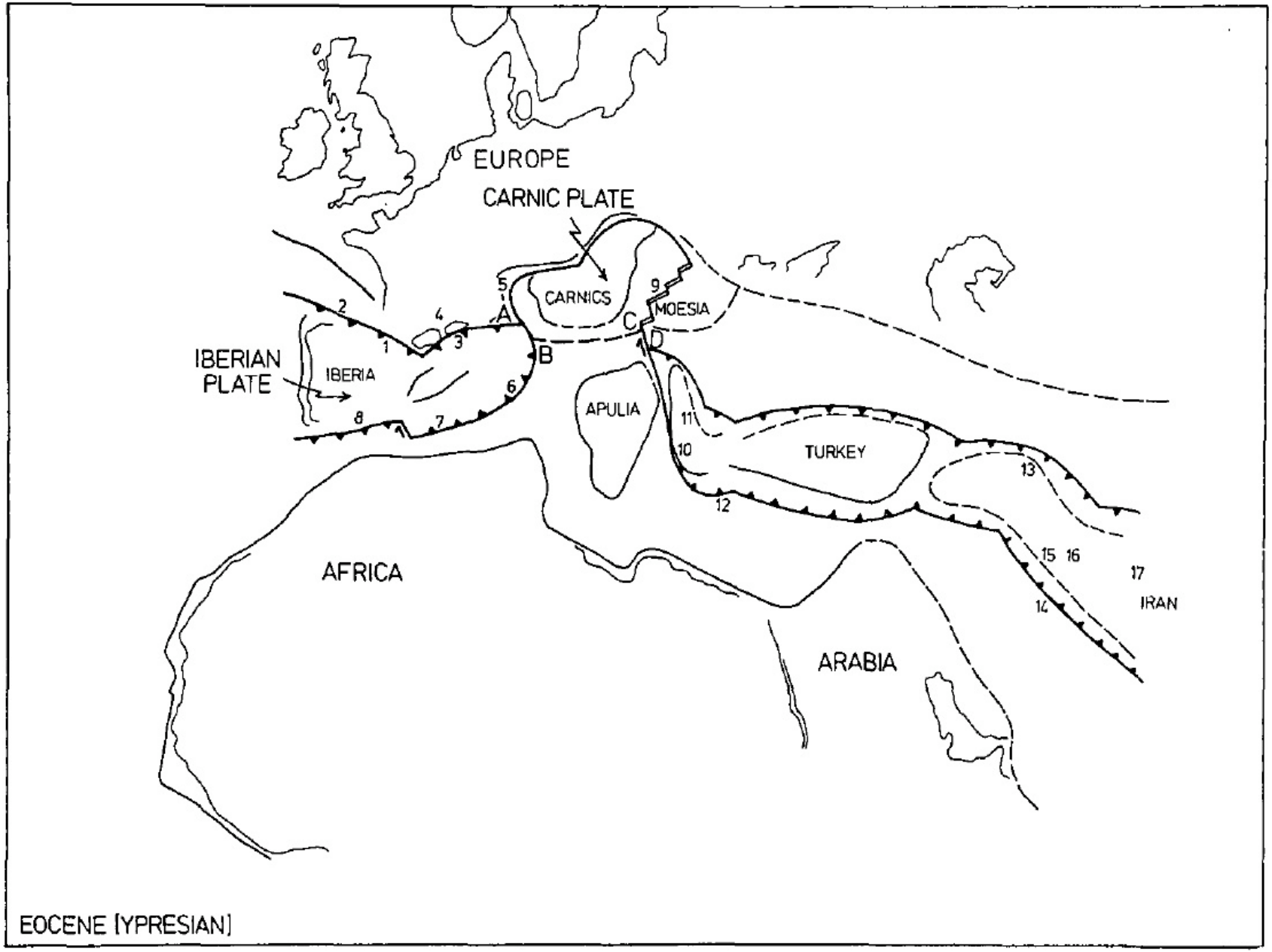

Figure 17. Proposed Ypresian plate-boundary scheme. Numbers indicate key data referred to in the text. Key to symbols in Figure 9.

Dewey et al 1973

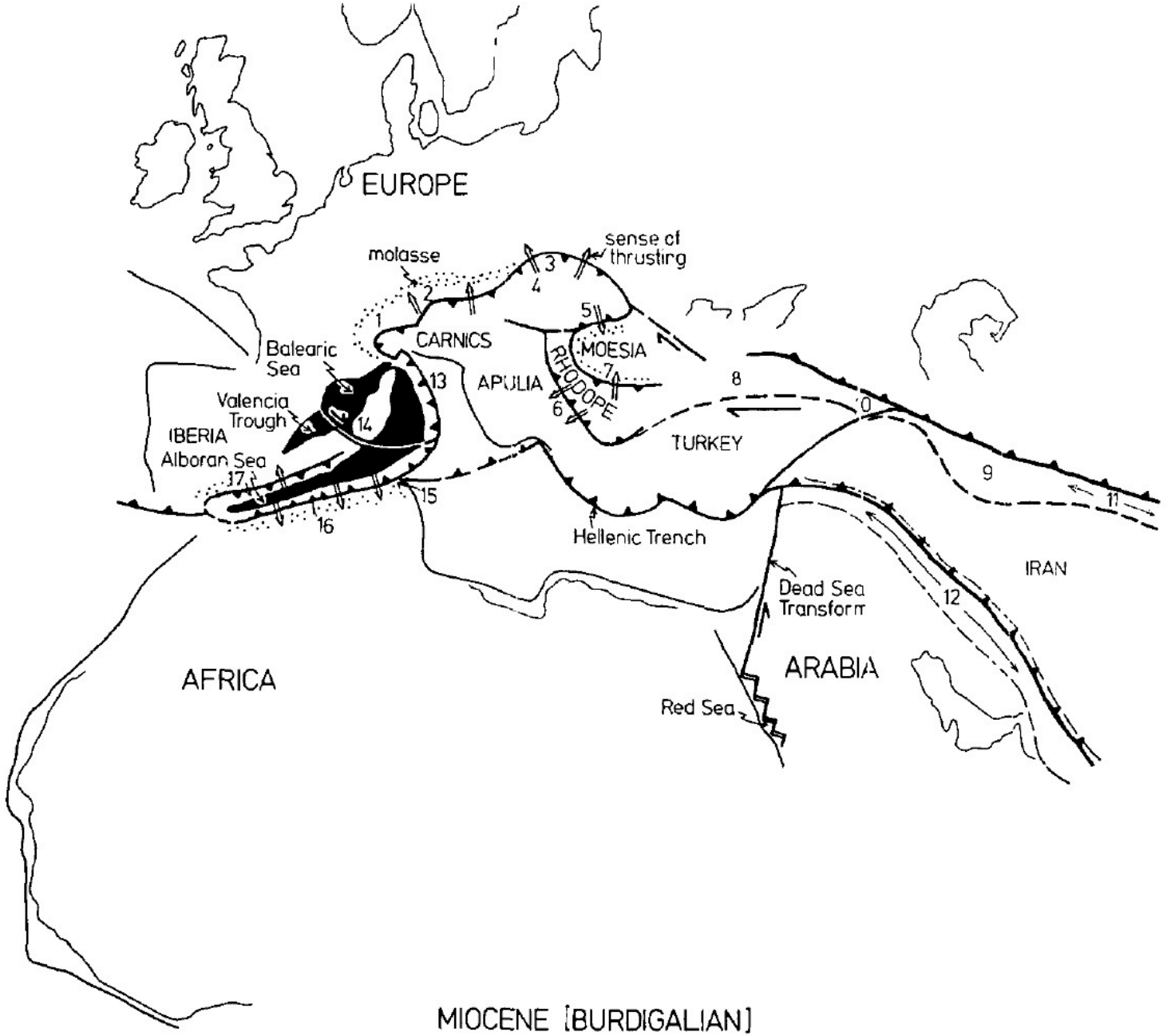

Figure 18. Proposed Burdigalian plate-boundary scheme. Numbers indicate key data referred to in the text. Key to symbols in Figure 9.

Dewey et al 1973

How might we improve on the work of Dewey, Pitman, Ryan, and Bonin?

- Improved knowledge of pre-Tethys paleogeography?
- Improved knowledge of Tethys rifted margin?
- Improved knowledge of Italian rotations?
- Improved knowledge of “Adriatic” or “Apulian” “plate”?
- Improved knowledge of the Dinaric belt?
- Something else?

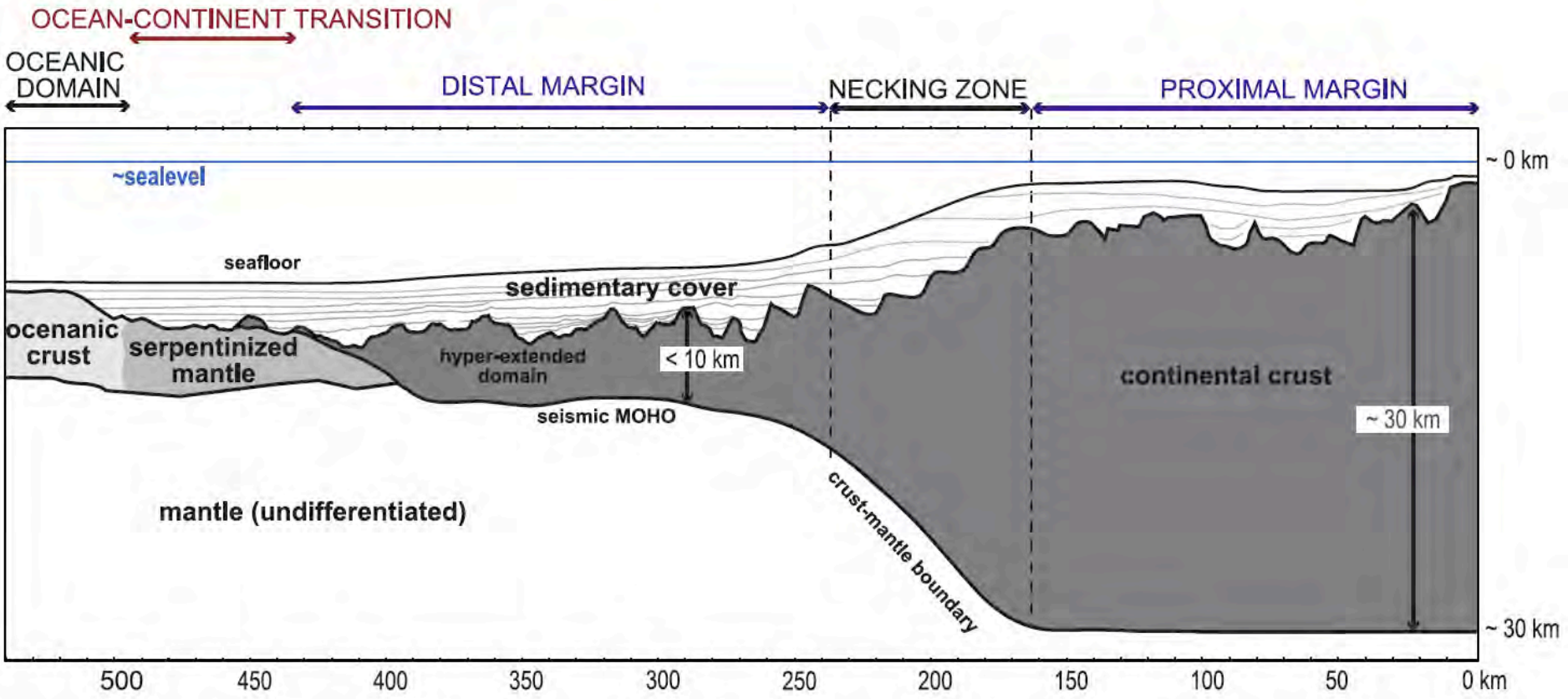

Figure 1. Idealized cross-section across a magma-poor rifted margin showing the different domains, crustal architecture and terminology used in this paper.

Mohn et al 2012

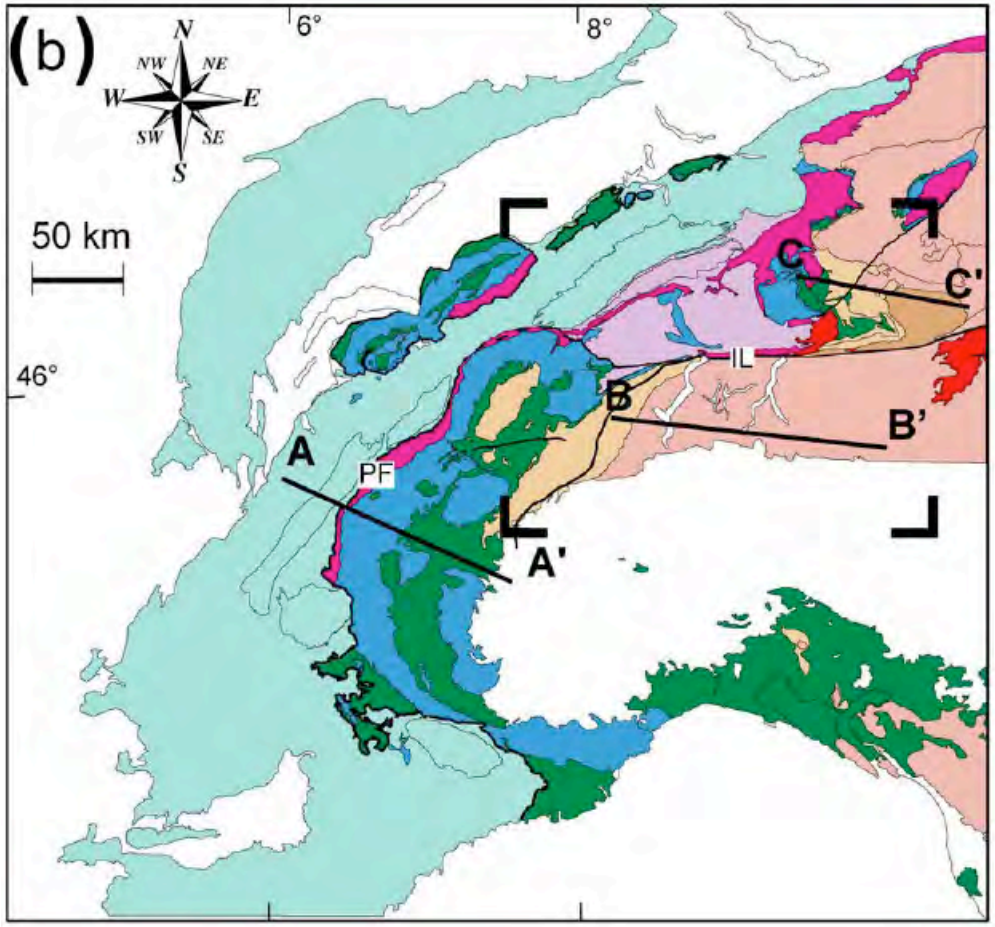

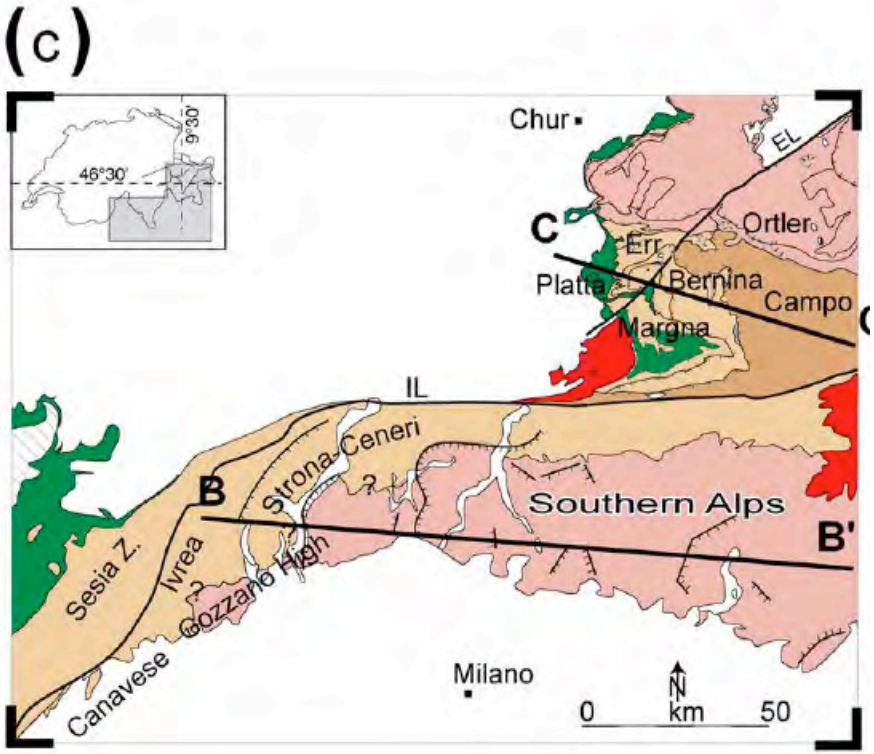

Mohn et al 2012

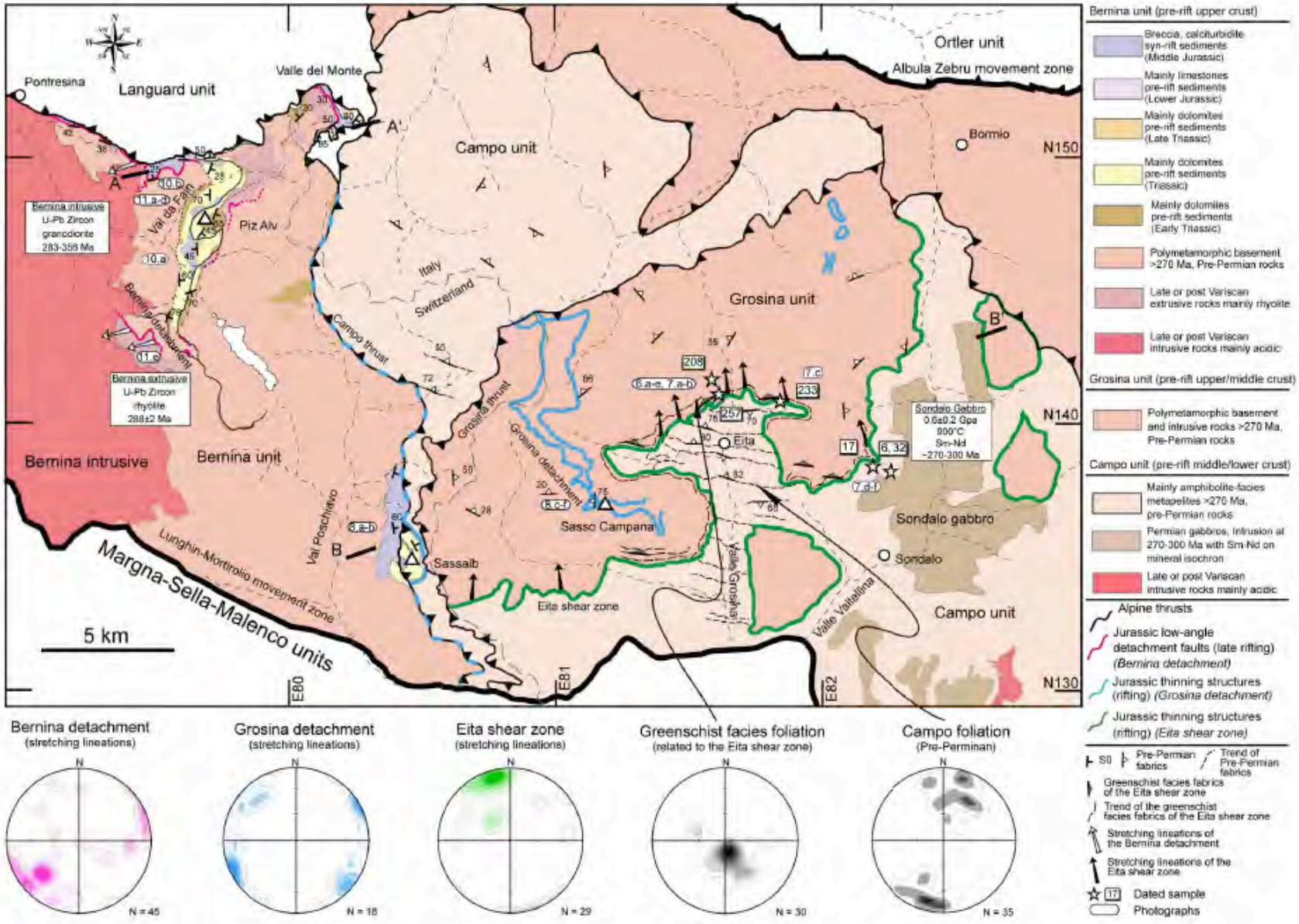

Figure 4. Geological map of the Bernina-Campo-Grosina units in SE-Switzerland and N-Italy. Map compiled from *Staub* [1946], *Bonsignore et al.* [1969], *Montrasio et al.* [1969], *Meier* [2003], and our own observations. Orientations of structural elements in the study area are presented in Lower hemisphere Schmidt projection. Note that localization of photographs of the Figures 6, 7, 8, 10, and 11 and $^{40}Ar/^{39}Ar$ samples (Figure 9) are indicated on the map as well as the trace of the cross sections of Figure 5.

Mohn et al 2012

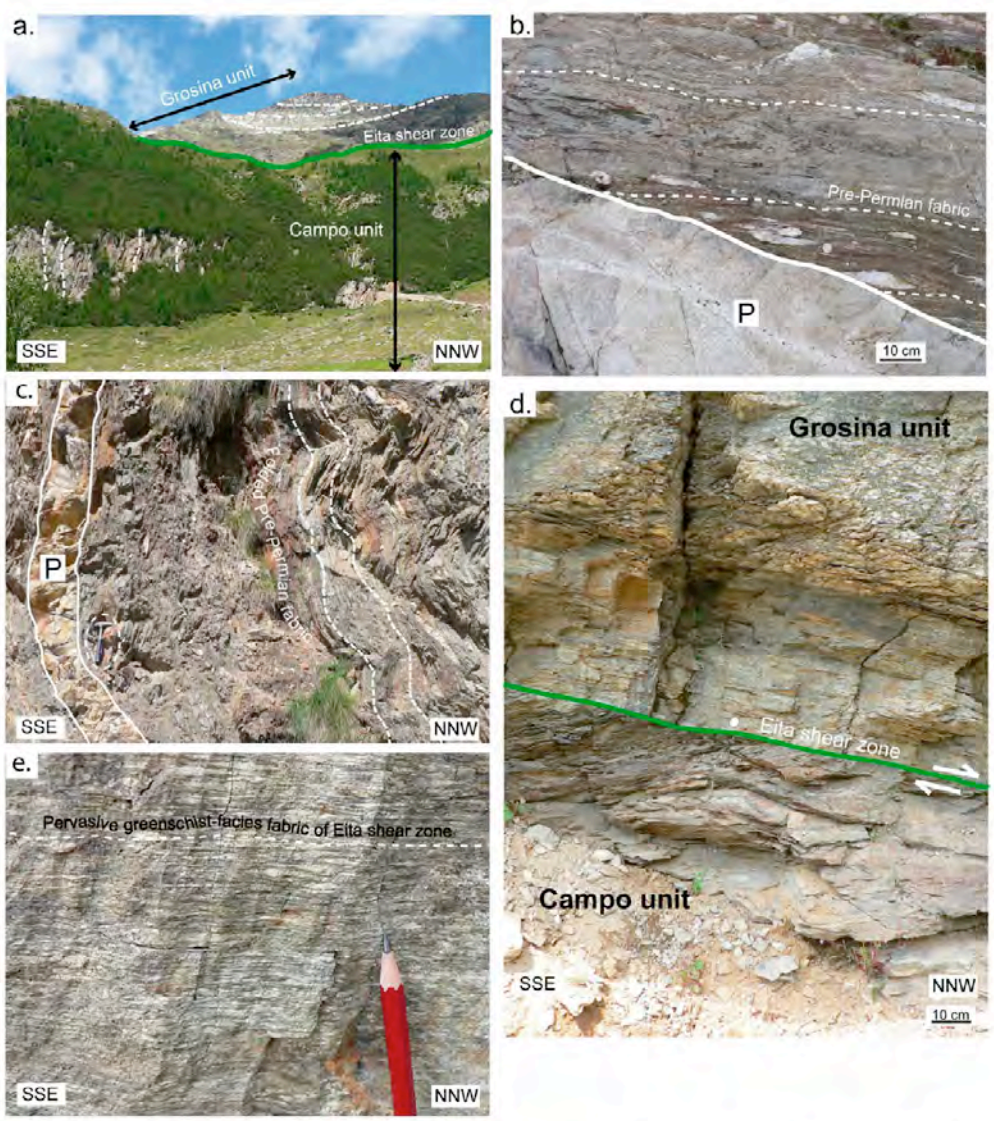

Figure 6. Field photographs showing the structural elements of Campo, Grosina units and Eita shear zone in Valle Grosina near Eita (for the location of photographs see Figures 4 and 5). (a) Large scale structures observed in Valle Grosina: note the angular discordance between the steep Pre-Permian Campo fabric and the flat pervasive greenschist pervasive foliation linked with the Eita shear zone (in green) within the Grosina basement (816305/139771). (b) Amphibolite-facies metapelites of the Campo unit crosscut by Permian pegmatite (P) (816315/139716) (c) In the vicinity of Eita shear zone, the pre-Permian Campo fabric associated with Permian dykes display recumbent folds (816467/141107). (d) Contact between Campo and Grosina basement formed by the Eita shear zone; note the drag of the Campo fabric due to the shearing indicating a top to NNW sense of shear (816481/141150). (e) North-dipping pervasive greenschist facies fabric related to the Eita shear zone (816510/141280). Coordinates are given with the Swiss grid.

Mohn et al 2012

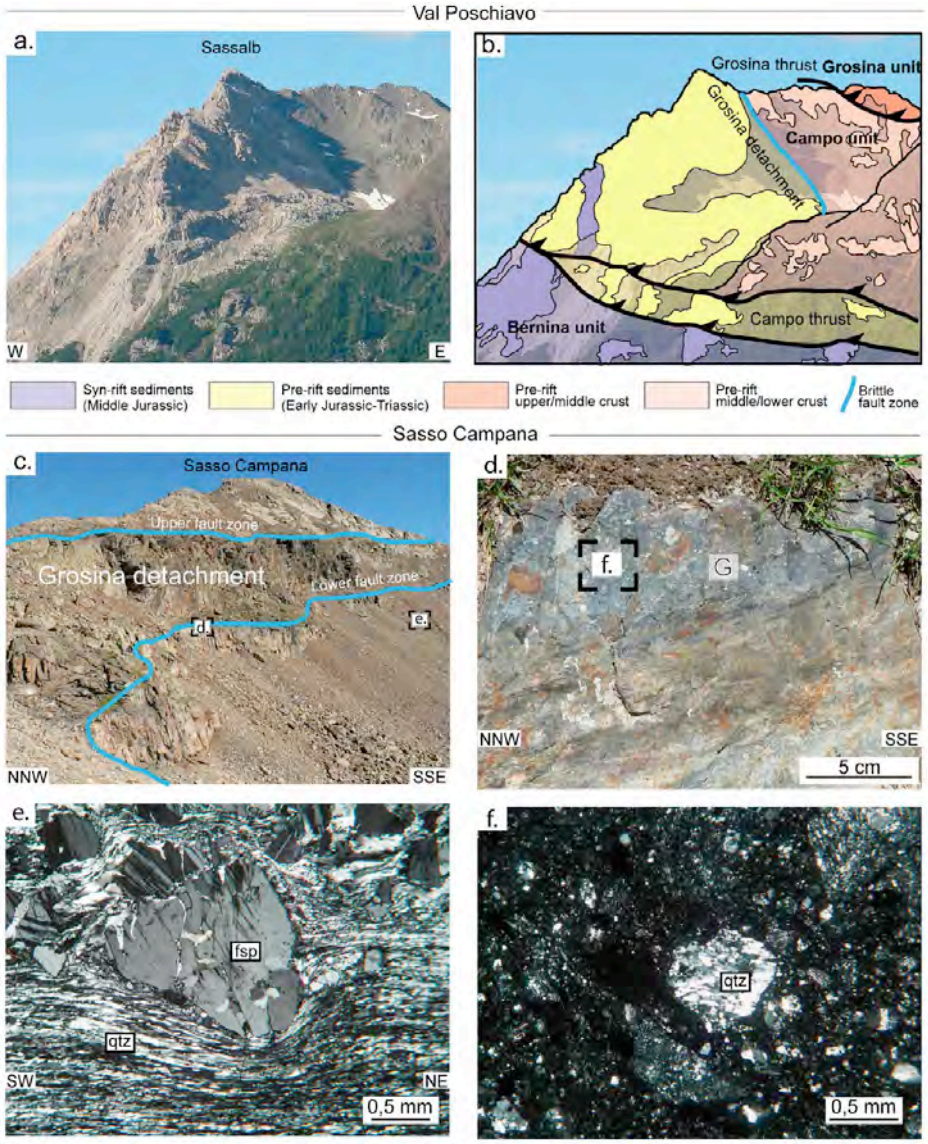

Figure 8. (a) Photograph and (b) line drawing from the Val Poschiavo at Sassalb showing the contact between Campo-Grosina and Bernina units. Campo unit is juxtaposed against the Bernina unit along a pre-Alpine contact referred to as Grosina detachment (in blue) crosscut by the Grosina and Campo thrust faults. Note that the photograph has been inverted to be compared with the map (Figure 4) and cross-section (Figure 5b) (804796/134771). (c) Grosina detachment at the top of Grosina unit in Sasso Campana. Note that two splays of the detachment can be observed (811306/137391). (d) Gouge zone as exposed along the Grosina detachment (811316/137314). (e) Photomicrographs of quartz mylonite from a shear zone crosscut by the Grosina detachment. Note the dynamically recrystallized quartz flows around the feldspar clast (811311/137194). (f) Photomicrographs of clast of quartz mylonite within a gouge from the Grosina detachment (811316/137314). Coordinates are given with the Swiss grid. For the location of photographs see Figure 4 and 5. (For mineral abbreviations see caption of Figure 7).

Mohn et al 2012

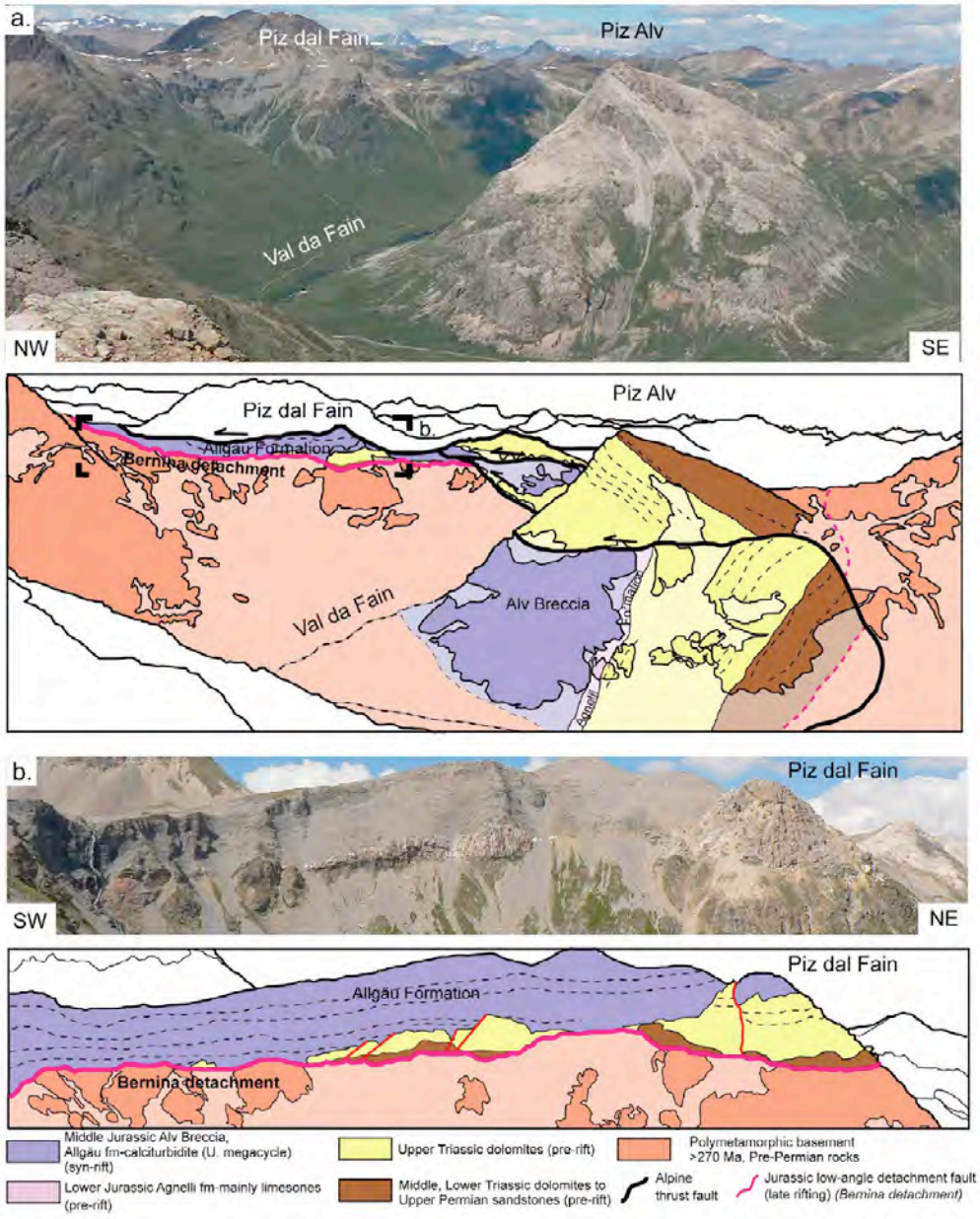

Figure 10. Photograph and line drawing from the Piz Alv–Val dal Fain area (Bernina unit) (for location of the photograph see Figures 4 and 5a). (a) Large-scale structure of Piz Alv-Val da Fain area viewed from the S showing the relationship between pre- and syn-rift sediments and basement rocks (796000/148000) (for restoration see Figure 5c). (b) View of Piz dal Fain from the S showing the syn-rift sediments (Allgäu Fm. (upper mega-cycle)) onlapping either onto exhumed basement or pre-rift sediments. (795000/149000) (for more details see text). Coordinates are given with the Swiss grid.

Mohn et al 2012

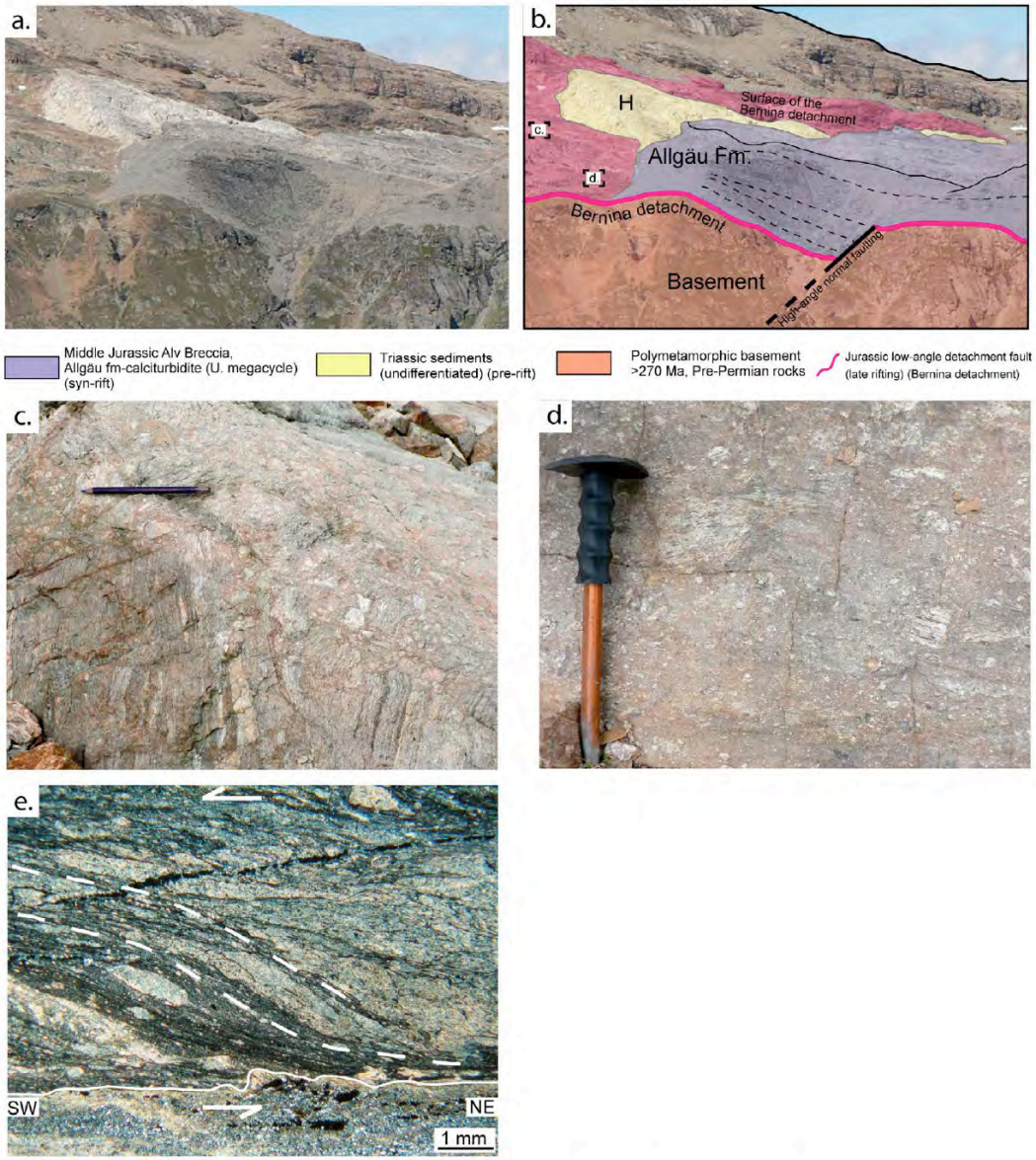

Figure 11. (a) Photograph and (b) line drawing of the Bernina detachment (Bernina unit) (view from the south). High-angle normal faults crosscutting the Bernina detachment can be locally observed. The syn-rift Allgäu Fm. thickens toward this fault, indicating that these sediments were deposited during the activity of this structure (794983/149072). View of the fault rocks related to the Bernina detachment. (c and d) Cataclastically deformed Paleozoic basement of the Bernina unit (794832/149133). (e) Photomicrographs under crossed polarizers of a gouge layer showing rotation of the shear fabric during shearing indicating a top to SW sense of shear (794643/143200). Coordinates are given with the Swiss grid. For location of the photographs see Figure 4 and 5.

Mohn et al 2012

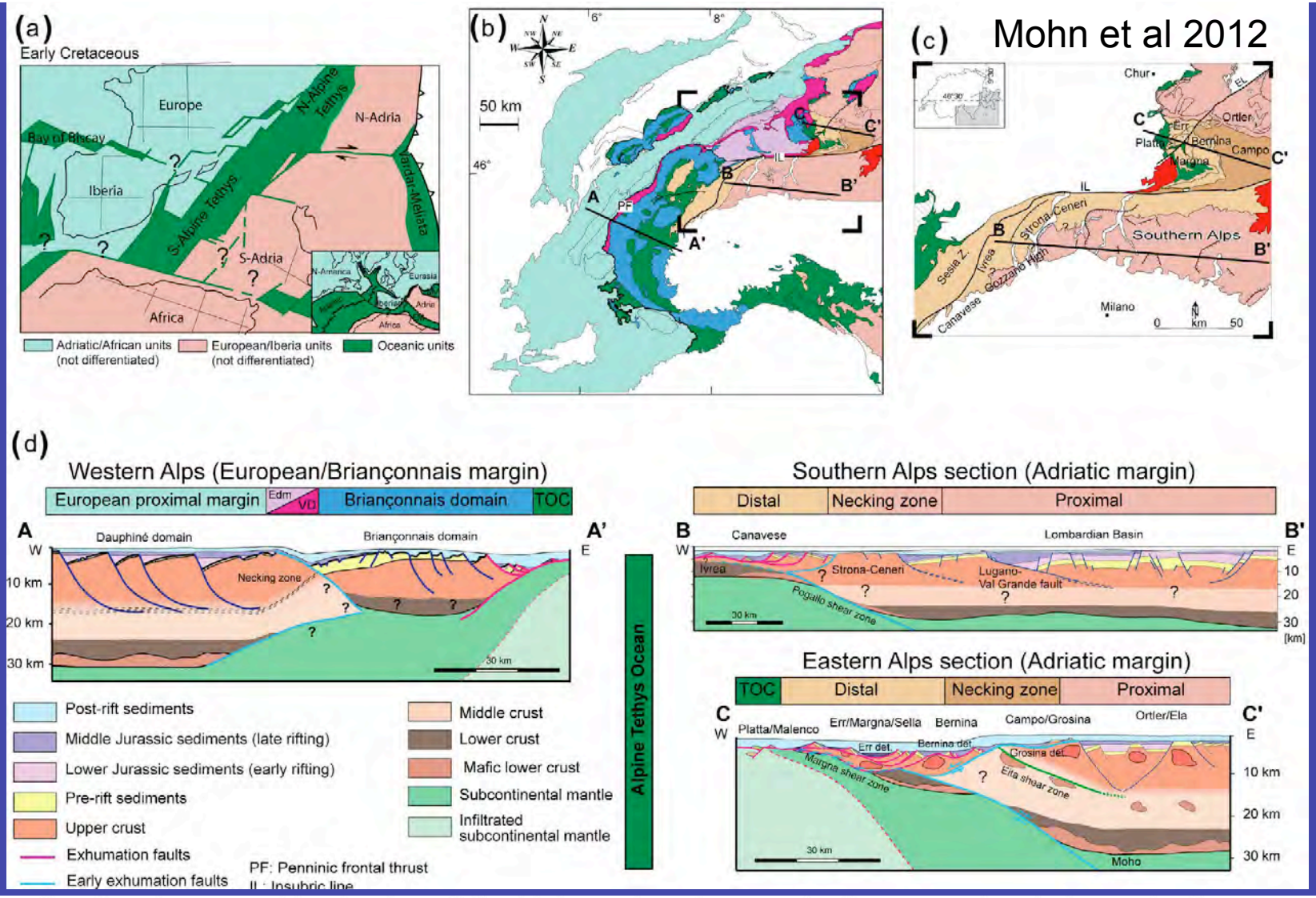

Figure 2. (a) Paleogeographic situation of the Alpine Tethys Ocean and adjacent margins during Early Cretaceous time [*Manatschal et al.*, 2011]. (b) Tectonic map of the Alps showing the distribution of the major palaeogeographic domains (modified after *Schmid et al.* [2004]). (c) Geological overview of the Eastern and Southern Alps modified after *Bernoulli et al.* [1990] and *Manatschal and Bernoulli* [1999]. (d) Reconstructed palaeogeographic sections across the European/Briançonnais and Adriatic rifted-margins, European/Briançonnais transect (section A-A′ modified after *Lemoine et al.* [1986] and *Mohn et al.* [2010]), Southern Alps transect (section B-B′ modified after *Bertotti et al.* [1993] and *Handy et al.* [1999]) and Eastern Alps transect (section C-C′ modified after *Froitzheim and Manatschal* [1996] and *Mohn et al.* [2010]) (for traces of sections see maps above).

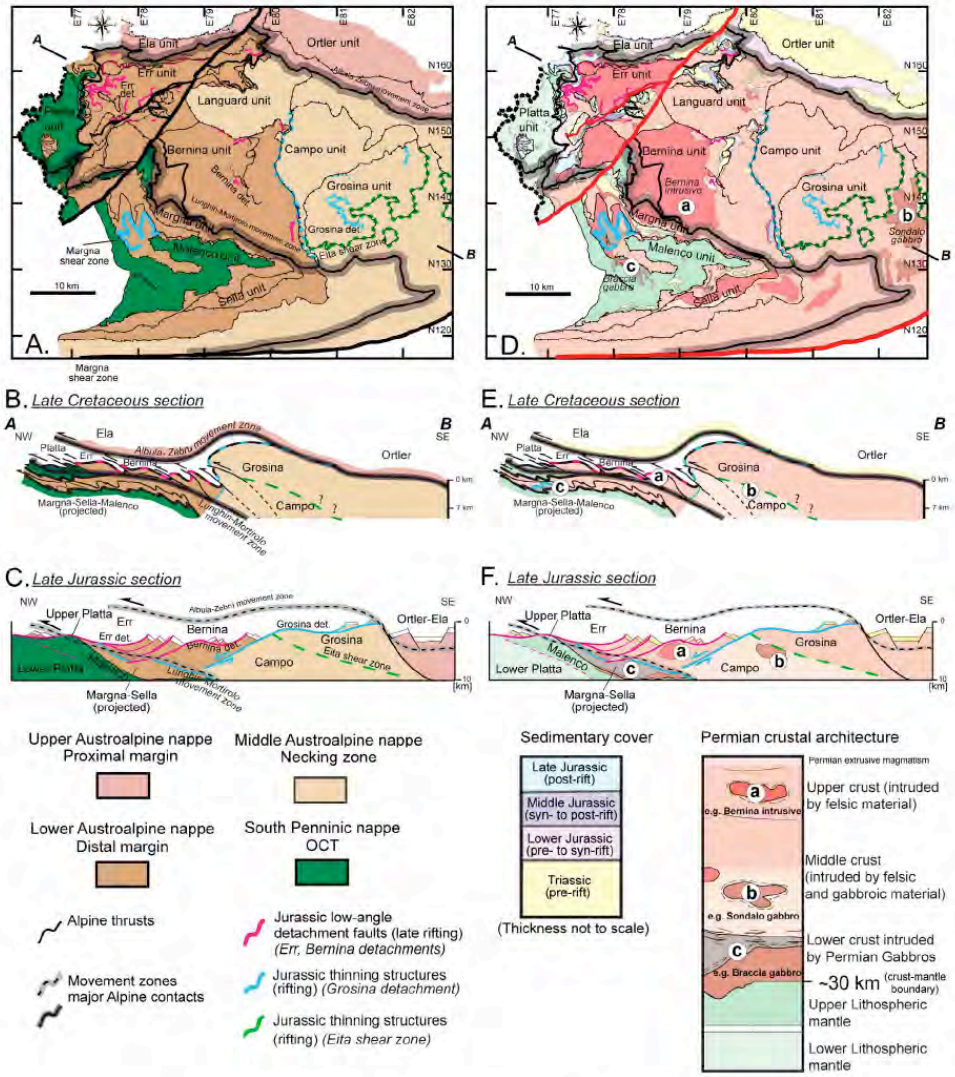

Figure 3. (a) Map showing the paleogeographic domains of the Austroalpine and Upper Penninic nappe systems in SE Switzerland and N-Italy. (b) Late Cretaceous section showing the distribution of paleogeographic units of the former Adriatic rifted margin after the west-directed convergence (modified from *Mohn et al.* [2011]). (c) Late Jurassic architecture of the Adriatic (Austroalpine) rifted margin showing the initial position of the paleogeographic units (modified from *Mohn et al.* [2010]). (d) Lithological map of the Austroalpine and Upper Penninic nappe systems in SE Switzerland and N-Italy. (e) Late Cretaceous section showing the reactivation of the former Adriatic rifted margin during the D1 west-directed convergence (modified from *Mohn et al.* [2011]). (f) Late Jurassic crustal architecture of the Adriatic (Austroalpine) rifted margin (modified from *Mohn et al.* [2010]). The section to the bottom right shows a simplified cross section of Permo-Jurassic cover associated with a cross-section through the crust in later Permian time, indicating the original position of the rocks found today in the different tectonic units (after *Mohn et al.* [2011]). Note that the Albula-Zebru and Lunghin-Mortirolo movement zones are major Alpine discontinuities inherited from the Jurassic rifting (for further details see *Mohn et al.* [2011]). Coordinates given in the maps refer to the Swiss grid.

Mohn et al 2012

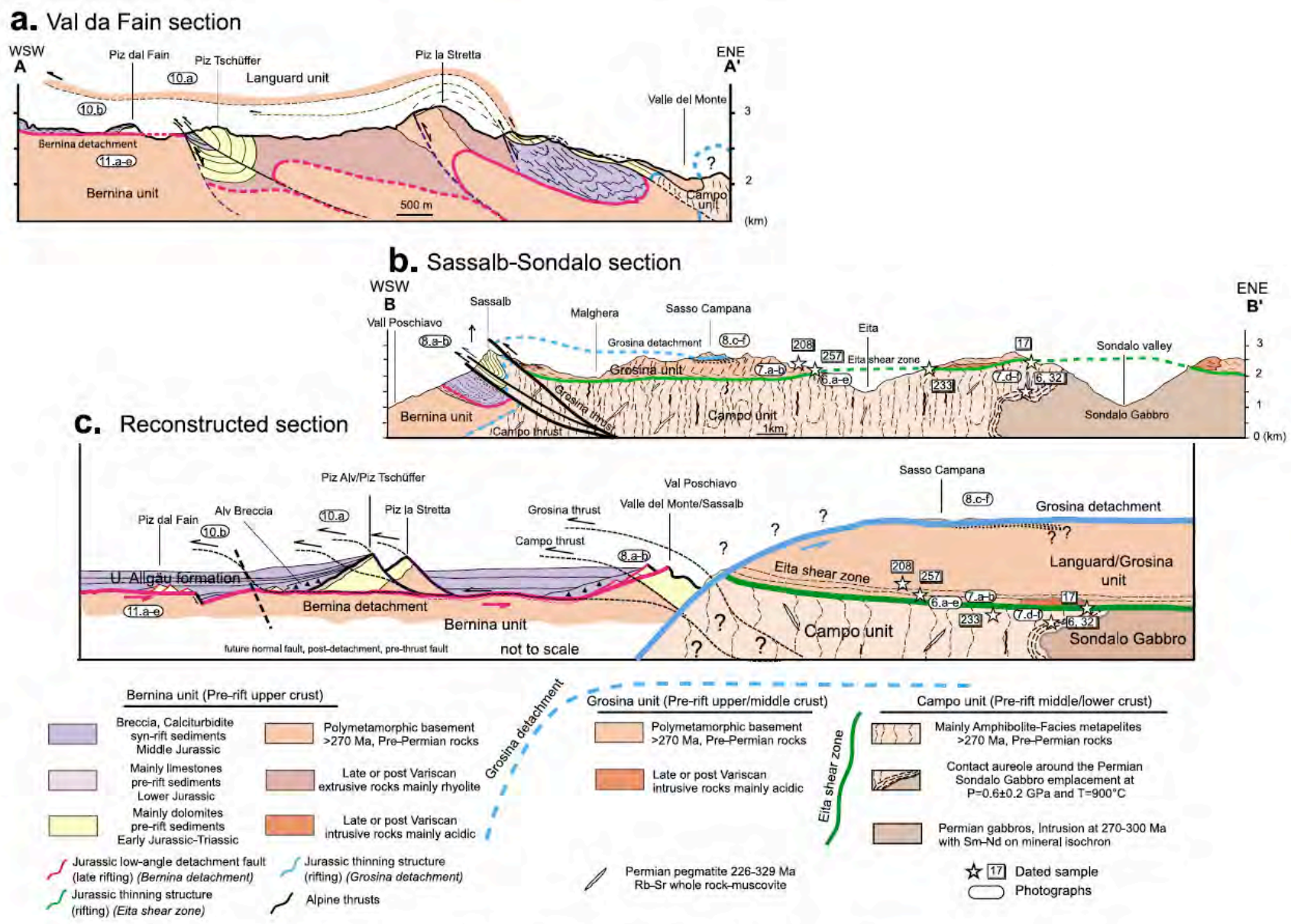

Figure 5. Geological sections across (a) Val dal Fain and (b) Sassalb–Sondalo and (c) restored section showing the pre-Alpine structures and their relation to the sediments and basement rocks in the Bernina, Campo-Grosina units. Localization of the cross-sections is shown in Figure 4 (modified after *Mohn et al.* [2011]). Note that localization of photographs of the Figures 6, 7, 8, 10, and 11 and $^{40}Ar/^{39}Ar$ samples (Figure 9) are indicated on the cross-sections.

Mohn et al 2012

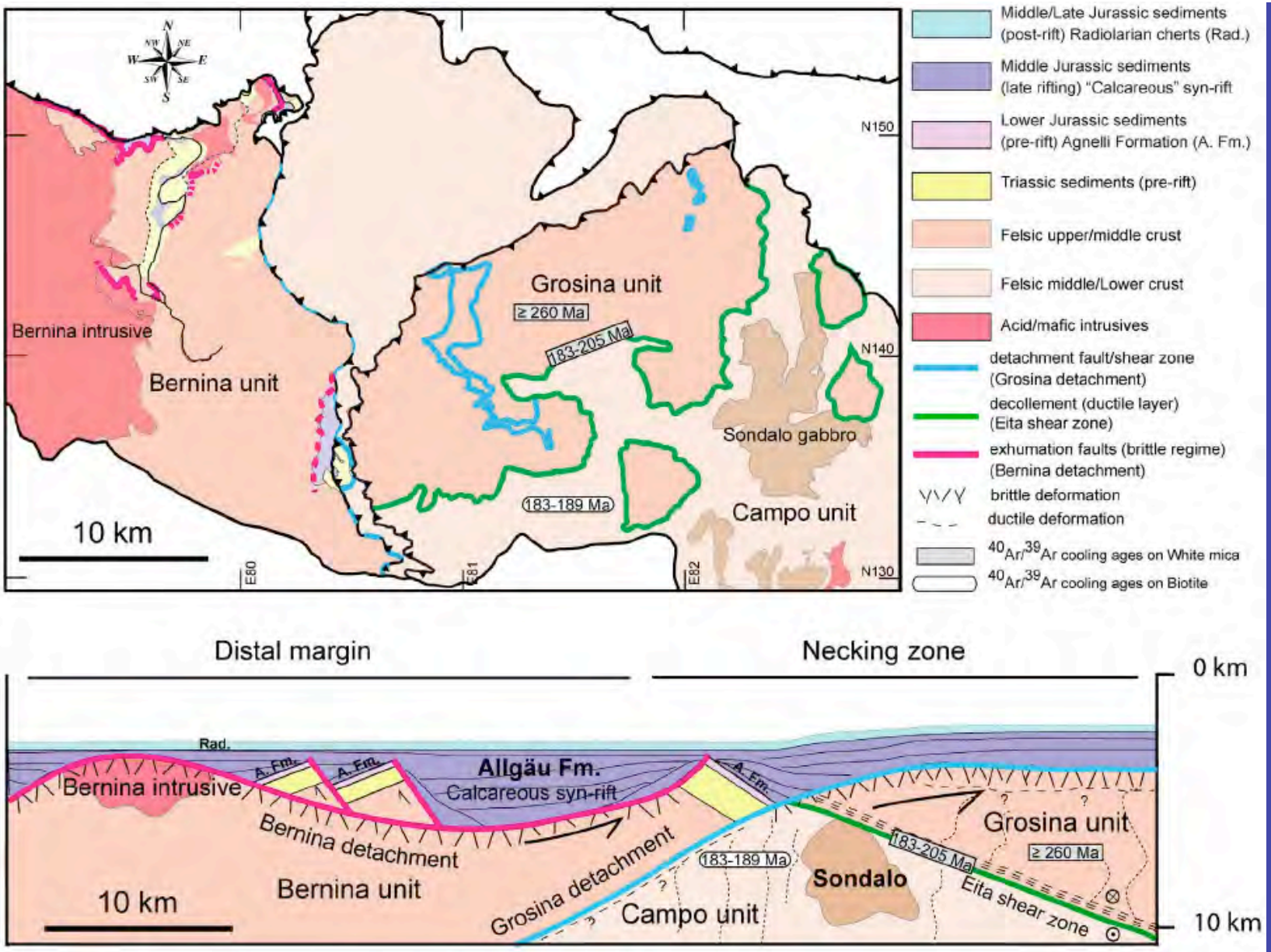

Figure 12. Present-day geological map associated with a restored cross-section of the necking zone of the Adriatic rifted margin across the Bernina-Campo-Grosina units. The cross section summarizes the sediment architecture, fault geometry, $^{40}Ar/^{39}Ar$ data, and strain distribution observed in these units.

Mohn et al 2012

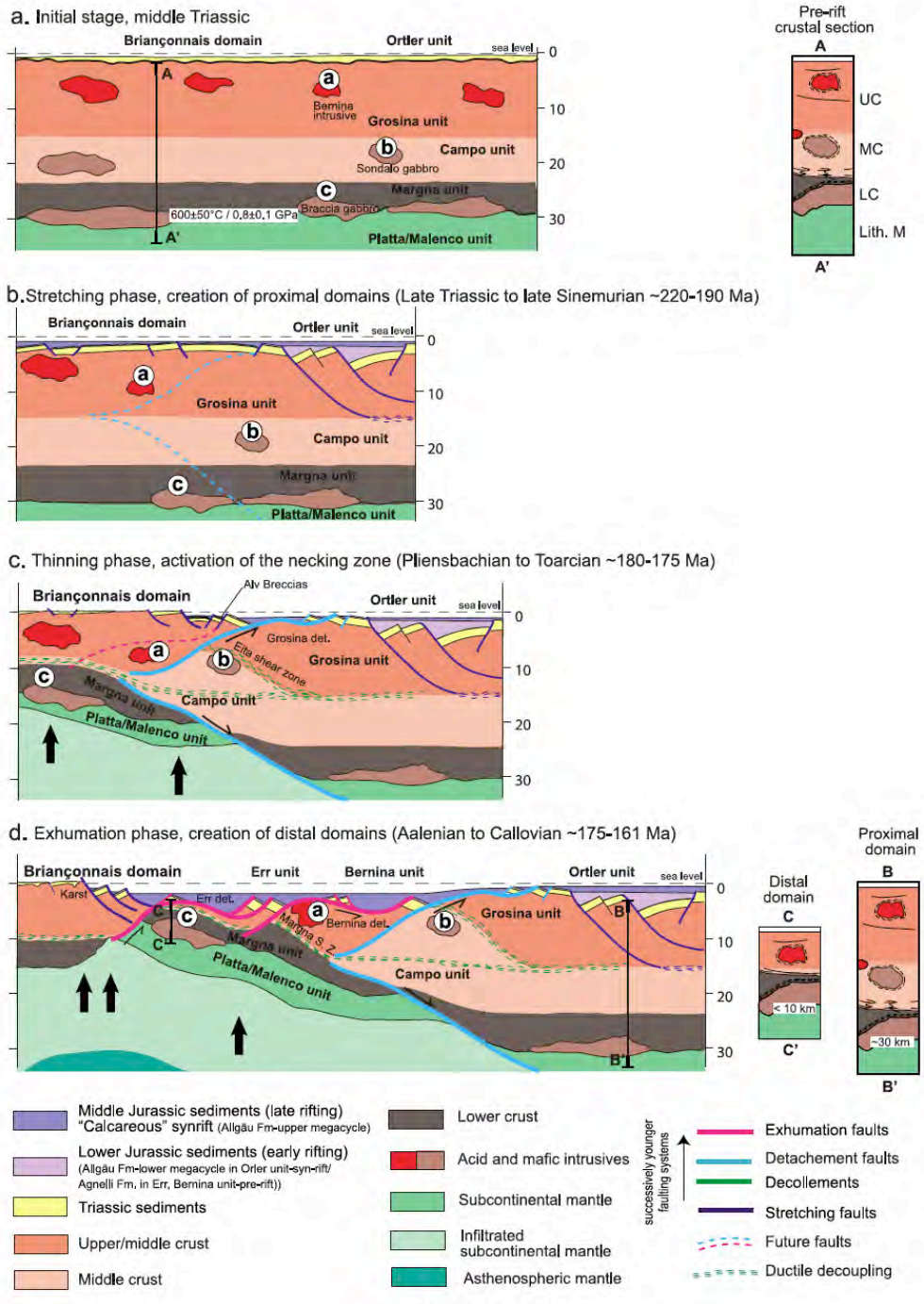

Figure 13

Mohn et al 2012

Maffioni et al 2010

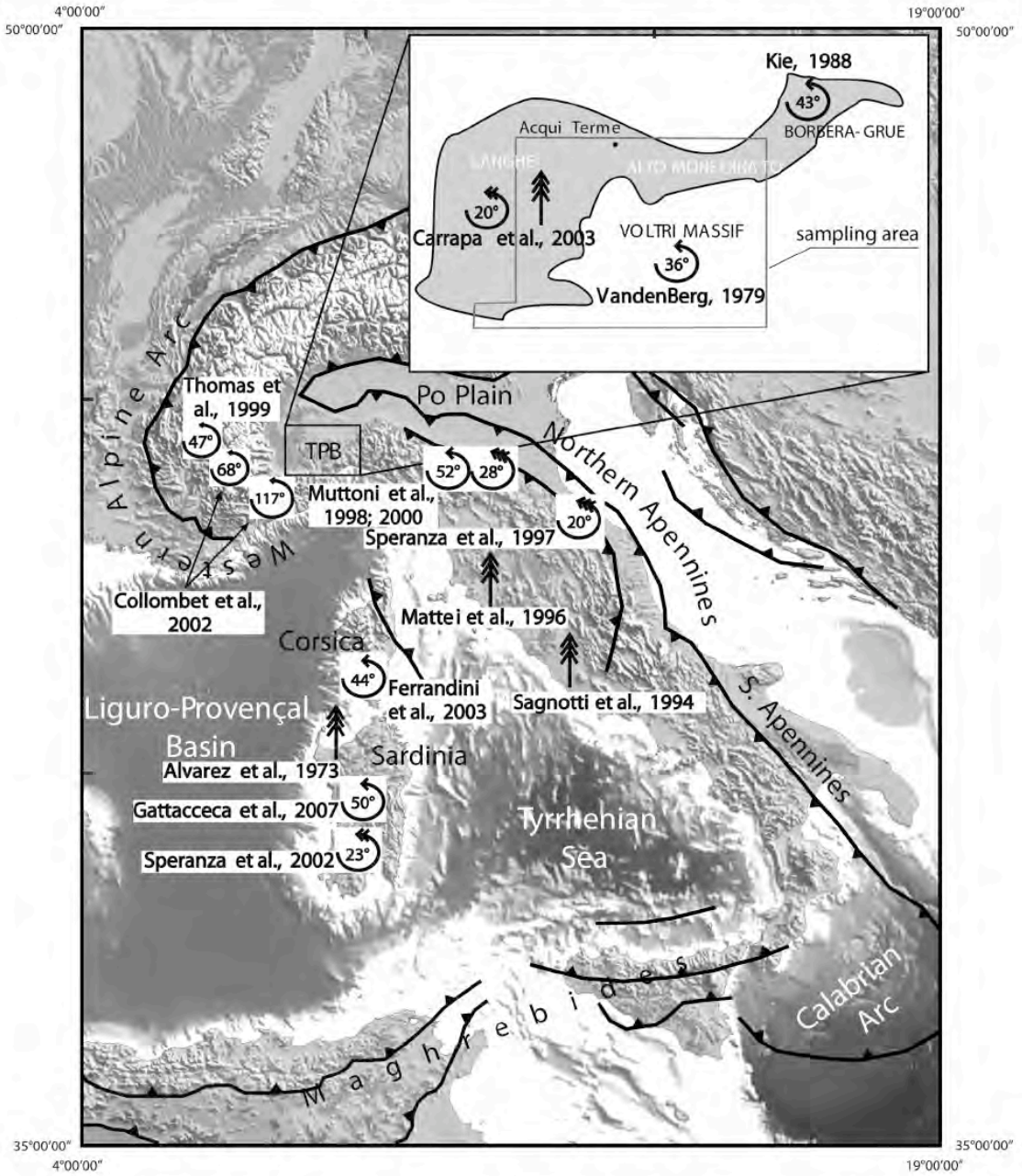

Figure 1. Digital elevation model of the central Mediterranean domain, and mean paleomagnetic rotation values (within circular arrows) with respect to nearby African/European plates for the internal western Alps, the northern Apennines, and the Corsica-Sardinia block (see text for details). Circular arrows with simple, double, and triple tips indicate post-Oligocene, post-Burdigalian, and post-Pliocene rotations, respectively. Vertical arrows indicate non-rotated areas after Late Miocene-Pliocene times.

***Table 1**. Paleomagnetic directions from the Tertiary Piedmont Basin*

Site	Formation	Geographic coordinates Latitude N	Geographic coordinates Longitude E	Nannofossil Zone	Age	Age (Ma)	Bedding (°)	Chrons	Cleaning Strategy	Tilt corrected D (°)	Tilt corrected I (°)	In situ D (°)	In situ I (°)	k	α95 (°)	n/N	Rotation (°)	Flattening (°)
BTP01	Molare	44° 18' 35.0"	8° 03' 12.2"	-	Rupelian	30.5-33.5	252-14	C12n-C13n	AF ; TH	317.4	39.7	308.4	32.8	332.1	4.2	5/12	-38.2 (6.6)	13.6 (5.4)
BTP06	Rocchetta	44° 32' 17.4"	8° 18' 59.3"	NP24	Rupelian	28.7-29.7	284-11	C10r-C11n1n	AF	124.2	-51.0	130.9	-61.3	94.0	5.3	9/11	-51.3 (0.4)	2.5 (6)
BTP07	Rocchetta	44° 32' 26.8"	8° 18' 19.6"	NP24	Rupelian-Chattian	28.0-29.4	327-6	C9r-C10r	AF	131.7	-55.7	128.7	-61.8	19.5	12.0	9/10	-43.9 (17.7)	-2.2 (10)
BTP09	Rocchetta	44° 36' 31.4"	8° 21' 26.7"	NP24	Rupelian-Chattian	28.0-29.7	18-9	C9r-C11n1r	AF	140.5	-54.6	128.7	-58.5	12.7	14.1	10/11	-35.1 (20.1)	-1 (11.8)
BTP11	Rocchetta	44° 35' 34.8"	8° 33' 01.5"	NP23	Rupelian	30.0-30.5	319-16	C11r	AF	106.2	-48.7	91.4	-59.2	96.9	8.4	6/9	-74.2 (11)	5.7 (7.8)
BTP12†	Rocchetta	44° 36' 38.0"	8° 32' 11.6"	-	Rupelian-Chattian	21.6-32.0	23-21	-	AF ; TH	-	-	-	-	-	-	-	-	-
BTP13	Rocchetta	44° 38' 30.8"	8° 29' 52.8"	NP23	Rupelian	29.9-30.9	236-35	C11n2n-C12n	AF	269.2	32.5	296.5	57.8	56.7	6.5	10/12	-86.4 (7.9)	21.1 (6.6)
BTP15	Cremolino	44° 39' 47.5"	8° 30' 39.1"	MNN4a	Burdigalian	16.5-17.6	359-9	C5Dn-C5Cn3n	AF ; TH	0.5	26.4	0.9	38.9	62.1	9.8	5/10	-1.8 (9.1)	32 (8)
BTP18	Rocchetta	44° 37' 45.0"	8° 40' 08.0"	NP23	Rupelian	30.1-32.3	325-23	C11r-C12r	AF	134.1	-45.1	124.8	-67.5	43.0	9.3	7/8	-51.6 (11.5)	8.5 (8.4)
BTP19*	Rocchetta	44° 36' 20.0"	8° 34' 0.8"	NP23	Rupelian	29.9-30.9	356-23	C11n2n-C12n	AF ; TH	4.4	26.2	7.5	48.9	499.2	2.5	8/8	8.7 (5.5)	27.4 (4.7)
BTP25†	Rocchetta	44° 36' 21.4"	8° 27' 49.1"	NP23	Rupelian	29.9-30.9	325-23	-	AF ; TH	-	-	-	-	-	-	-	-	-
BTP29*	Cremolino	44° 38' 54.8"	8° 27' 22.0"	MNN5a	Langhian	15.0-15.2	29-12	C5Bn2n	AF	5.5	42.7	359.7	53.2	165.0	3.5	12/13	3.3 (4.9)	15.7 (3.5)
BTP30*	Serravalle	44° 43' 44.2"	8° 28' 58.6"	MNN4a	Burdigalian-Langhian	16.0-17.6	21-12	C5Cn	AF ; TH	10.1	40.9	7.4	52.2	202.0	4.3	7/8	7.8 (5.5)	17.5 (4)
BTP31*	Cessole	44° 41' 20.0"	8° 47' 38.0"	MNN5b	Langhian	14.2-14.6	336-22	C5ADn	AF	350.5	34.3	357.3	55.2	46.2	6.8	11/11	-11.8 (7.2)	24 (5.7)
BTP38	Cessole	44° 41' 20.0"	8° 48' 38.0"	MNN5a/b	Langhian	14.8-15.2	310-49	C5Bn1n-C5Bn2n	AF	337.3	36.1	35.6	68.4	96.4	4.7	11/11	-25 (5.5)	22.4 (4.3)
BTP39	Rocchetta	44° 38' 10.0"	8° 45' 53.0"	NP23	Rupelian	30.1-32.3	356-25	C11r-C12r	AF	155.1	-18.5	161.4	-38.7	50.4	7.3	9/9	-20.6 (7.9)	35 (7)
BTP41	Rocchetta	44° 22' 35.0"	8° 13' 50.0"	NP23	Rupelian	29.9-30.9	38-3	C11n2n-C12n	AF	302.4	41.8	299.5	41.4	79.4	4.9	12/12	-53.2 (7.2)	11.6 (5.8)
BTP43	Rocchetta	44° 22' 50.0"	8° 12' 28.0"	NP24	Rupelian-Chattian	28.3-29.9	197-7	C10n-C11n1n/2n	AF	309.4	65.4	321.4	59.6	38.4	9.4	8/10	-44 (17.2)	-9.6 (8.5)
BTP47	Rocchetta	44° 38' 08.0"	8° 41' 42.4"	NP23	Rupelian	29.9-30.9	325-18	C11n2n-C12n	AF ; TH	312.9	42.1	307.8	58.5	62.1	11.7	4/10	-42.8 (13.4)	11.5 (10)
BTP53	Rocchetta	44° 35' 21.9"	8° 32' 47.1"	NP23	Rupelian	29.9-30.9	280-12	C11n2n-C12n	AF	311.7	19.4	314.8	29.7	128.9	3.7	13/13	-44 (5.9)	34.2 (5.2)
BTP57	Rocchetta	44° 34' 22.8"	8°19' 57.0"	NP23	Rupelian	29.9-30.9	253-17	C11n2n-C12n	AF	287.3	43.5	300.1	56.4	101.2	4.8	10/12	-68.3 (7.3)	10 (5.7)
BTP60	Rocchetta	44° 34' 26.7"	8° 19' 54.6"	NP23	Rupelian	29.9-30.9	11-9	C11n2n-C12n	AF	343.9	48.6	338.1	56.2	51.3	8.5	7/9	-11.7 (11.3)	4.9 (7.9)
BTP61	Rocchetta	44° 34' 28.1"	8° 19' 53.6"	NP23	Rupelian	29.9-30.9	245-27	C11n2n-C12n	AF	302.6	52.4	343.2	58.9	86.6	5.6	9/11	-53 (8.8)	1.1 (6.2)
BTP62	Rocchetta	44° 34' 33.1"	8° 19' 51.2"	NP23	Rupelian	29.9-30.9	276-9	C11n2n-C12n	AF	316.6	44.7	323.6	51.2	119.0	4.2	11/11	-39 (6.9)	8.8 (5.4)
BTP64	Rocchetta	44° 34' 43.5"	8° 19' 40.6"	NP23	Rupelian	29.9-30.9	257-2	C11n2n-C12n	AF	306.1	55.1	308.6	56.5	64.9	6.9	8/12	-49.5 (10.7)	-1.6 (6.9)
BTP65*	Monesiglio	44° 35' 08.7"	8° 19' 29.5"	MNN2a	Aquitanian	20.5-20.7	329-10	C6An1n	AF	357.0	49.3	3.7	57.4	72.9	5.1	12/13	-7 (7.5)	7 (5.2)
BTP66	Cremolino	44° 35' 25.0"	8° 18' 41.2"	MNN2b	Burdigalian	19.2-20.2	308-4	C6n	AF ; TH	9.8	36.7	12.3	38.4	226.0	4.5	6/13	5.8 (6.2)	19.6 (4.9)
BTP69*	Cremolino	44° 35' 34.6"	8° 15' 37.9"	MNN4a	Burdigalian-Langhian	16.0-17.6	247-4	C5Cn-C5Dn	AF	0.6	59.2	5.7	57.7	398.2	3.5	5/11	-1.6 (6.2)	-0.9 (3.6)
BTP72*	Cassinasco	44° 38' 17.7"	8° 14' 15.9"	MNN5a	Langhian	14.8-15.2	352-9	C5Bn	AF	359.0	43.3	0.4	52.2	111.3	4.6	10/10	-3.2 (5.9)	15.1 (4.2)
BTP73*	Cassinasco	44° 38' 15.8"	8° 14' 13.8"	MNN5a	Langhian	14.8-15.2	27-4	C5Bn	AF	5.2	49.5	3.2	53.4	97.3	6.8	6/11	3 (8.8)	8.9 (5.8)
BTP75*	Cassinasco	44° 34' 46.4"	8° 08' 11.4"	MNN5a	Langhian	14.8-15.2	296-10	C5Bn	AF	350.3	48.5	1.0	53.6	139.3	3.7	12/13	-11.9 (5.4)	9.9 (3.7)
BTP80	Monesiglio	44° 26' 07.3"	8° 14' 0.8"	MNN1c	Aquitanian	22.9-23.8	322-7	C6An2n/C6Cn	AF	320.8	39.2	320.6	45.9	51.9	8.5	7/11	-39.8 (10.1)	18 (7.7)
BTP84	Rocchetta	44° 28' 36.2"	8° 24' 56.1"	NP23	Rupelian	29.9-30.9	295-9	C11n2n-C12n	AF	334.2	20.0	336.8	27.1	42.6	6.7	12/12	-29.6 (7.5)	33.3 (6.8)
BTP85	Molare	44° 29' 54.3"	8° 25' 09.2"	-	Rupelian	30.9-33.1	263-5	C12r	AF	110.4	-51.4	113.7	-55.9	280.0	3.6	7/13	-65.2 (6.8)	2.1 (5.1)

Table 1. Paleomagnetic directions from the Tertiary Piedmont Basin. The geographical coordinates are referred to ED50 datum. Nannofossil zones are from Martini, (1971) and Fornaciari and Rio, (1996). Age in Ma is from the geological timescale of Gradstein *et al.* (2004), and is inferred considering both the magnetic polarity (chron boundary ages) and our new biostratigraphic data. Bedding is expressed in dip azimuth and dip values. Cleaning strategy is alternating field (AF) and/or thermal (TH). D and I are site mean declination and inclination calculated before and after tectonic correction. k and α_{95} are statistical parameters after Fisher, (1953). n/N is number of samples giving reliable results/number of studied samples at a site. Site mean rotation and flattening values, according to Demarest, (1983), are relative to coeval D and I African values expected at Tertiary Piedmont Basin (errors are in parentheses). The reference African paleopoles are from Besse and Courtillot, (2002). † Sites yielding scattered demagnetization diagrams. *Remagnetized sites (see text).

Maffioni et al 2010

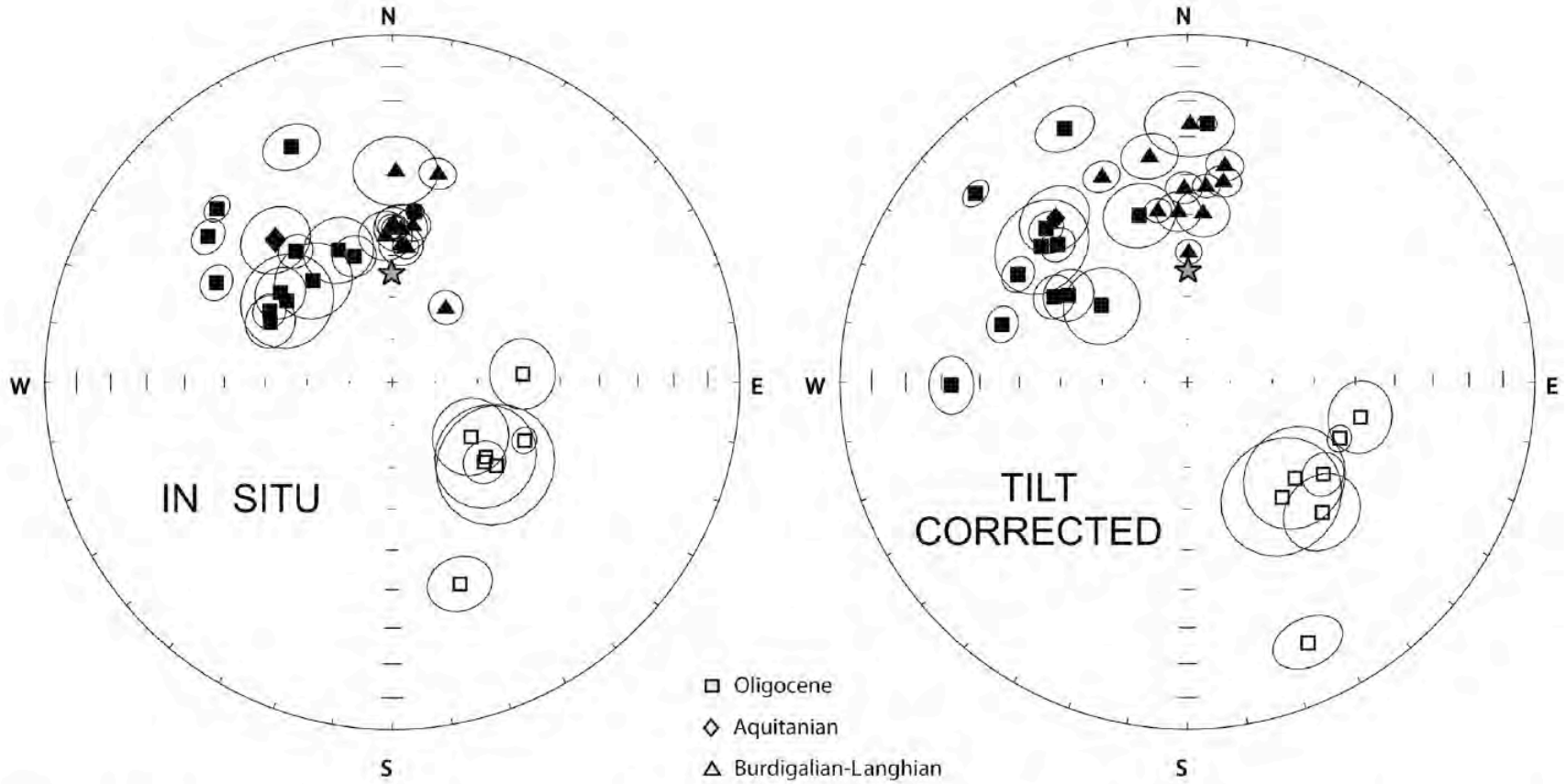

Figure 2. Equal-area projections of the site mean paleomagnetic directions from the TPB. Solid symbols represent projection onto the lower hemisphere (normal polarity magnetization components), while open symbols is the projection onto the upper hemisphere (reverse polarity magnetization components). Open ellipses are the projections of the α_{95} cones about the mean directions. The star represents the normal polarity geocentric axial dipole (GAD) field direction (D = 0°, I = 63.0°) for the study area.

Maffioni et al 2010

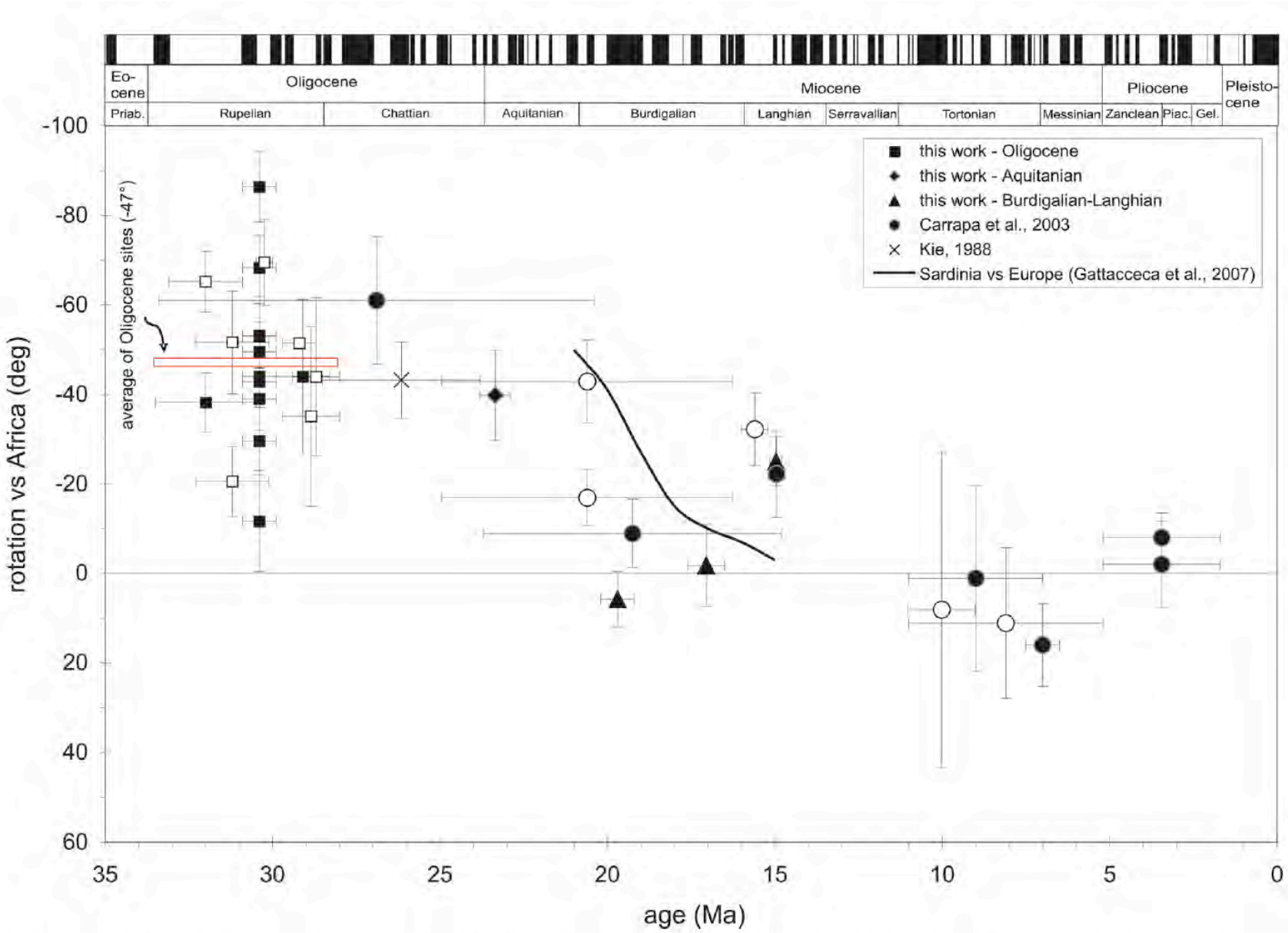

Figure 3. Site-mean paleomagnetic rotation with respect to Africa vs. age, for sites from the TPB. Solid symbols indicate sites yielding normal magnetic polarity, while open symbols indicate sites yielding reverse magnetic polarity. Geological and geomagnetic polarity time scales are from Gradstein *et al.* (2004). Error bars for declination site mean values are the $\alpha_{95}/\cos$ (I) values. Error bars for rotations were computed according to Demarest (1983). Error bars for ages were drawn considering both biostratigraphic information and paleomagnetic polarity (see text and Table 1).

Maffioni et al 2010

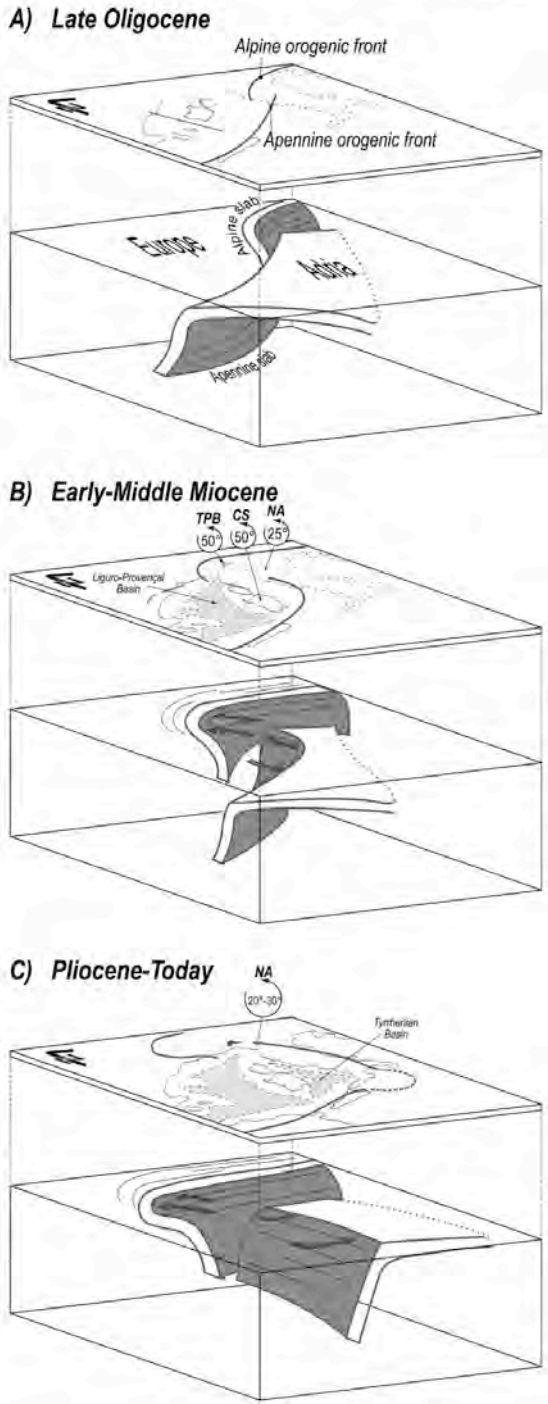

Figure 4. Schematic 3D-block diagram suggesting a possible kinematic reconstruction of the Alps-Apennines belt system since the Late Oligocene. The evolution in time and space of both the Alpine and the Apennine orogenic fronts are correlated together with the deep subduction geometry. The mean paleomagnetic rotation values for each stage are also reported. (TPB) Tertiary Piedmont Basin, (CS) Corsica-Sardinia block, (NA) Northern Apennines.

Maffioni
et al 2010

Stampfli and Borel 2002

80 Ma Alpine Tethys Sea Floor Spreading

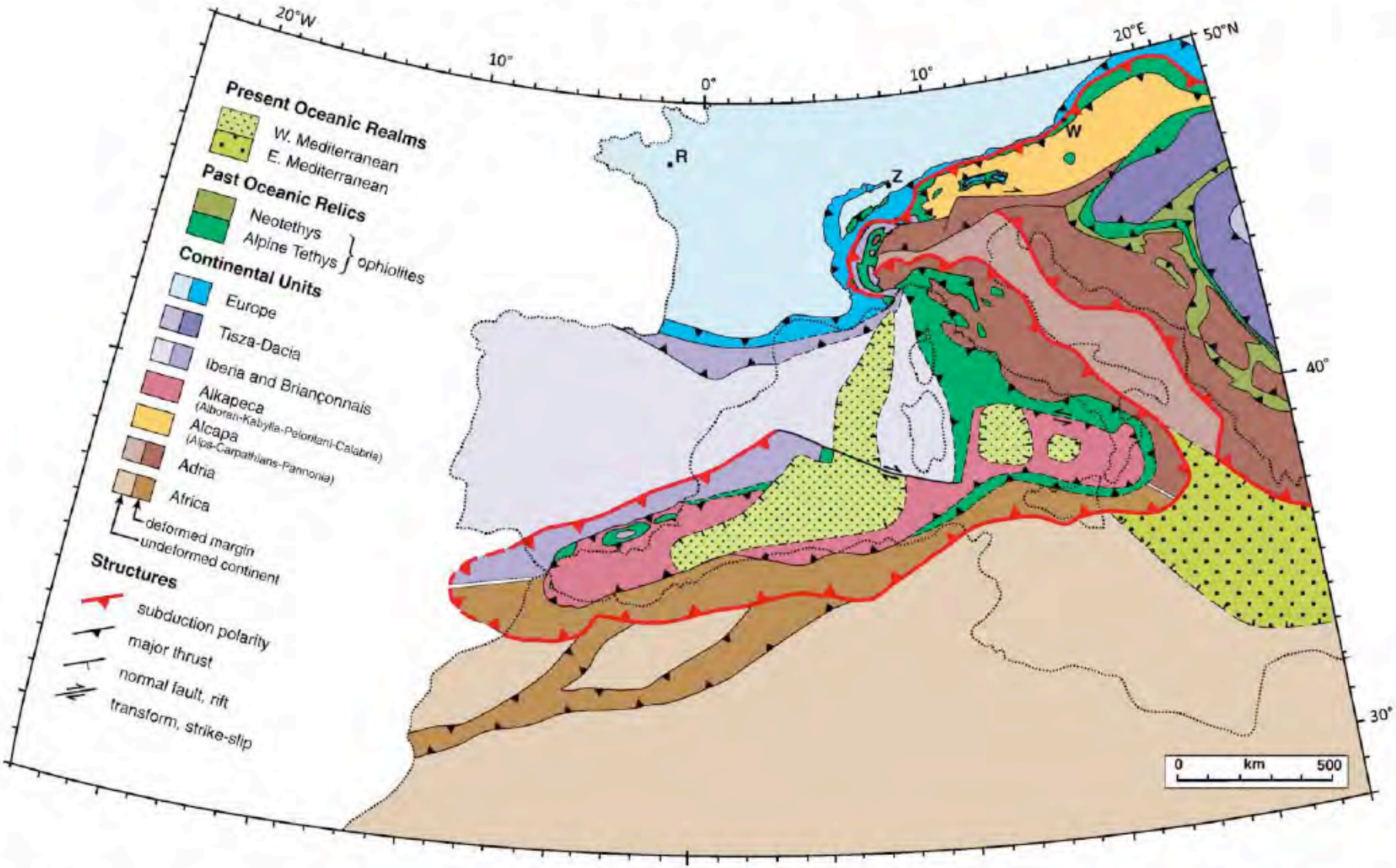

Fig. 1. Tectonic map of Mesozoic–Cenozoic mountain belts and ocean basins in the Alpine–Western Mediterranean area. The tectonic units in this map are plates or fragments of plates that have moved independently since Jurassic time and were amalgamated in Cenozoic–Recent time. Subduction polarities shown in red are determined from the dip of subducted lithospheric slabs imaged by seismic tomography (see Fig. 3). Note that some of these subduction polarities pertain to ancient plate boundaries (e.g. parts of the Alps), while others relate to boundaries that are still active (e.g. External Dinarides, Southern Apennines, Calabria, Betic–Rif). References: Alps, Dinarides, Carpathians (Schmid et al., 2004a, 2008); Italy (Bigi et al., 1989), Betic Cordillera, Alboran block, Northern Africa (Frizon de Lamotte et al., 2000; Michard et al., 2006); Western Mediterranean Sea (Roca et al., 2004); Ionian Sea (Chamot-Rooke et al., 2005).

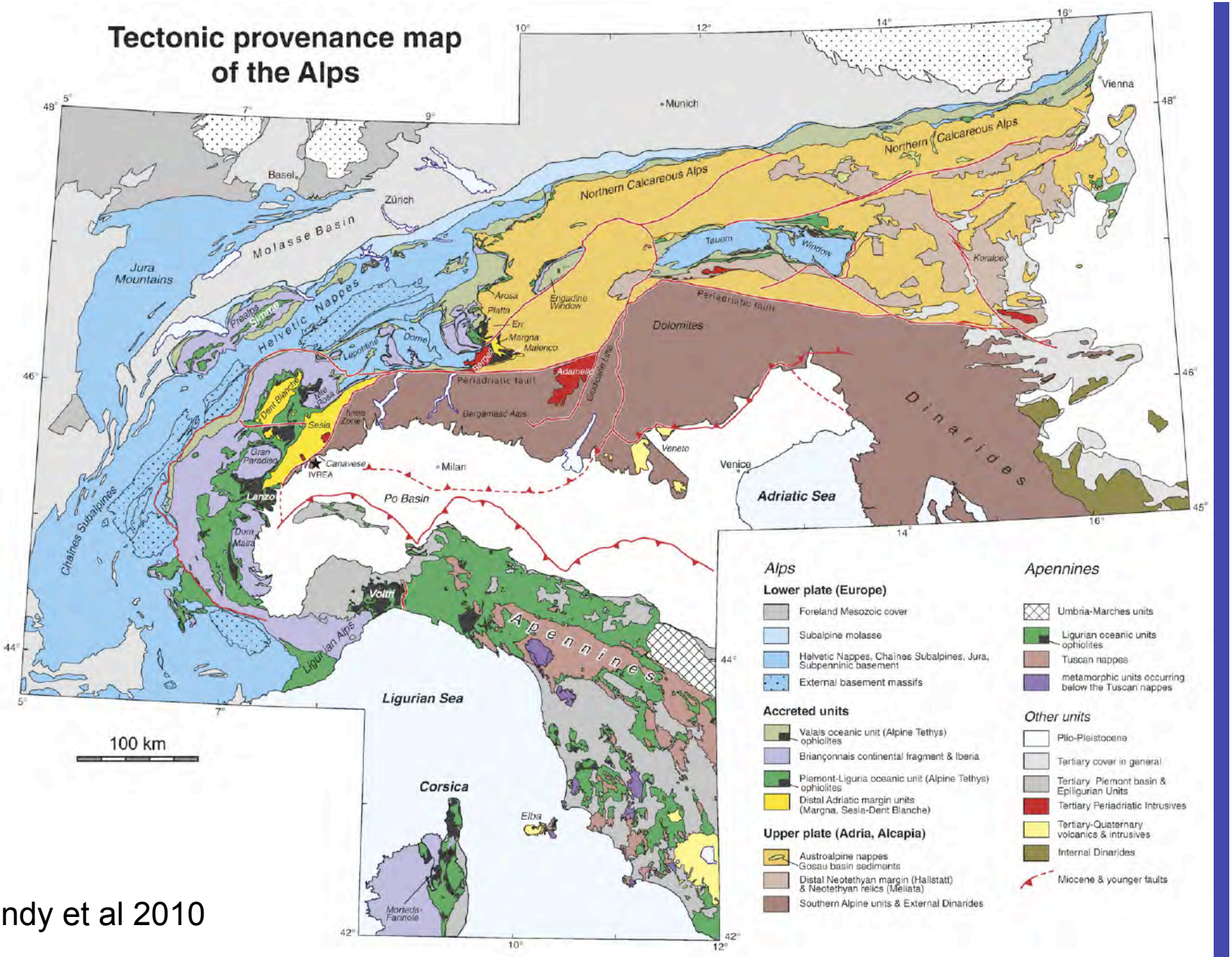

Handy et al 2010

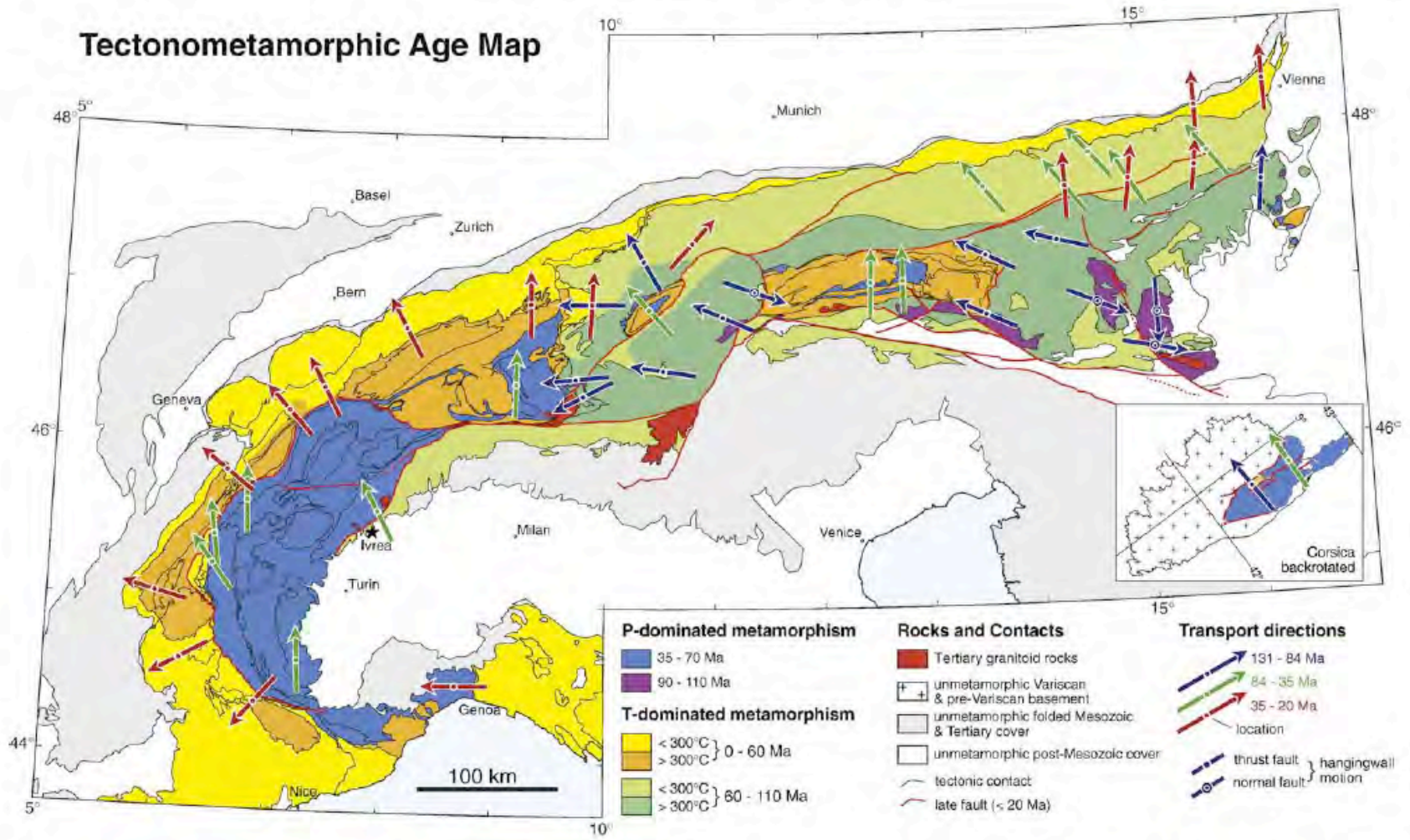

Fig. 5. Age of metamorphism and kinematics in the Alps and Corsica. Corsica is depicted in its pre-late Oligocene back-rotated orientation. Distribution of metamorphic ages is modified from inset map of Oberhänsli et al. (2004) as described in Handy and Oberhänsli (2004). Pressure-dominated metamorphism (blue and purple areas) includes blueschist-, eclogite- and HP greenschist-facies assemblages as well as UHP minerals (e.g., coesite); Temperature-dominated metamorphism includes assemblages ranging from sub-greenschist- (yellow, light green) to greenschist- and amphibolite-facies (orange, dark green). Arrows indicate transport direction taken from the following sources: Corsica (Malavieille et al., 1998; Molli, 2008); Ligurian Alps (Vignaroli et al., 2008), Western Alps (Malavieille et al., 1984; Choukroune et al., 1986; Vuichard, 1989; Philippot, 1990; Fügenschuh et al., 1999; Loprieno, 2001; Ceriani and Schmid, 2004); Central Alps (Babist et al., 2006; Pleuger et al., 2008; Nagel, 2008), Lower Austroalpine and adjacent Piemont–Liguria units of E. Switzerland (Ring et al., 1989; Liniger and Nievergelt, 1990; Handy, 1996); Engadin Window (Ring et al., 1989; Bousquet et al., 2002); Eclogite Zone in the Tauern Window (Kurz et al., 2008); Northern Calcareous Alps (Eisbacher and Brandner, 1996; Peresson and Decker, 1997), Austroalpine basement units including eclogite-bearing rocks of the Koralpe-Wölz unit (Ratschbacher et al., 1989; Froitzheim et al., 2008) and Radstadt Tauern (Becker, 1993).

Handy et al 2010

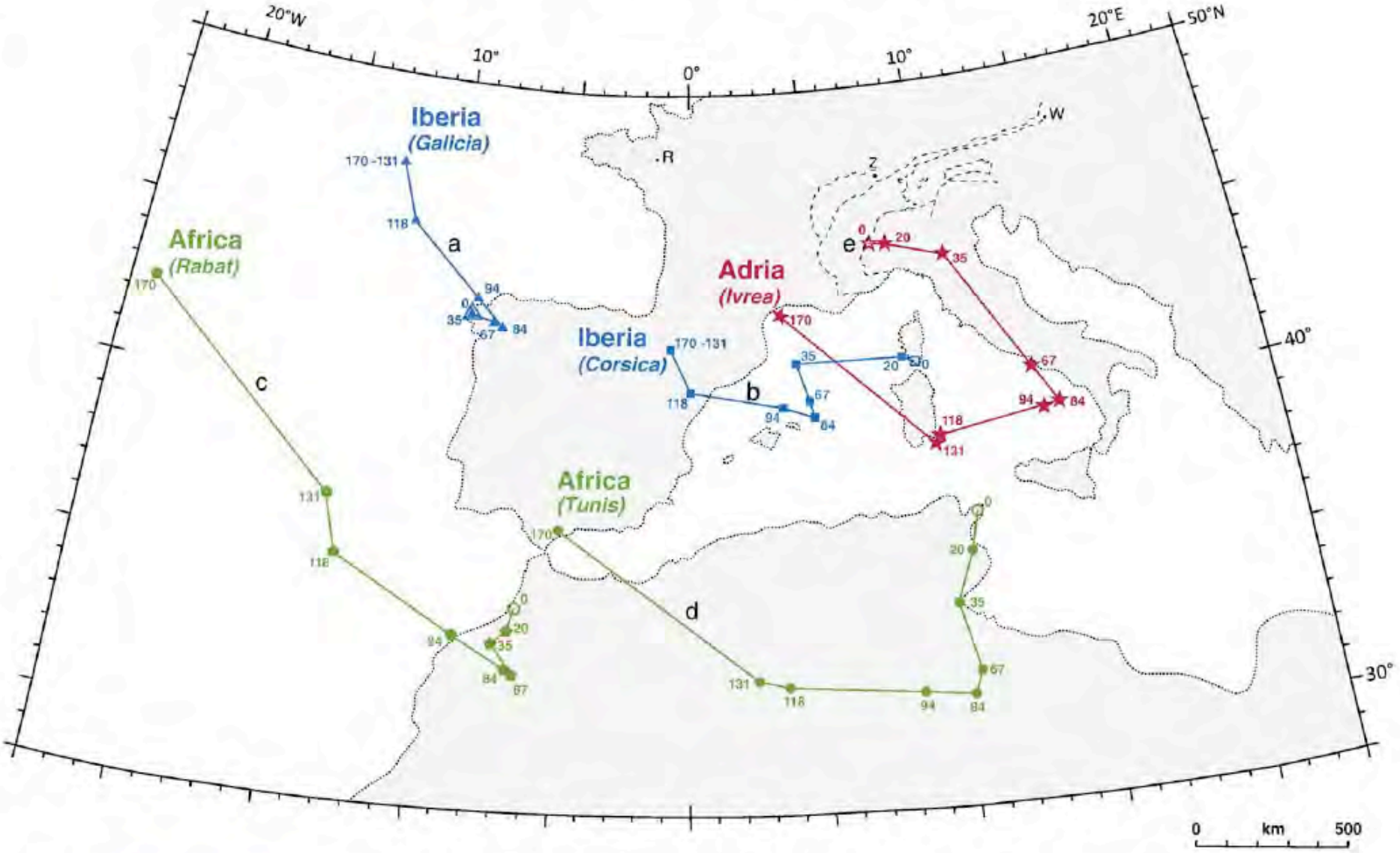

Fig. 7. Motion paths of five points labelled a to e located on tectonic plates and constructed according to criteria discussed in the text (Sections 3.2 and 3.3). Equal-area map projection modified from Capitanio and Goes (2006). Scale shows linear distances for center of map and is valid at the map edges to within 0.5 mm (6.8 km). Dotted lines = present coastal outlines. Dashed lines = Alpine nappe edifice. City locations for reference on stable Europe: R = Rennes, W = Wien (Vienna), Z = Zürich.

Handy et al 2010

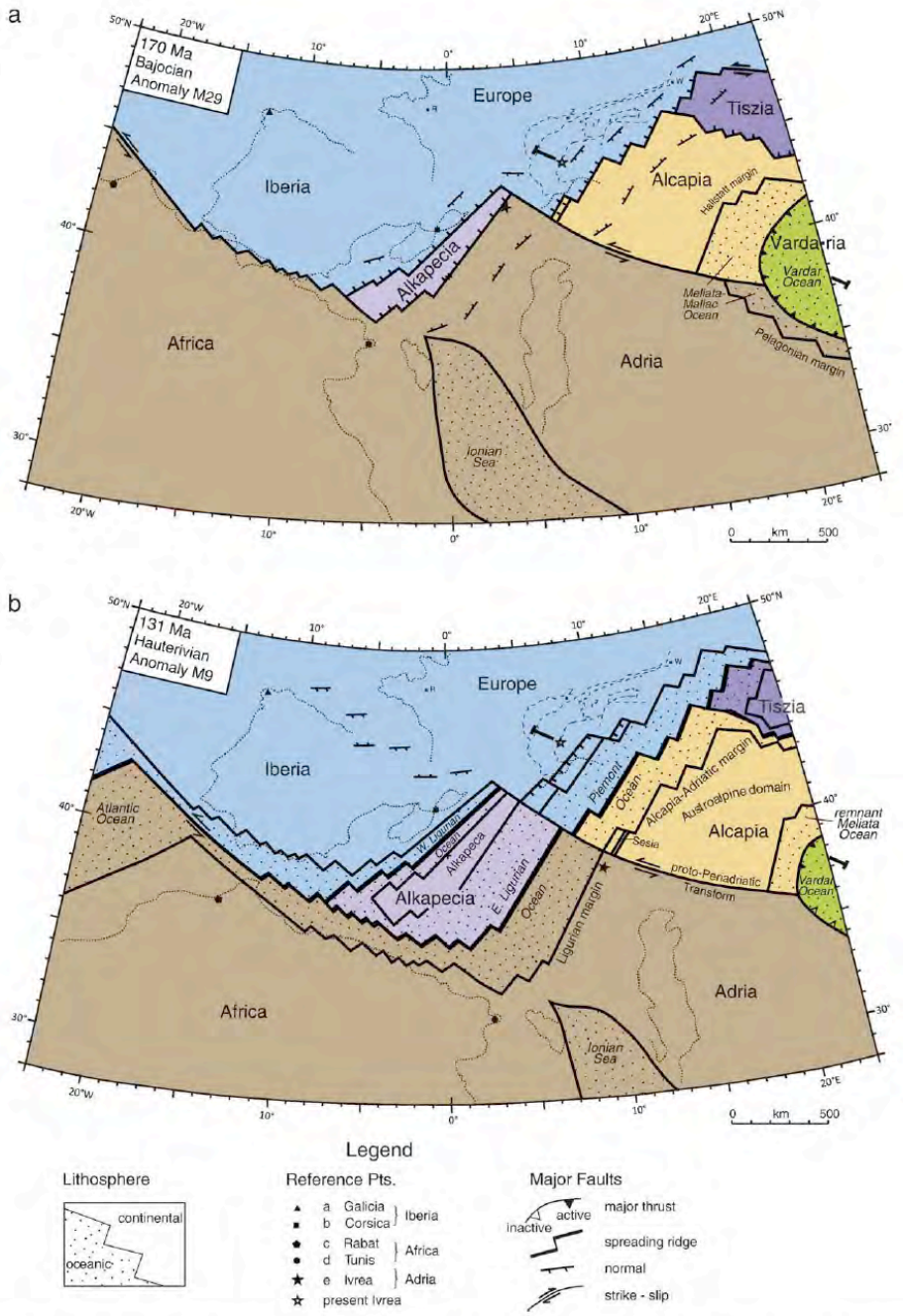

Fig. 8. Plate tectonic maps of Alpine Tethys and the western embayment of Neotethys: (a) 170 Ma, Africa, Alcapia and Tiszia break away from Europe; the Jurassic Vardar Ocean is obducted westward onto Triassic Meliata–Maliac oceanic crust; (b) 131 Ma, end of spreading in the Piemont–Liguria Ocean. A sinistral transform fault links this spreading with subduction and obduction of Vardar oceanic crust. Line shows trace of cross sections in Fig. 9. Dotted lines = coastal outlines of Western Europe, Iberia, islands in the Western Mediterranean Sea (Corsica, Sardinia), southernmost Italy (Apulia) and northern Africa. Dashed lines = current outline of Alpine nappe edifice. City locations for reference on Europe: R = Rennes, W = Wien (Vienna), Z = Zürich.

Handy et al 2010

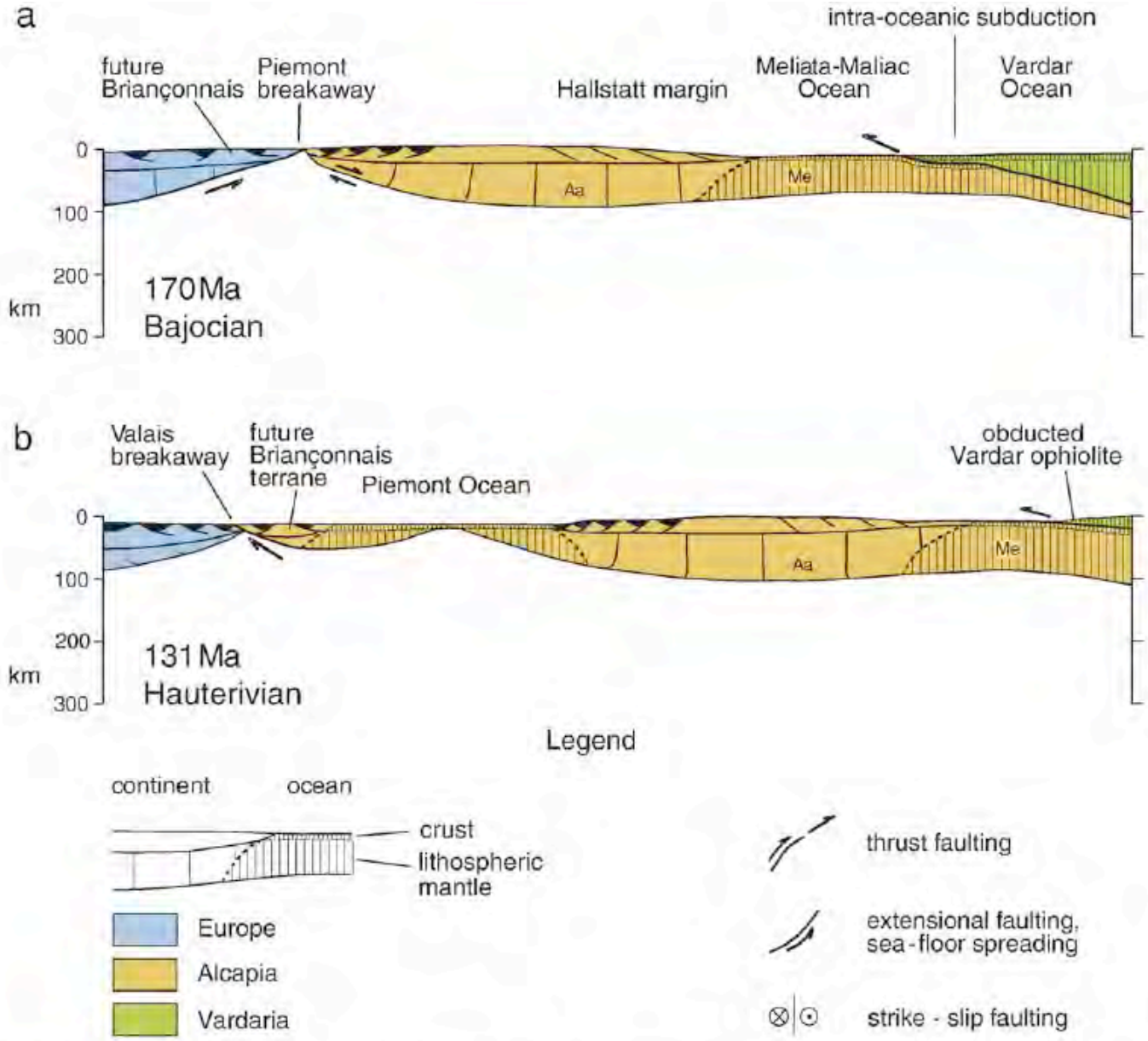

Fig. 9. Cross sections through Alpine Tethys and part of Neotethys: (a) 170 Ma, onset of spreading in Piemont part of Alpine Tethys; intra-oceanic obduction of Vardar oceanic lithosphere; (b) 131 Ma, end of spreading in Piemont part of Alpine Tethys and onset of Eo-alpine orogenesis; Location of cross sections shown in Fig. 8. Horizontal scale equals vertical scale. Aa = Austroalpine (Alcapia) continental lithosphere, Me = Meliata–Maliac oceanic lithosphere.

Handy et al 2010

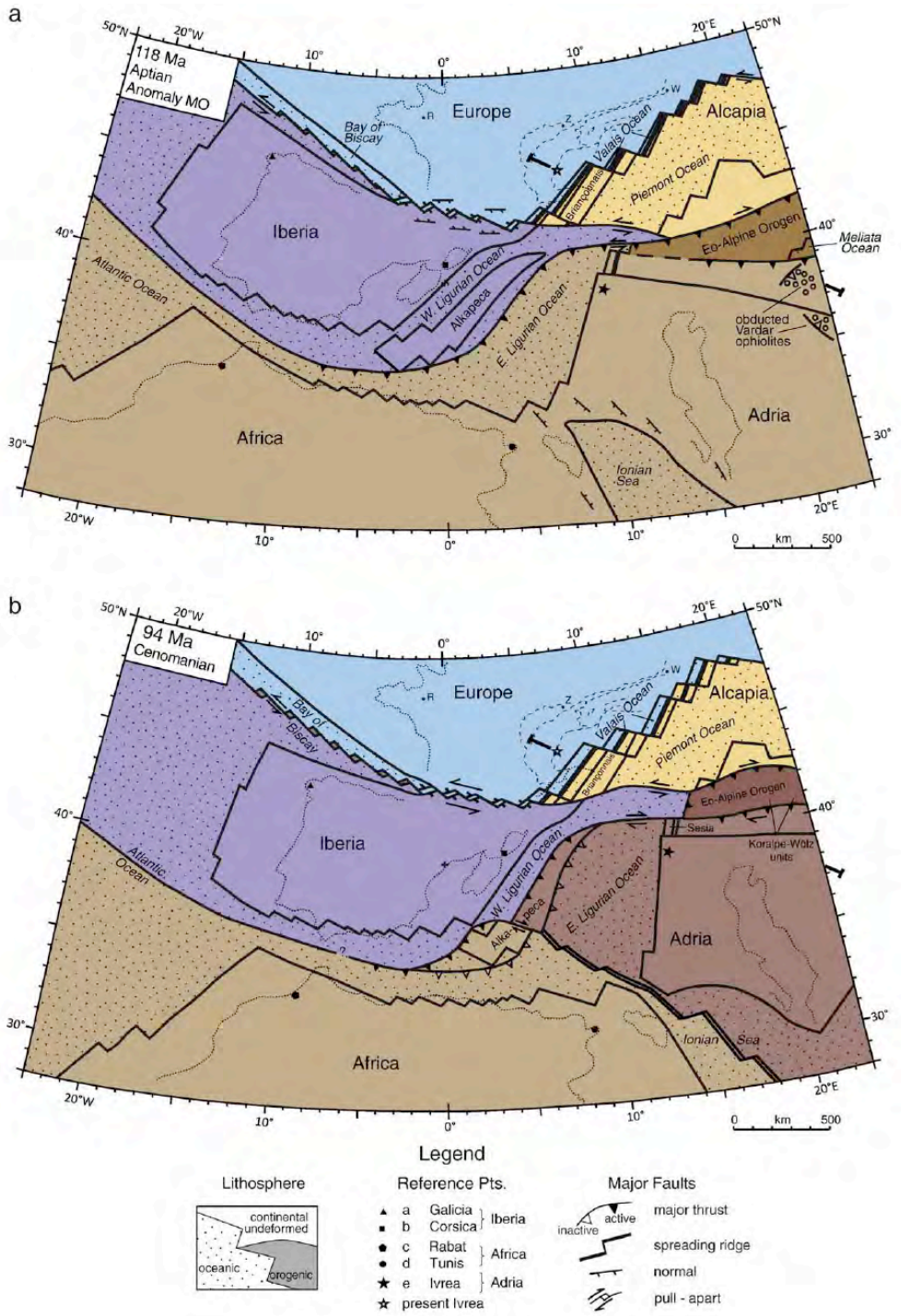

Handy et al 2010

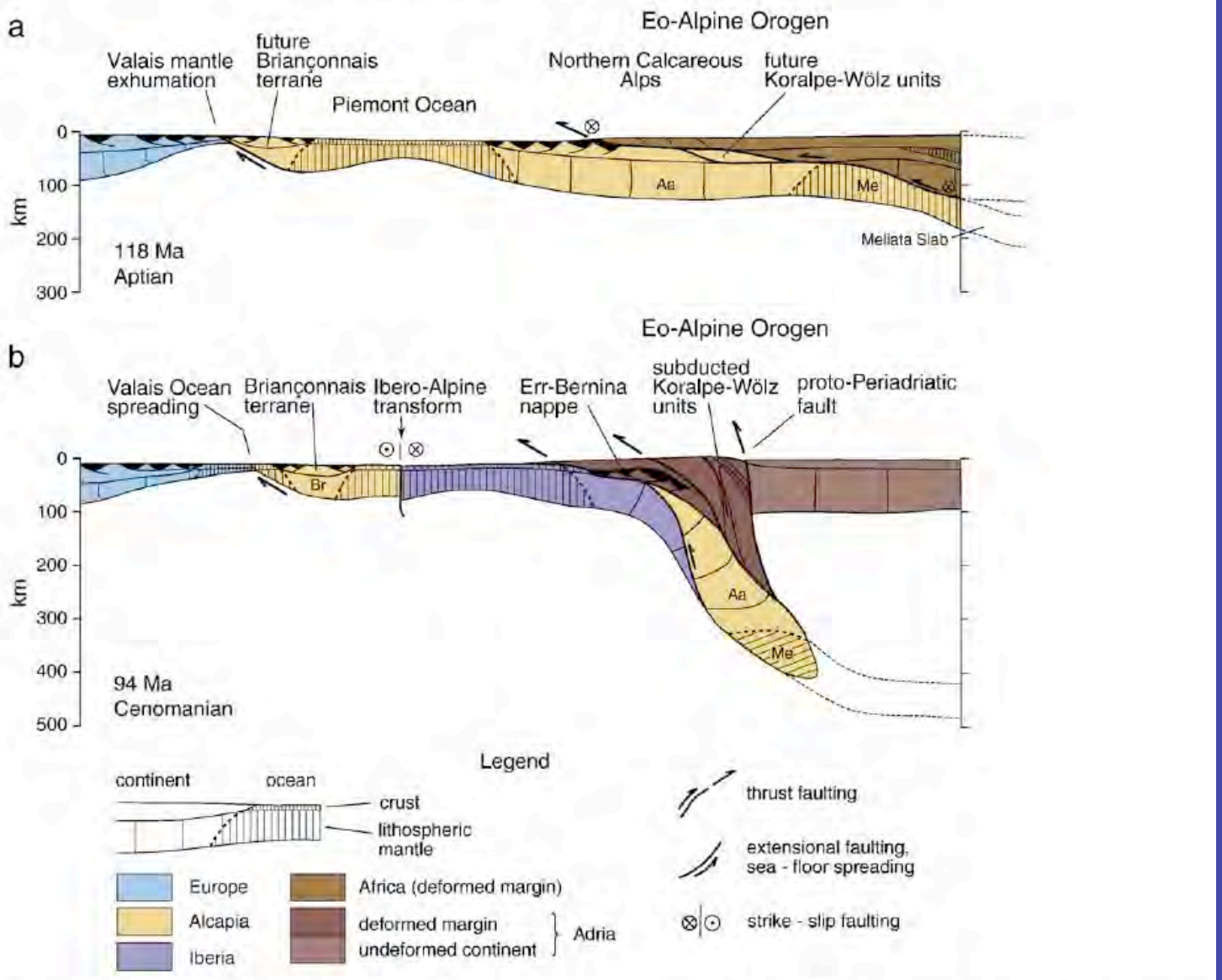

Fig. 11. Cross sections through Alpine Tethys and adjacent continental margins in Late Cretaceous time: (a) 118 Ma, spreading of Valais Ocean linked to Eo-alpine orogenesis, with dashed lines showing probable eastward continuation of the Adriatic lithosphere and the subducted slab of Alcapia (including Meliata oceanic lithosphere); (b) 94 Ma, onset of active margin tectonics only at western end of Eastern Alps due to convergence of Iberia and Alcapia; intracontinental subduction in Eastern Alps. The dashed lines indicate the lateral continuation of the slab of Neotethyan (Me = Meliata–Maliac) oceanic lithosphere behind, i.e., ENE of the plane of the cross section. Location of cross sections shown in Fig. 10. Horizontal scale equals vertical scale. Aa = Austroalpine (Alcapia) continental lithosphere, Br = Briançonnais continental fragment, Me = Meliata–Maliac oceanic lithosphere.

Handy et al 2010

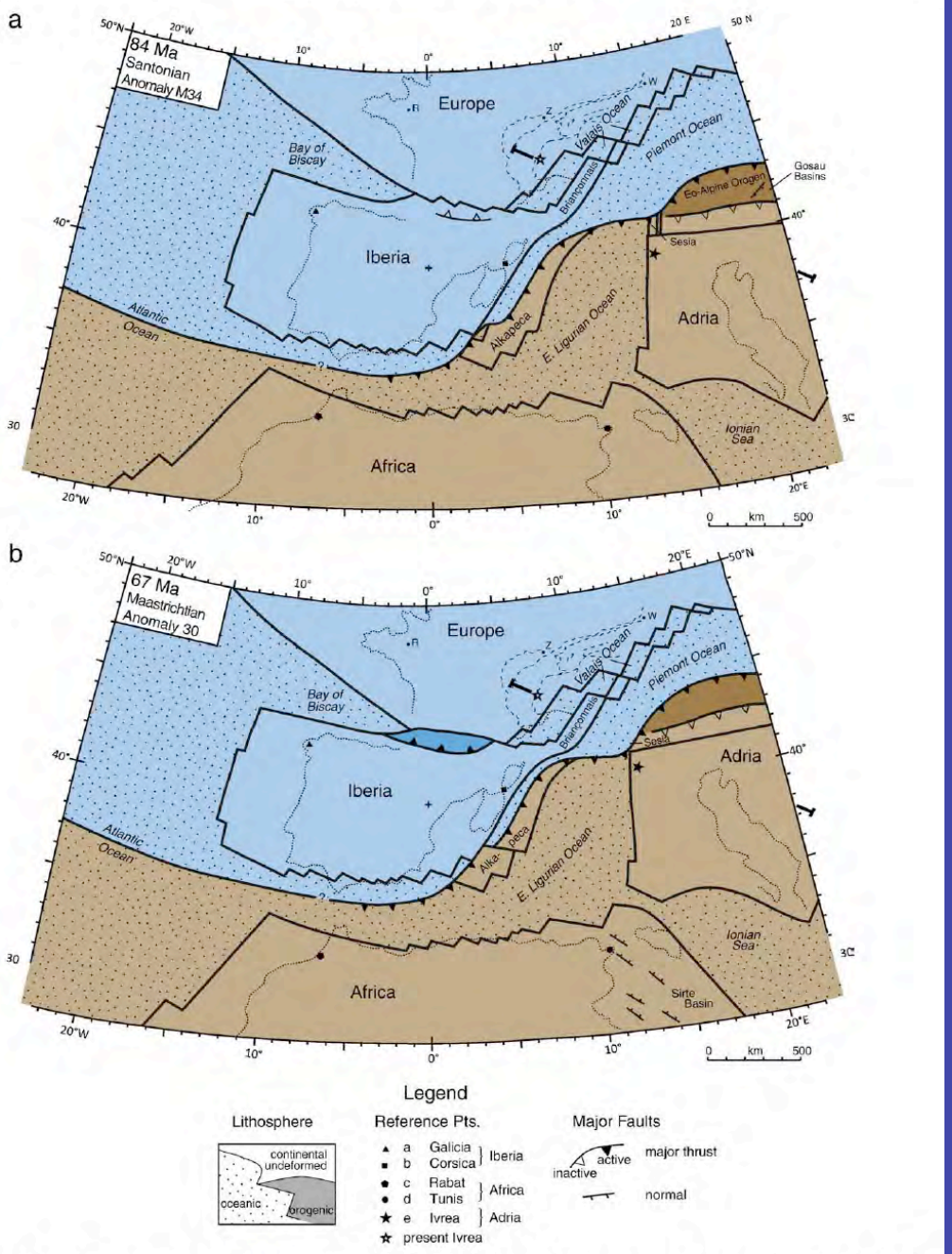

Fig. 12. Plate tectonic maps of Alpine Tethys and adjacent continental margins during NW motion of Africa: (a) 84 Ma, onset of S-directed subduction of Piemont Ocean along Eo-alpine active margin, continued subduction of western Ligurian Ocean; (b) 67 Ma, subduction of westernmost part of Austroalpine passive margin (Sesia Zone) and formation of Western Alpine accretionary wedge. Line shows trace of cross sections in Fig. 13. Dashed lines = current outline of Alpine nappe edifice. City locations for reference on Europe: R = Rennes, W = Wien (Vienna), Z = Zürich.

Handy et al 2010

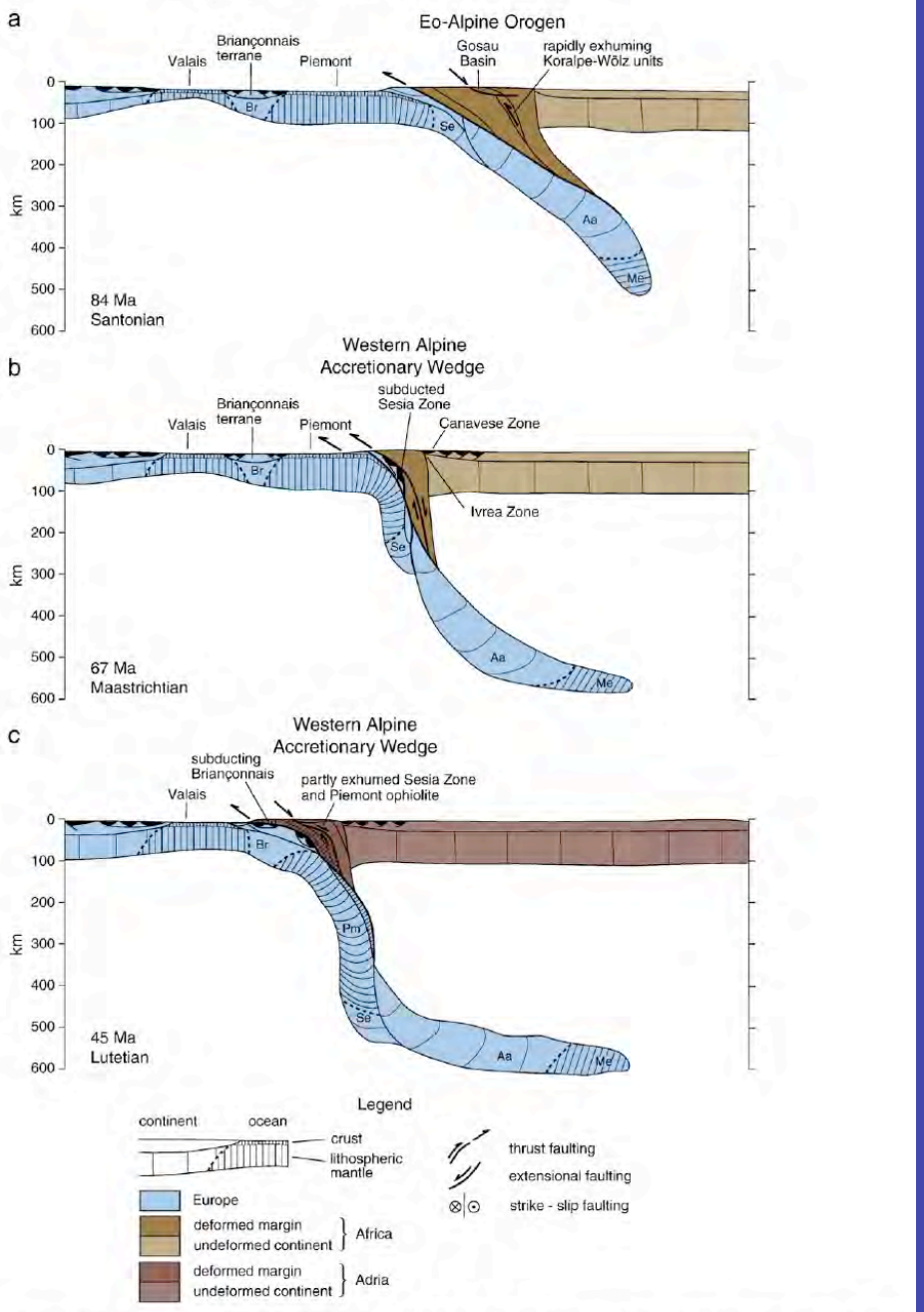

Fig. 13. Cross sections through Alpine Tethys during Late Cretaceous time: (a) 84 Ma, onset of subduction related to NW motion of Africa, rapid exhumation of Koralpe-Wölz unit; (b) 67 Ma, subduction of western tip of the Adriatic continental promontory (Se = lithosphere of the Sesia Zone) and formation of the Western Alpine accretionary wedge; (c) 45 Ma, Early Cenozoic accretion and imbrication of Piemont oceanic crustal slices, subduction of the Briançonnais continental fragment (Br). Location of cross sections shown in Fig. 12. Horizontal scale equals vertical scale. Aa = Austroalpine (Alcapia) continental lithosphere, Me = Meliata–Maliac oceanic lithosphere, Pm = Piemont oceanic lithosphere.

Handy et al 2010

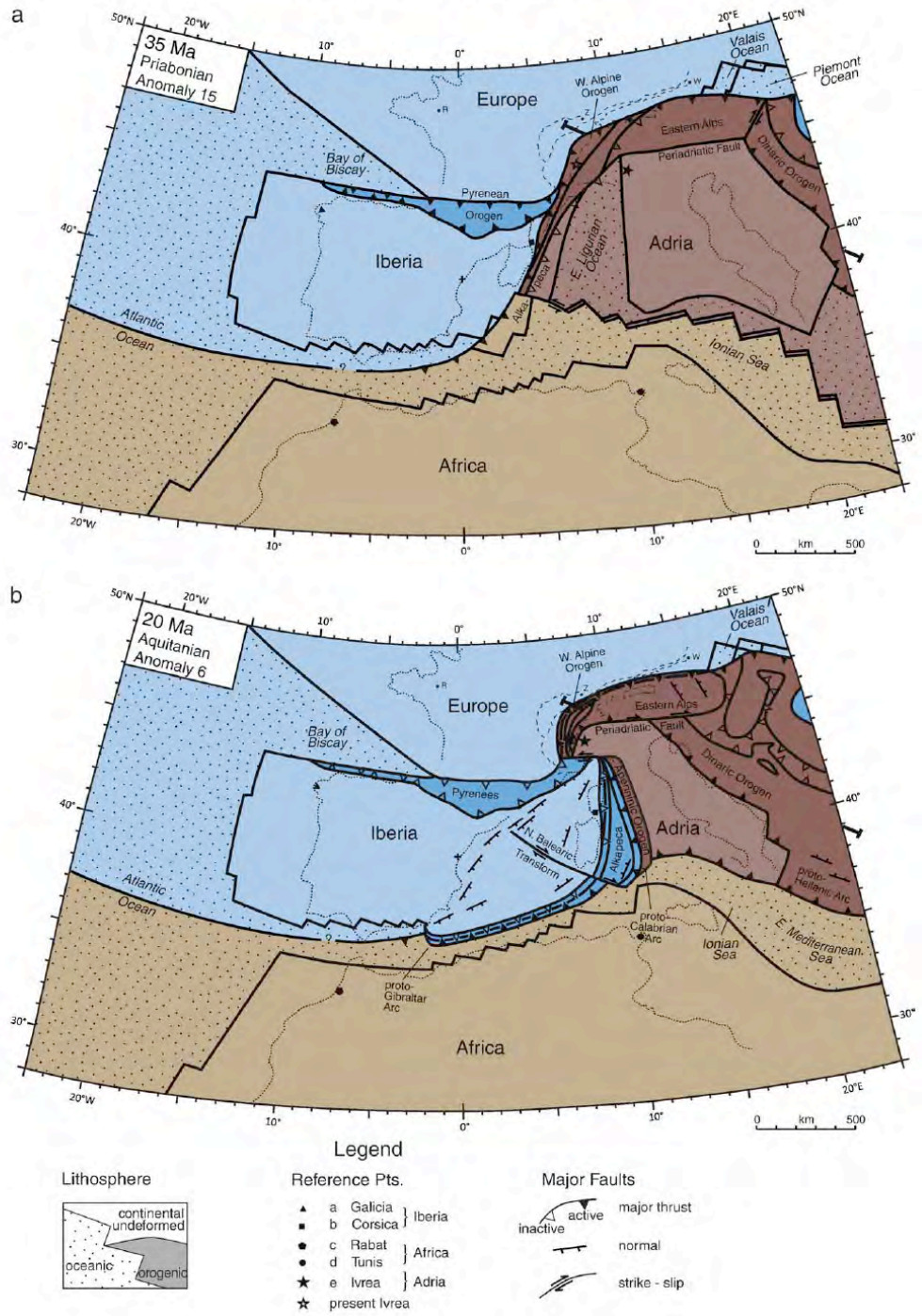

Handy et al 2010

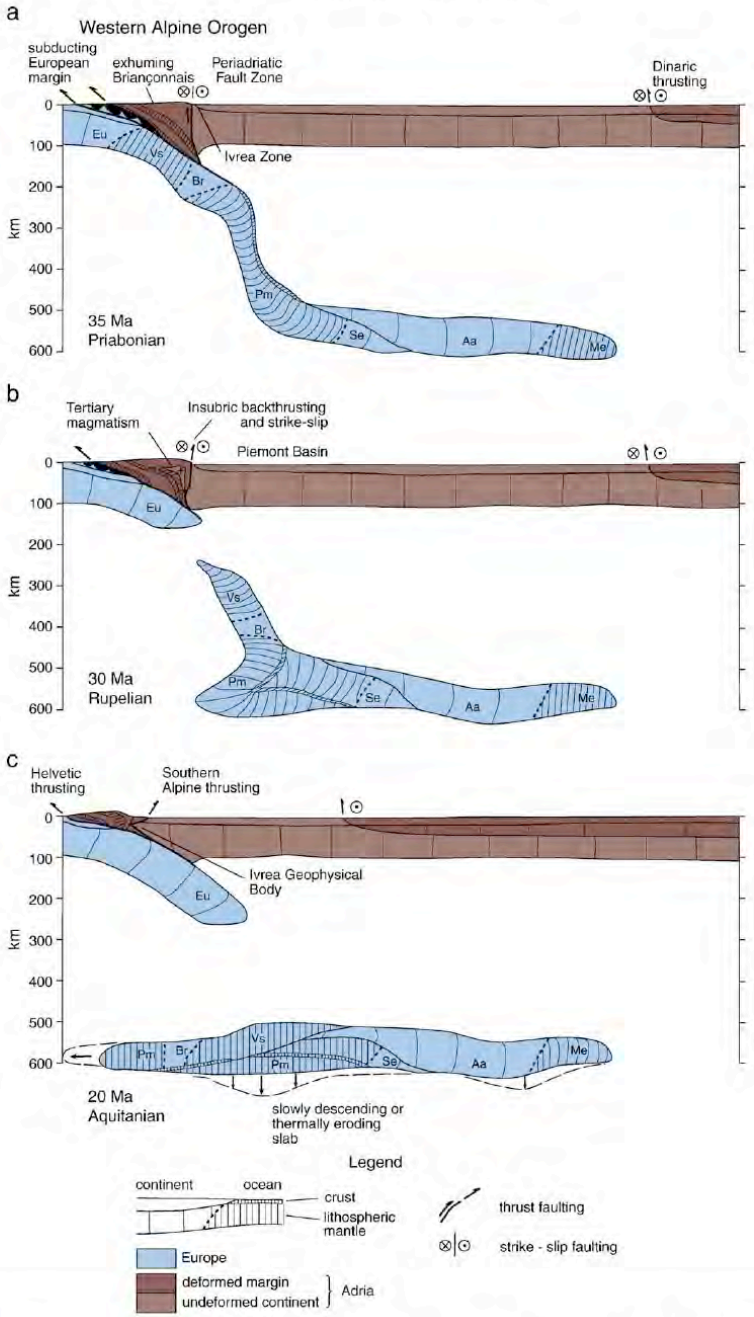

Fig. 15. Cross sections through Western Alpine Orogen and Adriatic plate with Dinaric thrusting: (a) 35 Ma, slab break-off and onset of collision in the Western Alps; (b) 30 Ma, Alpine collision and Adriatic indentation after slab break-off; (c) 20 Ma, late collisional backfolding of partly exhumed Early Cenozoic nappe edifice in the Western Alps. Location of cross sections shown in Fig. 14. Aa = Austroalpine (Alcapia) continental lithosphere, Br = Briançonnais continental fragment, Eu = distal European continental margin, Pm = Piemont oceanic lithosphere, Me = Meliata–Maliac oceanic lithosphere, Se = subducted part of Sesia continental lithosphere, Vs = Valais oceanic lithosphere.

Handy et al 2010

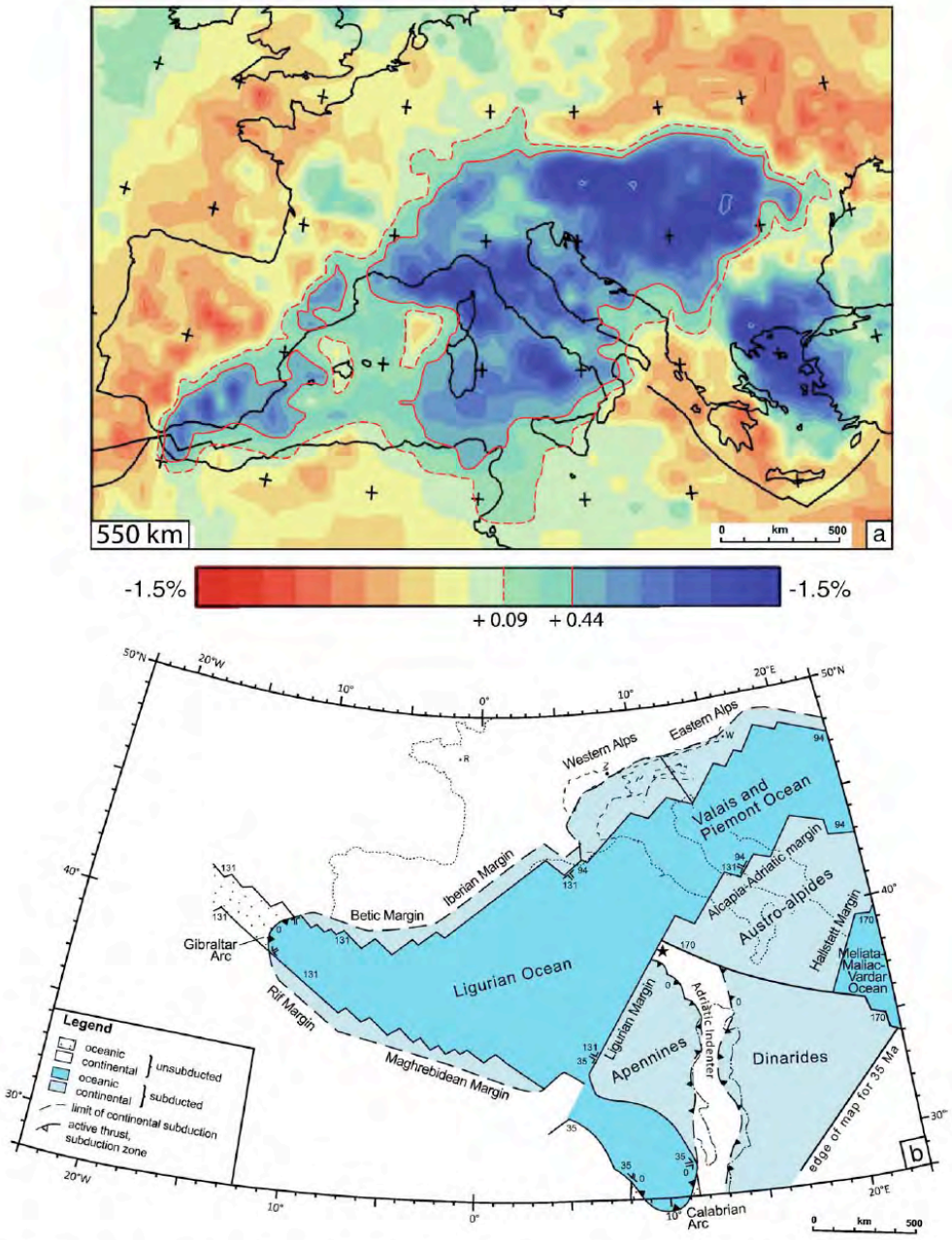

Fig. 17. Subducted lithosphere in the Alps and Mediterranean region. (a) P-wave anomalies at 550 km depth interpreted to be slabs of lithospheric mantle subducted in Late Cretaceous and Cenozoic time (courtesy of W. Spakman). Dashed and solid red lines mark the +0.09% and +0.44% contour lines, respectively, that enclose the positive P-wave anomaly and are used to estimate the amount of lithosphere in the mantle transitional zone in Fig. 18; (b) total area of subducted material comprising oceanic (dark blue) and continental margin (light blue) lithosphere. See text for details of construction. Areal estimates from a and b are shown in the right and left columns of Fig. 18, respectively.

Handy et al 2010

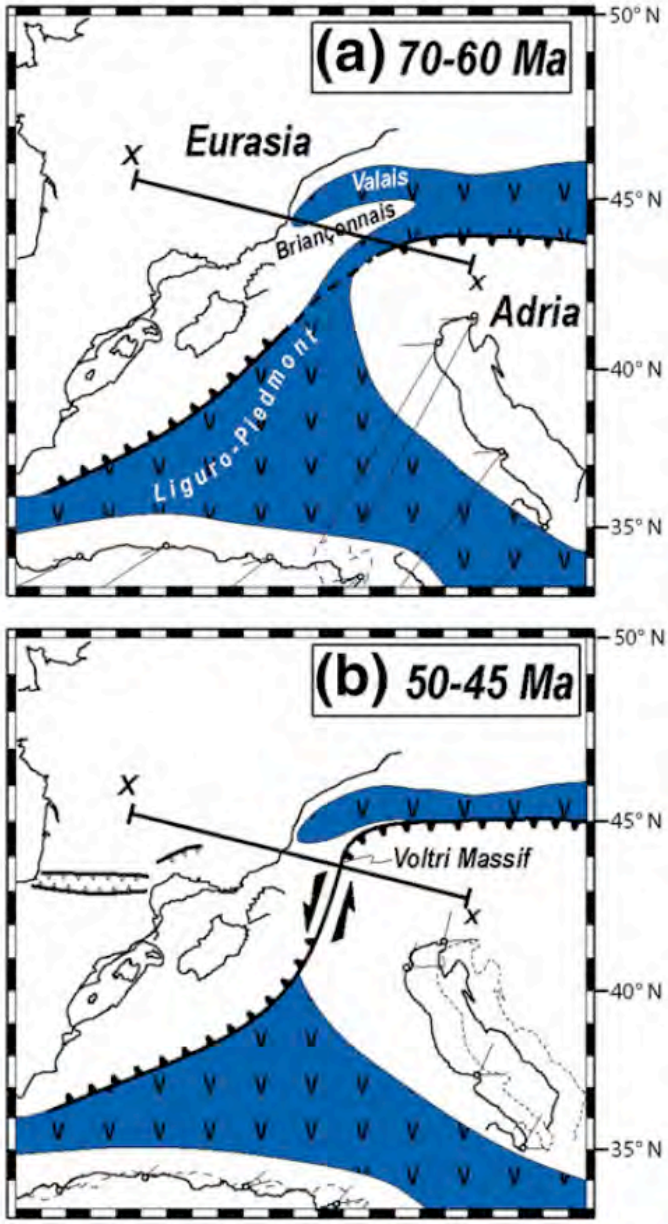

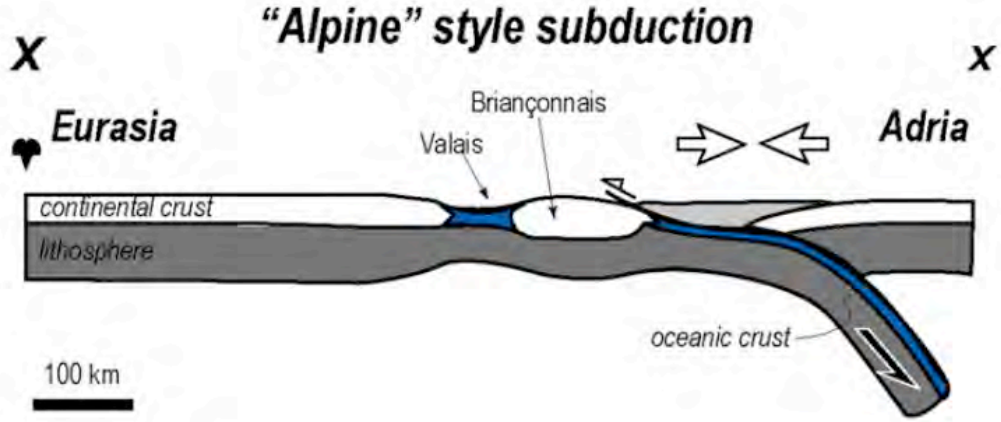

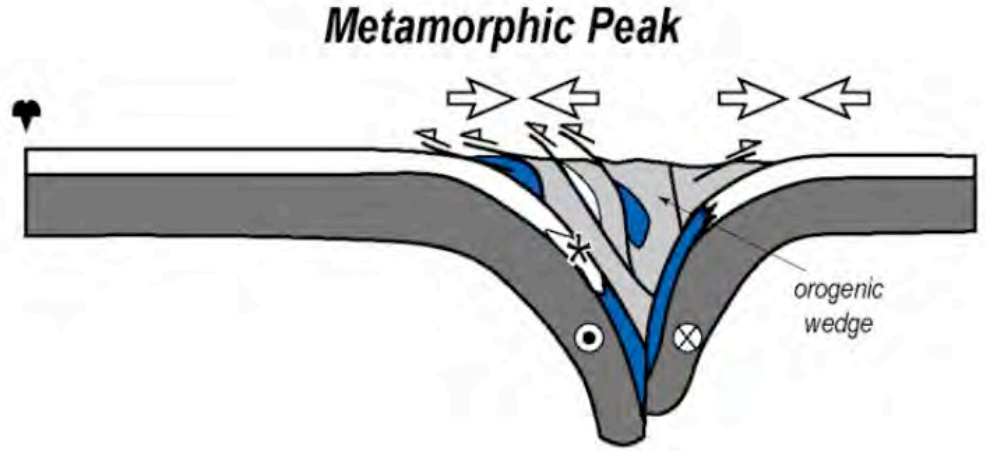

Western Alpine Tectonic History 70-45 Ma

Vignarolli et al 2008

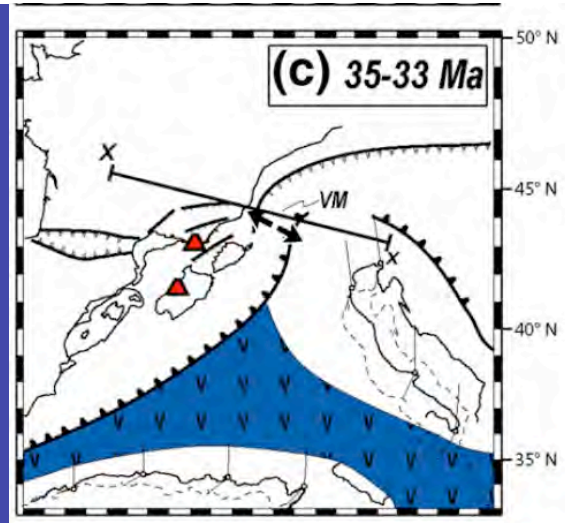

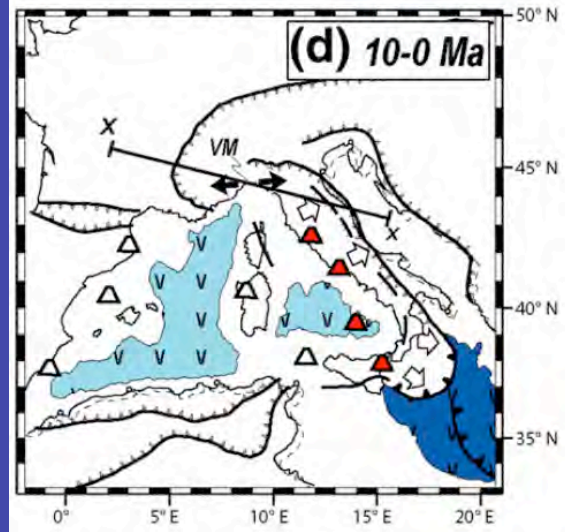

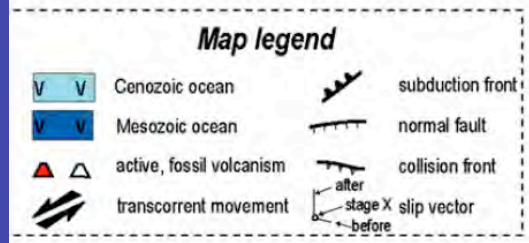

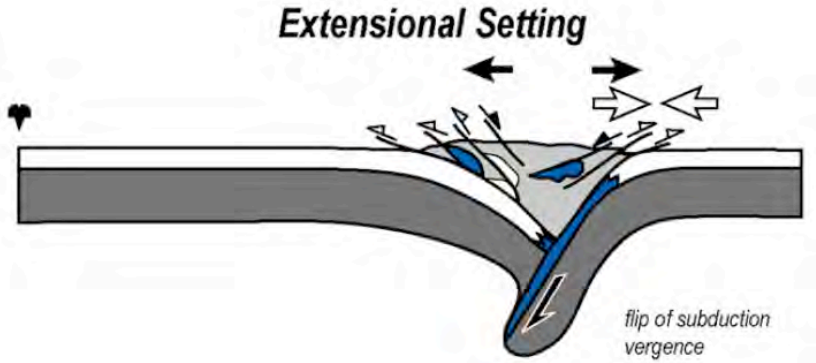

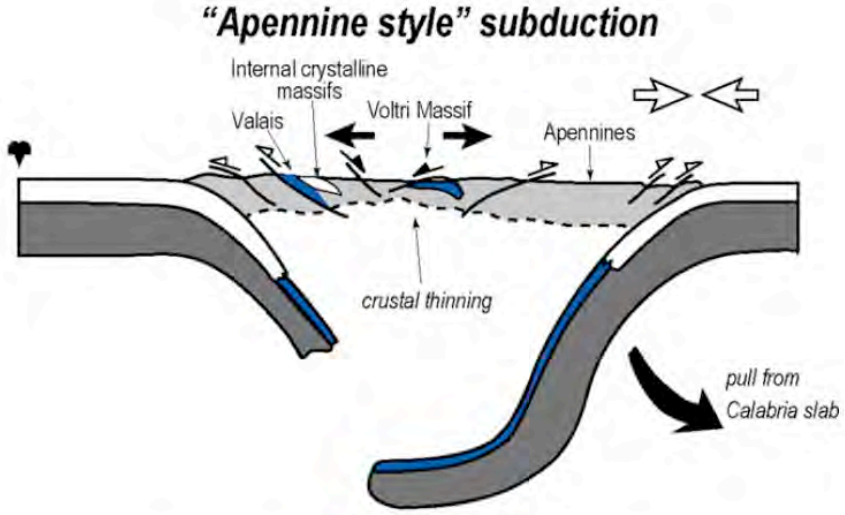

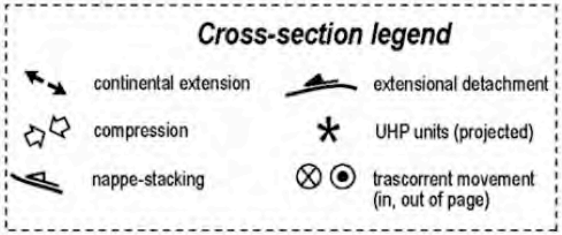

Western Alpine-Apennine Tectonic History 35-0 Ma

Vignarolli et al 2008

Western Alpine-Apennine Tectonic History 70-0 Ma

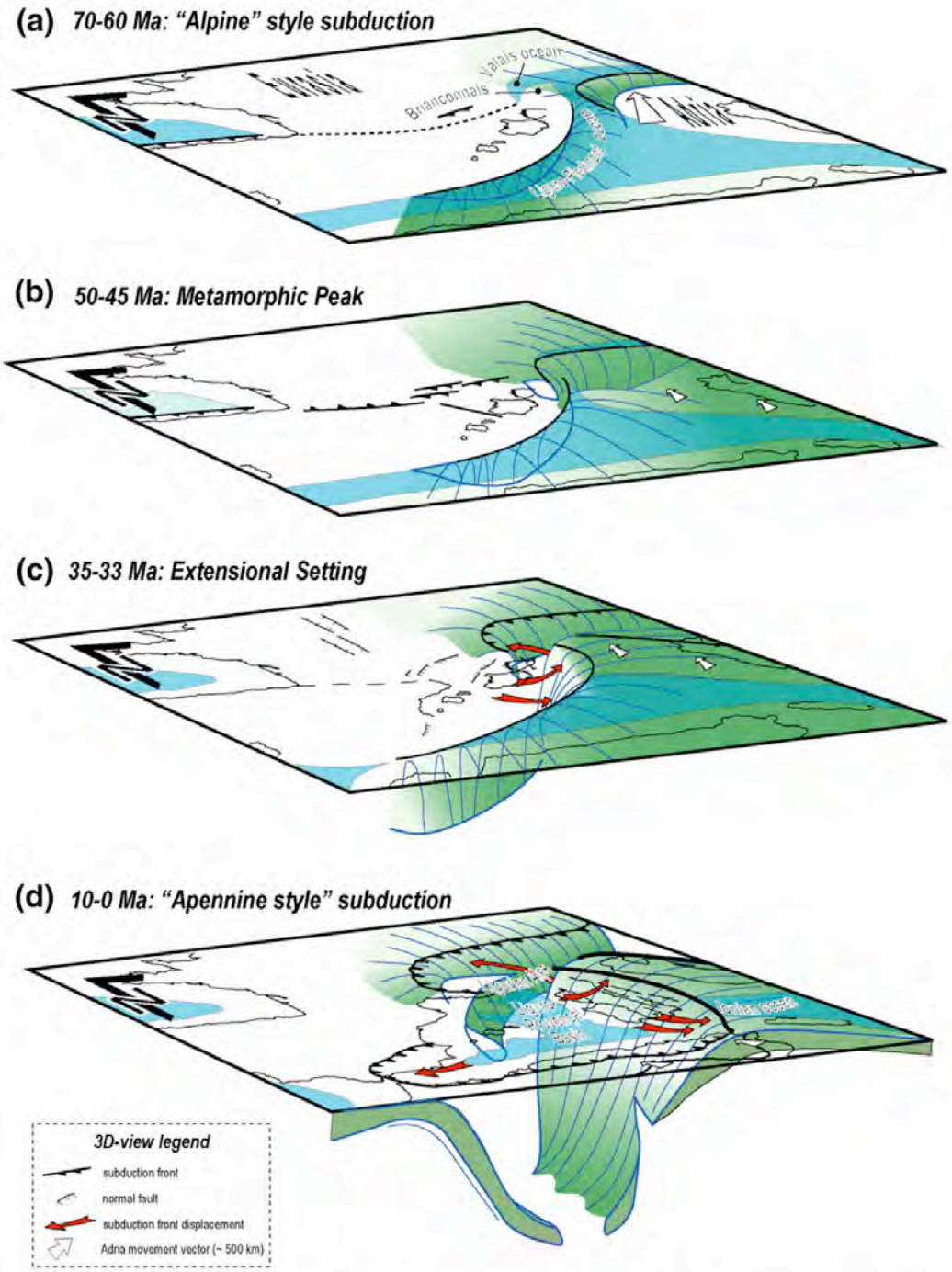

hematic 3D-view of the kinematic reconstruction of the Alps–Apennines belt system, showing as the two orogenic segments progressively separated and

Vignarolli et al 2008

Western Mediterranean Tectonic history ~23-10 Ma

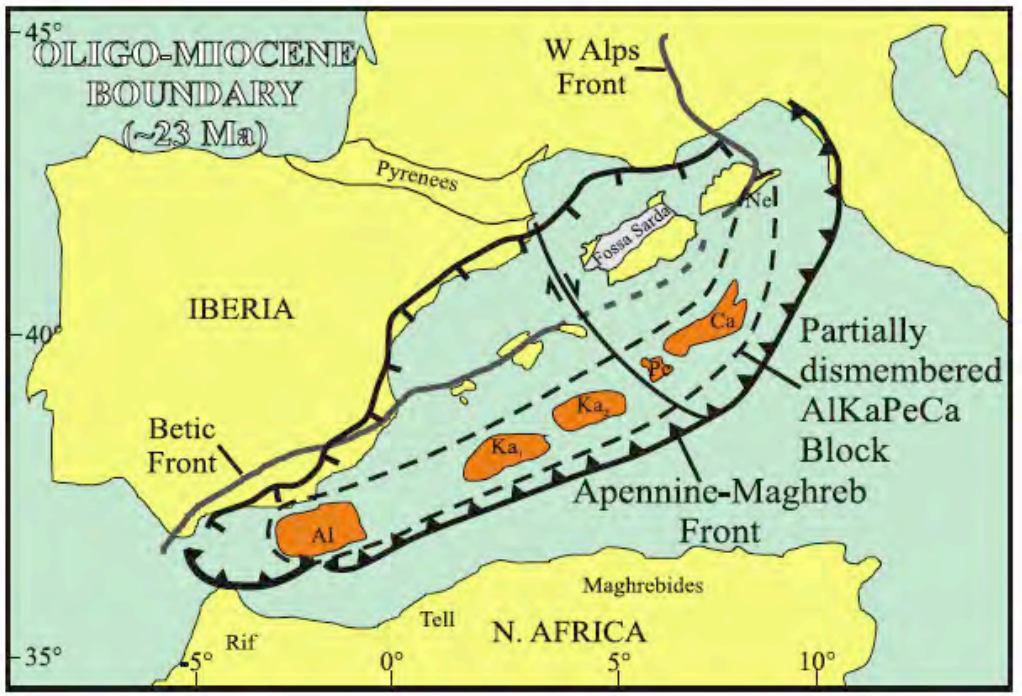

Lustrino et al 2009

Paleozoic Oceans consumed during construction of Pangea 490-420 Ma

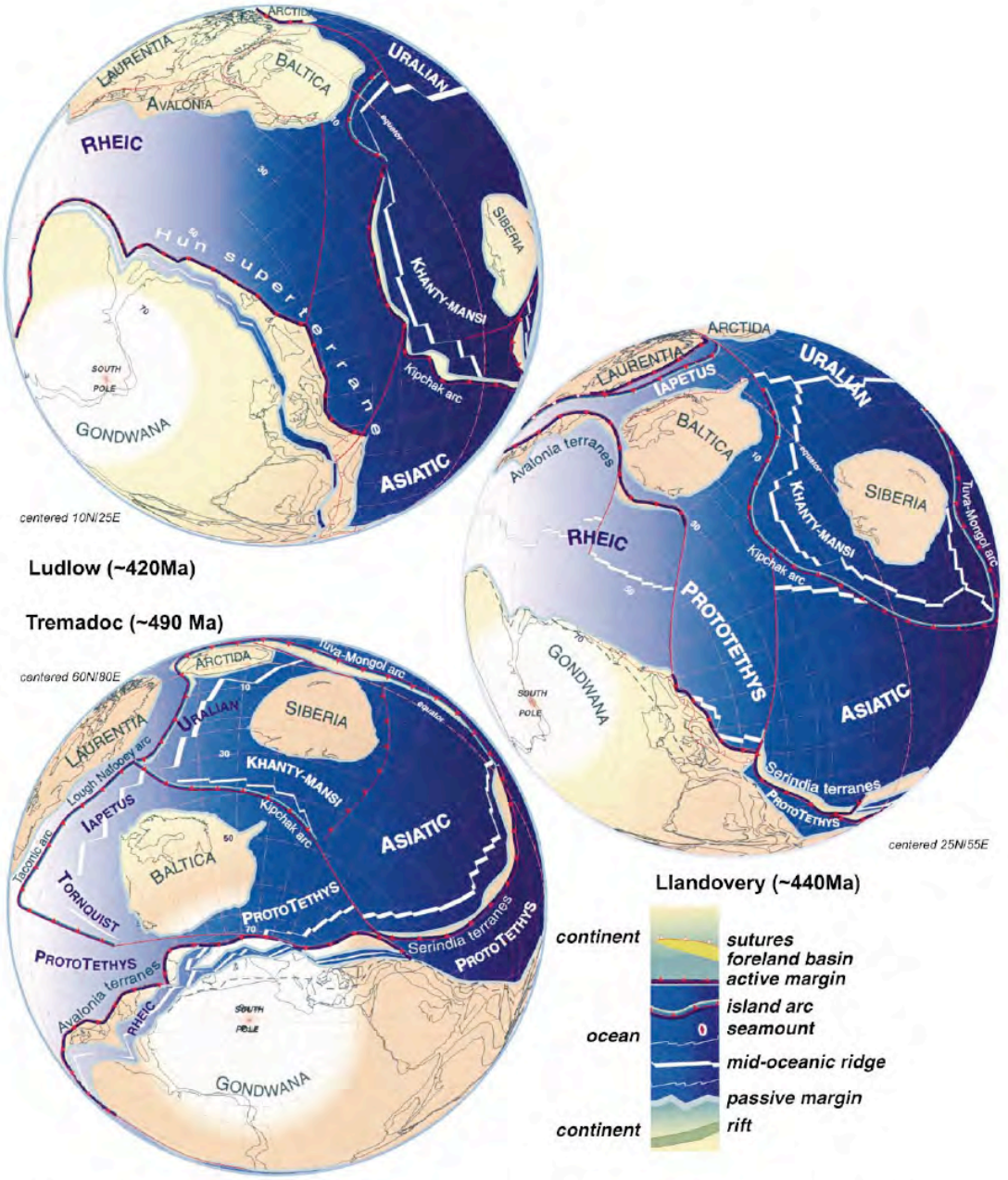

Fig. 3. Explanations in text. Orthographic projection with Europe fixed in its present-day position. Paleopoles of Baltica are used as reference for the paleolatitudes. A complete legend for selected key reconstructions (490 Ma, 360 Ma, 240 Ma, 155 Ma-M25 and 84 Ma-34) are available in the **EPSL Online Background Dataset**[1].

Stampfli & Borel 2002

Paleozoic Oceans consumed during construction of Pangea 400-360 Ma

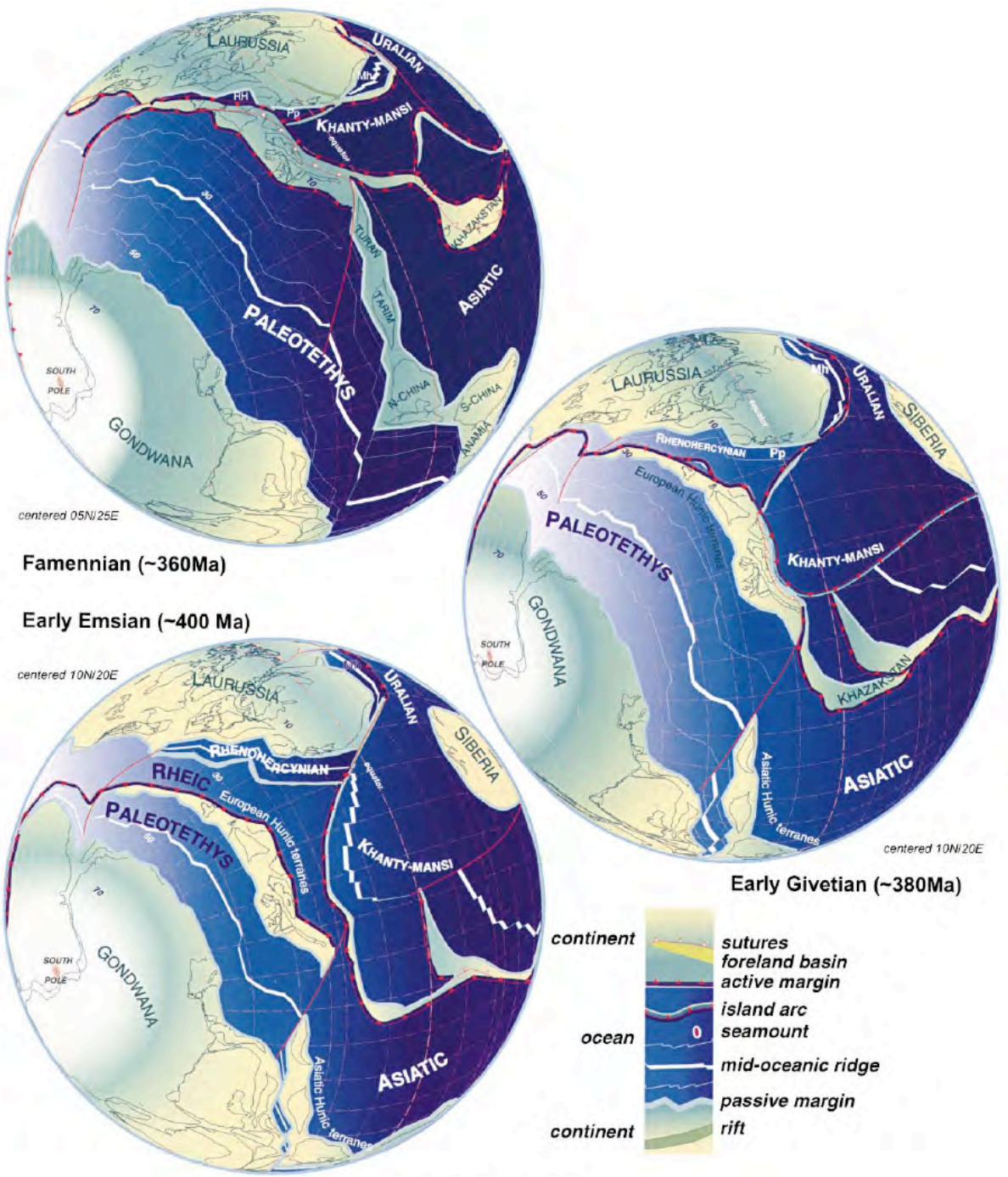

Fig. 4. See legend of Fig. 3.

Stampfli & Borel 2002

The Assembly of Pangea 340 to 300 Ma

Stampfli & Borel 2002

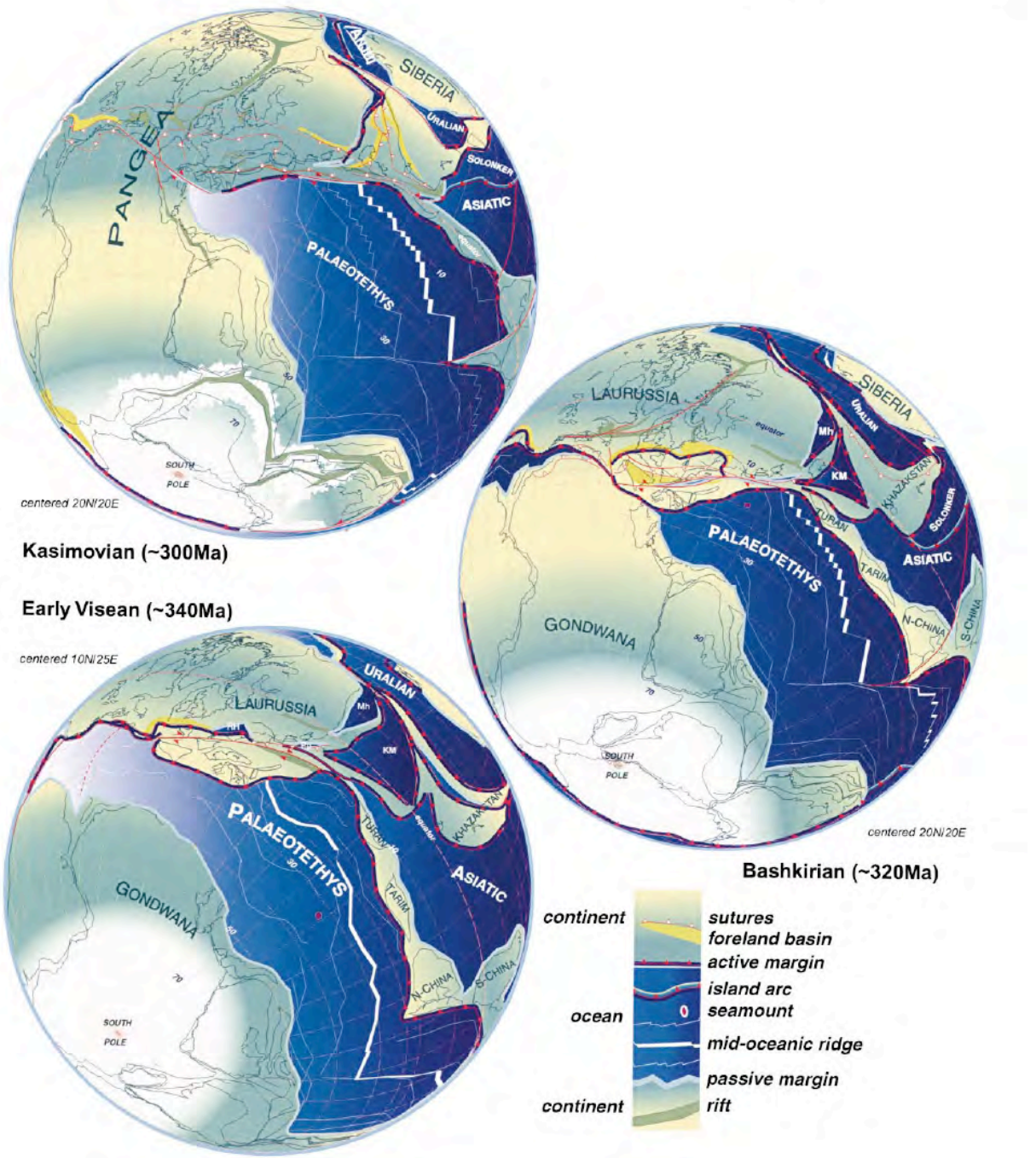

Opening of the Tethys Ocean 290-250Ma

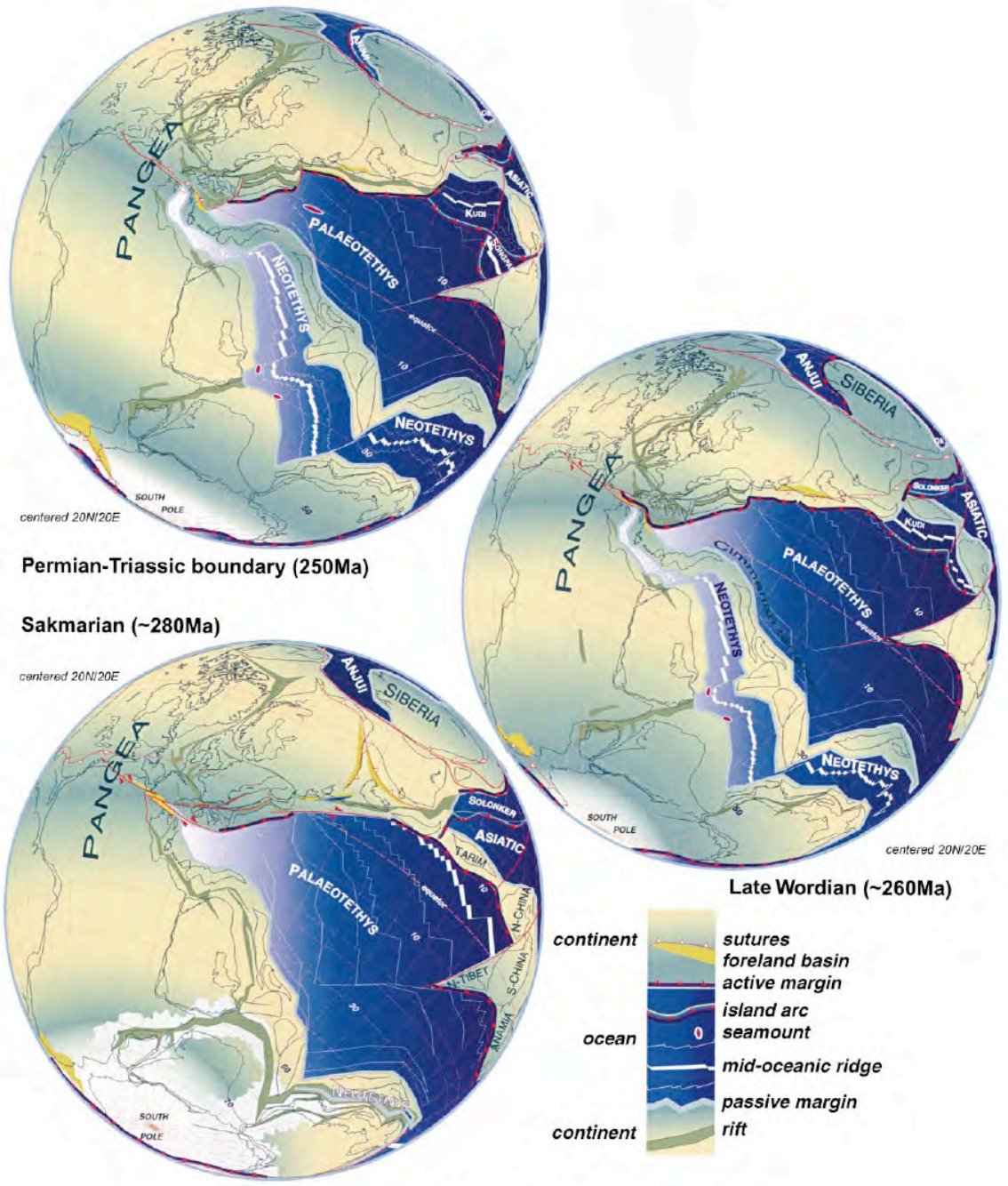

Fig. 6. See legend of Fig. 3.

Stampfli & Borel 2002

Opening of the Tethys Ocean 240-220Ma

Stampfli & Borel 2002

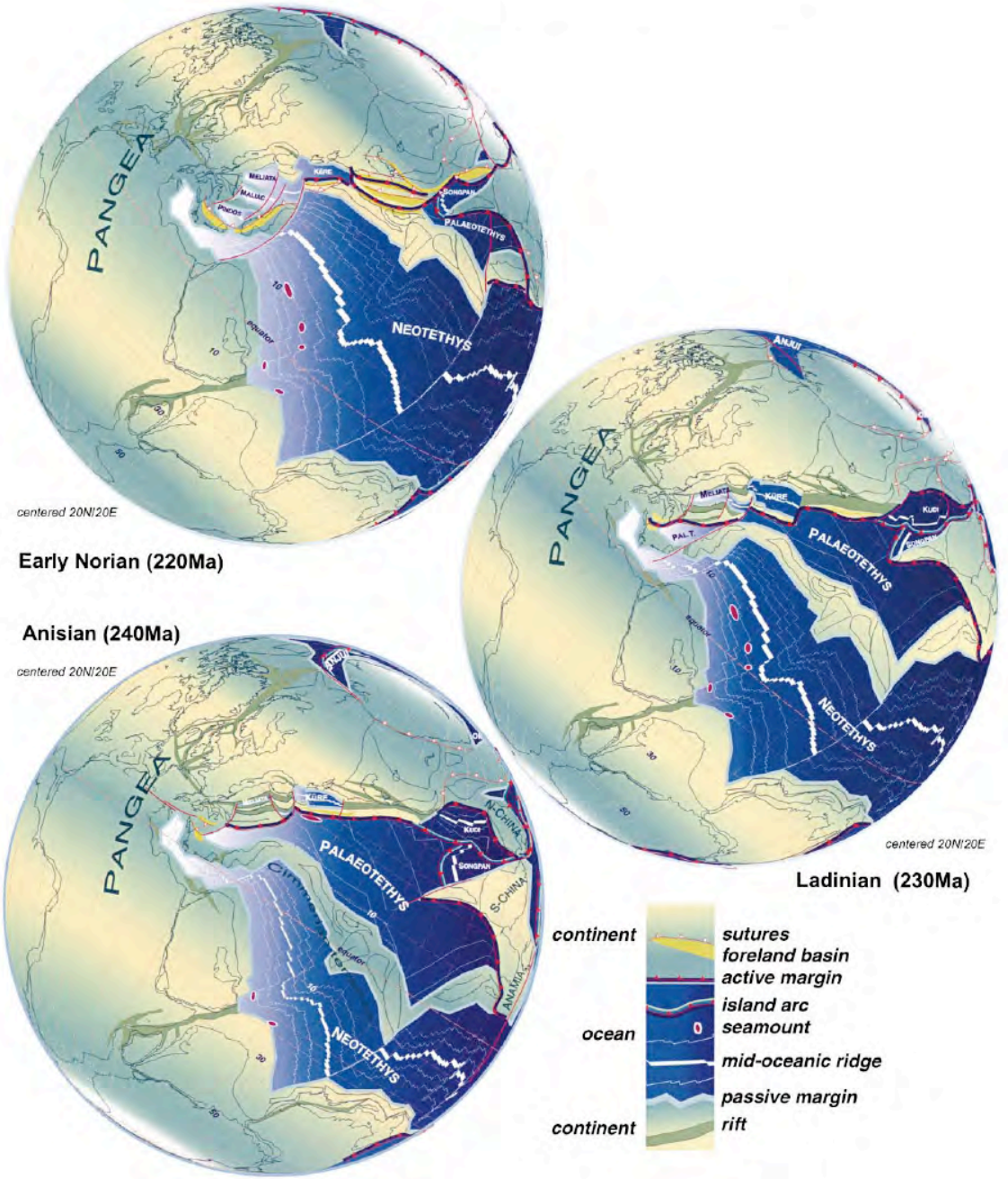

Fig. 7. See legend of Fig. 3.

Opening of the Neotethys Ocean Triassic-Jurassic

Stampfli & Borel 2002

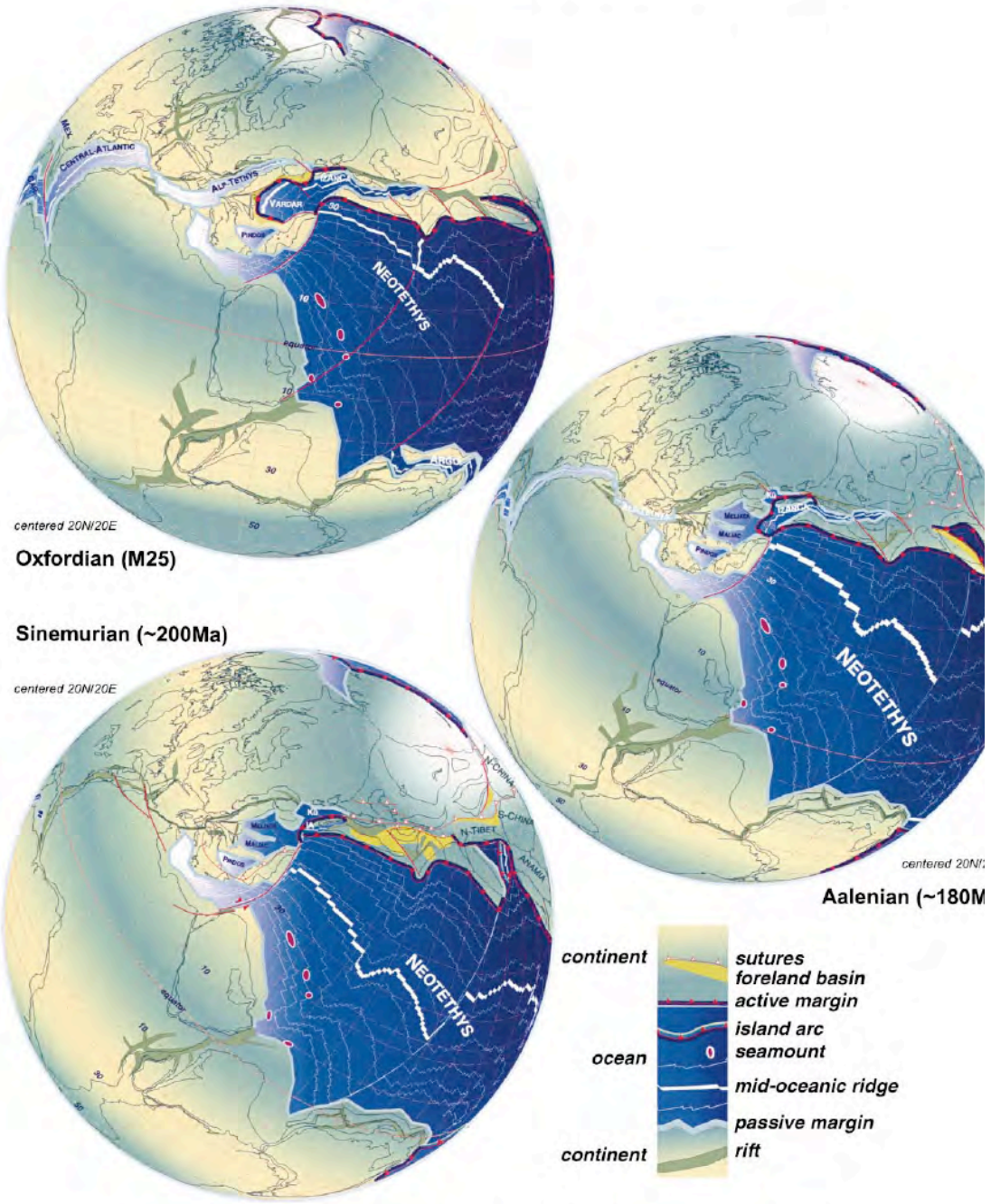

Fig. 8. See legend of Fig. 3.

Sea floor spreading In the Alpine Tethys And Vardar Seas 140-85 Ma

Stampfli & Borel 2002

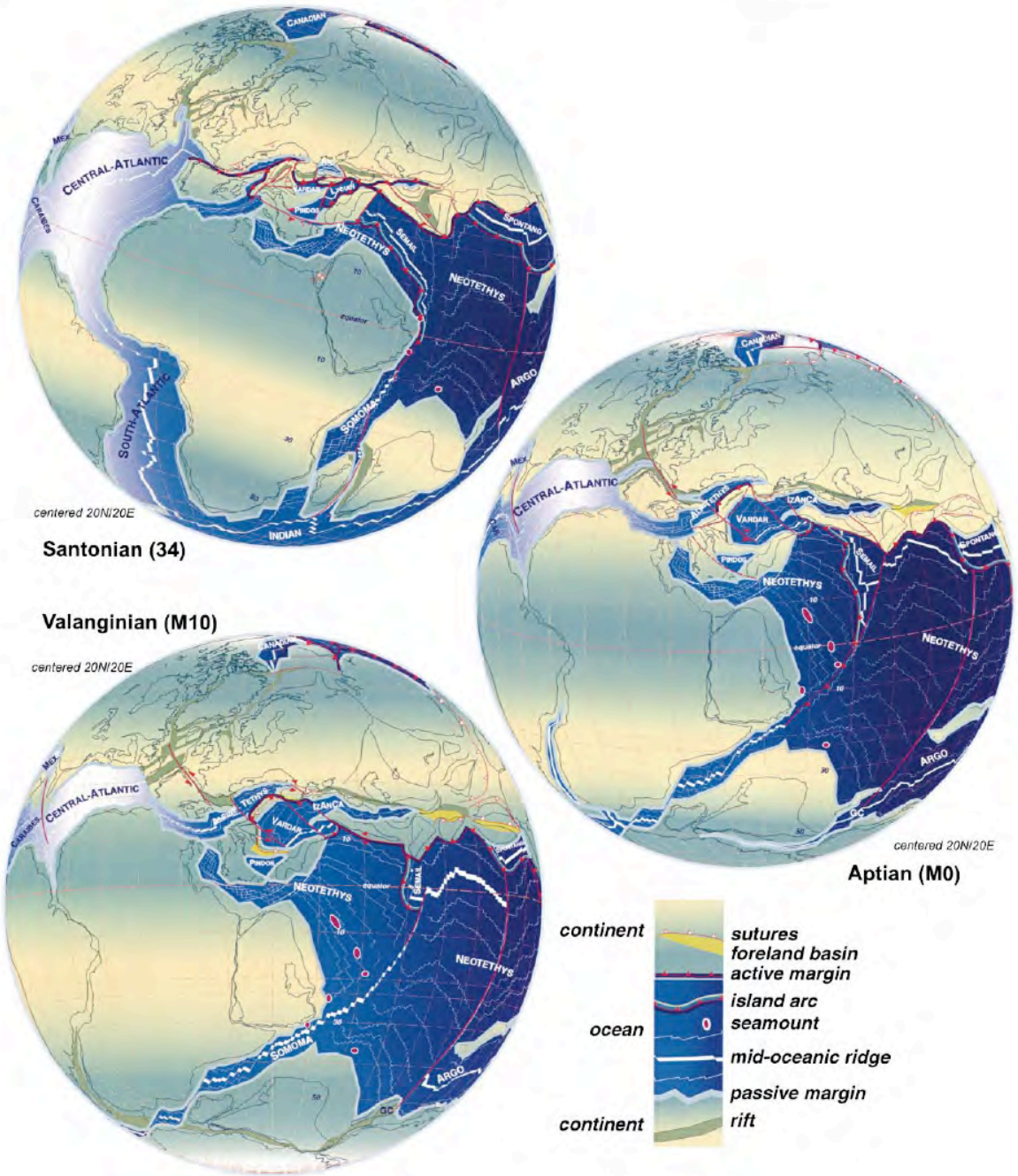

Fig. 9. See legend of Fig. 3.

Western Alpine-Apennine Tectonic History 70-0 Ma

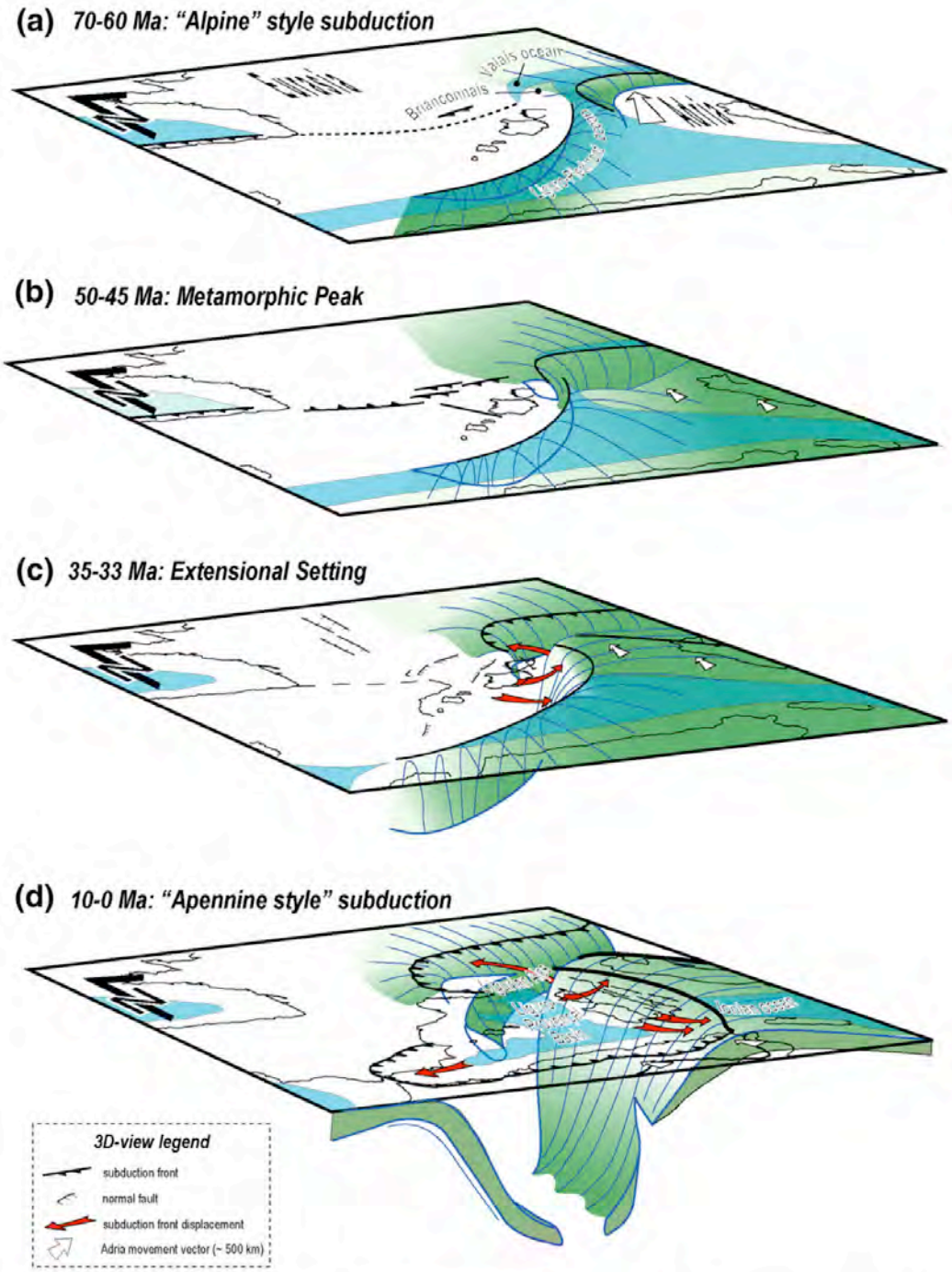

hematic 3D-view of the kinematic reconstruction of the Alps–Apennines belt system, showing as the two orogenic segments progressively separated and

Vignarolli et al 2008